Performance of MIMO Schemes in Radio-over-fibre-based Distributed Antenna System

A Thesis Submitted to The University of Kent for the Degree
of Doctor of Philosophy in Electronic Engineering

By

Anthony Efosa Aighobahi

May, 2017

ABSTRACT

The research presented in this thesis has focused on the use of MIMO wireless communications in a RoF-based DAS to improve wireless coverage and capacity performance in an indoor environment. The aim is to analyse the practical issues that cause throughput to deteriorate when commercial MIMO APs are used in a RoF-DAS, and also to verify that improved performance – lower error rates and higher capacities – can be achieved by a large physical separation between the RAUs when specific multi-antenna scheme algorithms are used.

The performance of an IEEE 802.11n MIMO-supported AP and IEEE 802.11g spatial-diversity-supported AP are investigated in a RoF-DAS when different fibre lengths are connecting the AP in the central unit to the RAUs, and when the RAUs are widely separated. The analysis indicates that for MIMO, the throughput drops rapidly due to severe ISI caused by differential delay when the fibre-length difference exceeds a certain distance, while for spatial diversity high throughputs can be maintained even at large fibre-length difference. Further, it was observed that largely separated RAU may lead to power imbalances and the throughput drops in specific wireless user's positions when the received power imbalance was above 12-15dB for MIMO-supported AP, while for spatial-diversity-supported AP the power imbalance does not affect the throughput.

The majority of previous works on RoF-DAS for improving MIMO systems were based on commercial products and the specific algorithms used within these products are unknown. An investigation was carried out at microwave frequency with SIMO algorithms in RoF-DAS uplink, MISO and MIMO algorithms in RoF-DAS downlink, and compared with the performance of a SISO system. This investigation was later extended to millimetre-wave frequency where larger bands of frequency are available enabling the possibility of wider bandwidth and higher data rates. The result shows significantly reduced error rate and modestly increased capacity for a wireless 1x2 SIMO uplink using MRC algorithm and 2x1 MISO downlink using Alamouti STBC algorithm. Also, error rate was reduced for a wireless 2x2 MIMO downlink using the zero-forcing algorithm while, most importantly, greatly increased capacity was achieved through the spatial multiplexing gain.

ACKNOWLEDGEMENT

TABLE OF CONTENTS

LIST OF PUBLICATIONS

[1]   U. Habib, **A. E Aighobahi**, M. Nair, H. Zhu, T. Quinlan, S. D Walker and N. J Gomes, "Performance Improvement for OFDM-RoF Transported 60GHz System using Spatial Diversity and Multiplexing," The 10th International Workshop on Evolutional Technologies & Ecosystems for 5G and Beyond, IEEE International Communication Conference (ICC), Paris, France, 2017 (Accepted)

[2]   U. Habib, **A .E. Aighobahi**, C. Wang and N. J. Gomes, "Radio over Fiber Transport of mm-Wave 2×2 MIMO for Spatial Diversity and Multiplexing," 13th Avionics and Vehicle Fiber-Optics and Photonics Conference and IEEE International Topical Meeting on Microwave Photonics (AVFOP/MWP), Long beach, USA, 2016, pp. 39 – 42.

[3]   **A. E. Aighobahi** and N. J. Gomes, "Capacity and Error Performance Verification of Multi-Antenna Schemes in Radio-over-Fiber Distributed Antenna System," Journal of Lightwave Technology, vol. 34, Issue 20, 2016, pp. 4779-4785.

[4]   **A. E. Aighobahi**, P. Assimakopoulos, and N. J. Gomes, "Experimental analysis of single and multiple antenna units in uplink of radio-over-fiber distributed antenna system," IEEE International Topical Meeting on Microwave Photonics (MWP), Paphos, Cyprus, 2015, pp. 1-4.

[5]   Y. Fan, **A. E. Aighobahi**, N. J. Gomes, K. Xu, and J. Li, "Performance analysis of commercial multiple-input-multiple-output access point in distributed antenna system," Optics Express, vol. 23, Issue 6, 2015, pp. 7500-7513.

[6]   Y. Fan, **A .E. Aighobahi**, N. J. Gomes, K. Xu and J. Li, "Performance of commercial MIMO access point in distributed antenna system with different fiber lengths," IEEE International Topical Meeting on Microwave Photonics and 9th Asia-Pacific Microwave Photonics Conference (MWP/APMP), Sapporo, Japan, 2014. pp. 17 – 20.

LIST OF ABBREVIATIONS

3G	Third generation of wireless communications
4G	Fourth generation of wireless communications
AP	Access Point
ASE	Amplified Spontaneous Emission
AWG	Arbitrary Waveform generator
BB	Baseband
BER	Bits Error Rate
BERT	Bit Error Rate Tester
BF	Beamforming
BPF	Bandpass filter
bps	Bit per second
BS	Base Station
CAS	Co-located antenna system
CN	Condition number
CNR	Carrier-to-noise ratio
COTS	Commercial off-the-shelf
CP	Cyclic prefix
CSI	Channel state information
CU	Central unit
CW	Continuous-wave
DAC	Digital-to-analogue converters
DAS	Distributed antenna system
dB	decibel
DD	Delay Diversity
DFB	Distributed Feedback
DSP	Digital signal processor/processing
DWDM	Dense Wavelength Division Multiplexing
EA	Electronic amplifier
EDFA	Erbium-doped fibre amplifier
EGC	Equal gain combining

EVM	Error vector magnitude
FEC	Forward error correction
FP	Fabry-Perot
Gbps	Gigabits per second
GHz	Gigahertz
GSL	Gain Switched Laser
I/Q	In-phase and quadrature components
ICI	Inter-carrier interference
IEEE	Institute of Electrical and Electronics Engineers
IF	Intermediate frequency
IIP3	Input power third-order intercept point
IM-DD	Intensity modulation direct detection
IMD3	Third-order intermodulation distortion
IP3	Third-order intercept point
ISI	Inter-symbol interference
ITU	International Telecommunication Union
LD	Laser diode
LMS	Least mean squares
LO	Local oscillator
LOS	Light-of-sight
LPF	Low pass filter
LS	Least square
LTE	Long Term Evolution
MAC	Media Access Control
Mbps	Megabits per second
MCS	Modulation and coding scheme
MDS	Minimum detectable signal
MER	Modulation error rate
MHz	Megahertz
MIMO	Multiple-input, multiple-output
MISO	Multiple-input, single-output
ML	Maximum likelihood

mm-wave	Millimetre-wave
MMF	multi-mode fibre
MMSE	Minimum mean square error
MRC	Maximal ratio combing
multi-antenna	Multiple antenna
mW	Mili-Watt
MZM	Mach-Zehnder modulator
NIC	Network Interface Cards
NLOS	Non-light-of-sight
nm	Nano-metre
OBPF	Optical band pass filter
OBSF	Optical band stop filter
OFDM	Orthogonal Frequency Division Multiplexing
OIP3	Output power third-order intercept point
OSTBC	Orthogonal space-time block code
PAPR	Peak-to-average power ratio
PC	Personal computer
PD	Photodiode
PM	Phase modulator
QAM	Quadrature Amplitude Modulation
RAU	Remote Antenna Unit
RF	Radio Frequency
RIN	Relative Intensity Noise
RoF	Radio-over-fibre
Rx	Receive
SC	Selection Combining
SD	Sphere detection
SDD	System description document
SDR	Software defined radio
SER	Symbols error rate
SFBC	Space-frequency block coding
SFDR	Spurious-free dynamic range

SG	Signal generator
SIMO	Single-input, multiple-output
SINR	Signal-to-interference plus noise
SISO	Single-input, single-output
SMF	Single-mode fibre
SNR	Signal-to-noise ratio
STBC	Space-Time Block Coding
SVD	Singular value decomposition
TAS	Transmit antenna selection
TCP	Transmission Control Protocol
Tx	Transmit
TxBF	Transmit beamforming
UDP	User Datagram Protocol
UE	User equipment
ULA	Uniform linear array
UTC-PD	Uni-Traveling-Carrier Photodiode
V-BLAST	Vertical-Bell Laboratories Layered Space-Time
VCSEL	Vertical-cavity surface-emitting laser
VNI	Visual Networking Index
VSA	Vector signal analyser
VSG	Vector signal generator
WLAN	Wireless local Area Network
WNIC	Wireless network interface card
ZF	Zero-forcing

LIST OF FIGURES

LIST OF TABLES

CHAPTER 1

INTRODUCTION

1.1. Motivation

Global data traffic is expected to grow from 7 exabytes per month in 2016 to 49 exabytes per month by the year 2021 as shown in Fig. 1.1, and according to Cisco Visual Networking Index (VNI), global mobile devices and connections grew to 8 billion in 2016, up from 7.6 billion in 2015 [1]. There is increasing demand for higher data rate by the growing numbers of wireless users, and this has motivated the development of alternative communication systems that will improve wireless coverage and capacity.
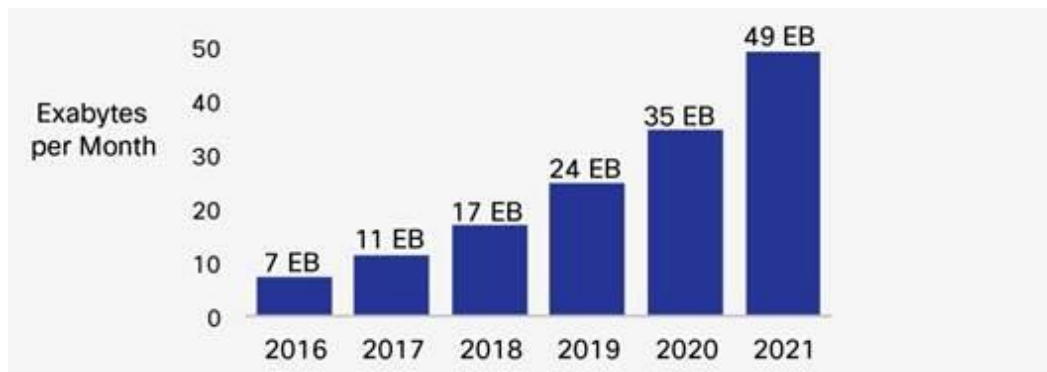
Figure 1.1 Global Mobile Data Traffic, 2016 to 2021 [1]

80%-90% of the data traffic originates from the indoor environment [2], and more traffic will be offloaded from cellular networks on to indoor wireless networks, increasing their need to offer high data rates. Various approaches are widely used to develop an efficient and flexible wireless network to provide adequate coverage and capacity in an indoor environment, and some of these approaches include: femtocells, relays and distributed antenna systems (DASs). Each of these approaches has their

pros and cons, with these depending on the building, design requirements for the current project, and the future needs of the building [3].

Femtocell technology was introduced in IEEE 802.16m SDD (system description document) [4] to bring about significant improvement to the indoor wireless network, by providing boosted cellular signal and high quality wireless services to indoor users. Femtocells are low power, short range and low cost internal base stations used within a building to provide wireless services to stationary or less mobile users within a coverage area (typically between 30-40m) [5]. A femtocell device operates by communicating with a broadband router that interfaces with the mobile operator network through the Internet, and since the femtocells and macrocells are both required to operate in these same limited bandwidths, there are certain to be interference issues [6], for example between neighbouring femtocells or between macrocell and femtocell. However, to cope with these challenges, many researchers have proposed solutions to solve the problems, some of which include interference cancellation and interference avoidance [7].

The integration of relay capability into the indoor wireless network is a promising architectural upgrade [8]; relays are used when a source (e.g. an access point) is communicating with the destination (e.g. a wireless user) and the direct communication path is obstructed. Instead of transmitting the signal through the obstructed direct path and suffering a severe level of path loss, the signal from the source can exploit other unobstructed line-of-sight paths, and with the help of a relay node, the source can still deliver a high-quality signal to its destination. Relay networks suffer from practical issues such as cooperative schemes involving signalling between relays, and difference in time of arrival between the direct path from source to destination and the paths between source-relay-destination [9].

The distributed antenna system (DAS) is an alternative to femtocell and relay networks. In DAS, remote antenna units (RAUs) are geographically deployed and connected to a central unit (CU) using either an out-of-band radio link, coaxial cables, a digital optical network or radio-over-fibre (RoF) links to extend the wireless coverage from the base station to indoor users [10]. DAS has attracted much attention [11-13] for the in-building environment because it can provide high quality signal coverage, with low interference and high signal-to-noise ratio (SNR). Also, DAS can

facilitate easy upgrade of existing services to emerging wireless services due to its centralized architecture [14] making it easier to adopt different techniques such as higher order modulation, orthogonal frequency-division multiplexing (OFDM), advanced coding schemes and, more recently, multiple-input multiple-output (MIMO) schemes to widely improve wireless access rates.
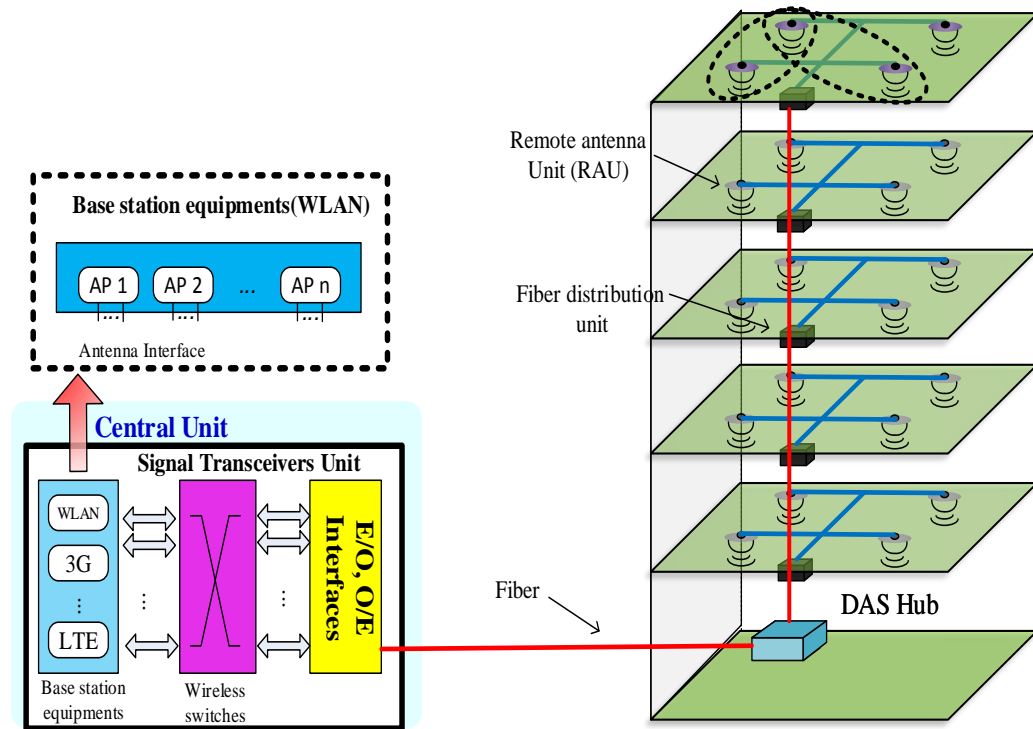
Figure 1.2 RoF-based DAS

Fig. 1.2 shows an illustrative radio-over-fibre (RoF)-based DAS infrastructure used to distribute wireless local area network (WLAN), 3G and Long Term Evolution (LTE) signals. The base station equipment and WLAN APs are co-located in the central unit (CU), and connected to the RAUs using RoF link. Although, coaxial cable and other electrical cables can be used to connect the CU to the RAUs, such electrical cables have very high attenuation, making longer transmission spans impractical and prohibiting the centralization of equipment in a single location in larger buildings [15]. Using RoF link in DAS has key advantages, such as simple configuration and low loss of optical fibre to improve signal transmission, and when using simple direct modulated laser and direct detection photodiode (PD), the

3

infrastructure cost can be reduced [16]. The RAUs are merely a distributed set of antennas, with little or no processing capability [17], that exchange RF signals with the CU where all the signal processing such as modulation, demodulation, multiplexing, de-multiplexing, handover, diversity and protocol transformations are carried out.

1.2. Objective of research

Early works on in-building DAS used IEEE 802.11b/a/g compliant APs with single-input, single-output (SISO) antenna configuration, where RF splitters were used to split the wireless signal from the CU to the RAUs. The introduction of the multiple-input, multiple-output (MIMO) antenna configuration in the IEEE 802.11n standard, and its integration into RoF-based DAS can bring about further improvement in throughput performance by taking advantage of the largely separated multiple RAUs (enabling greater spatial decorrelation). However, the geographical location of the RAUs has raised practical issues; for example, the unequal fibre lengths connecting the CU to the RAUs can introduce differential delays to the received OFDM signals resulting to Intersymbol Interference (ISI). Also, large antenna separation may lead to imbalances in the received power, which can cause deterioration in throughput performance because the signal strengths of the two received signals in MIMO should be relatively equal before combining them. Furthermore, previous works on RoF-DAS for improving MIMO systems were based on commercial products and the specific algorithms used within these products were unknown. Finally, there are interests in the technical convergence of millimetre-wave-over-fibre transport and MIMO schemes, but due to the highly directional antennas used at millimetre-wave frequencies to overcome the wireless channel path loss, it is unclear how well MIMO techniques will work within a line-of-sight (LOS) propagation given the shortage of multipath.

1.3. Contribution of the Thesis

The unique contributions of this thesis include:

- Performance analysis of two practical issues encountered when transmitting MIMO signals on RoF-DAS infrastructure i.e. fibre length difference and power imbalance effect. The experimental investigation involves the performance of a commercial IEEE 802.11n 2x2 MIMO-supported access point (AP) and a spatial-diversity-supported AP in a RoF-DAS. The analysis can greatly assist the DAS operator to make allocation decisions in a typical office environment; for example, the decisions can include which distributed antennas can cooperate and which cannot due to large fibre-length difference, and how much power each RAU should transmit so that received power imbalances can be reduced.

- An experiment to verify that improved performance – lower error rates and higher capacities – can be achieved by a large physical separation between the RAUs with spatial diversity single-input multiple-output (SIMO) algorithms in RoF-DAS uplink, spatial diversity multiple-input single-output (MISO) and spatial multiplexing MIMO algorithms in RoF-DAS downlink. The uplink experiment was carried out with one transmitting mobile unit placed at different locations in a typical office environment and the OFDM signals gathered through two RAUs and brought back to the central unit for processing. The downlink experiment was carried out when the signals from two transmitting RAUs are sent to a mobile unit and captured for processing.

- An experiment to verify that transmitting 1Gbps data in a 25GHz and 60GHz mm-wave-over-fibre MIMO system, the error vector magnitude (EVM) can be reduced using spatial diversity algorithm, and data rate can be increased using spatial multiplexing algorithm, when compared to a SISO system. The 25GHz experiment involves DWDM-RoF-transport of two MIMO signals to two RAUs for wireless transmission and the signals are captured at the mobile unit and saved for MIMO offline processing. The 60GHz experiment involves measuring the complex channel transfer matrix H together with the transmitted symbols to

emulate a 2x2 MIMO system, and the values are saved for MIMO offline processing.

1.4. Thesis Outline

Chapter 2 presents a detailed background study comparing in-building co-located antenna system (CAS) with DAS, in particular focussing on RoF link configurations, direct and external modulated RoF links, and specific performance metrics used to characterize the performance of such links. In addition, the principles of MIMO systems is presented focusing on the spatial diversity technique that is used to improve data reliability, spatial multiplexing technique that is used to increase data rates, and beamforming technique that is used to improve SNR. The performance metrics used to measure the amount of error and the channel capacity of wireless MIMO systems are also presented. Further, a literature review is carried out to determine the improvement in capacity, throughput and coverage the integration of RoF-DAS and MIMO system offers over DAS supporting only a SISO configuration.

Chapter 3 presents the analysis of practical issues with commercial IEEE 802.11n 2x2 MIMO-supported AP and a spatial-diversity-supported AP in RoF-DAS infrastructure. The two practical issues - fibre-length difference effect and received power imbalance - are first discussed before demonstrating these effects in an experimental RoF-DAS. The experimental setup is described, and the fibre length difference analysis results are presented for a single and multiple user case. Further, the power imbalance analysis results are presented showing the relationship between MIMO-DAS throughput performance and received power imbalance, and the relationship between the received power and throughput.

Chapter 4 presents the error and capacity performance of SIMO, MISO and MIMO schemes in RoF-DAS using specific algorithms. The selected coded algorithms used to process the multi-antenna signals are first discussed, before demonstrating them in an experimental RoF-DAS. The error and capacity performance results of the 1x2 uplink SIMO, 2x1 downlink MISO and 2x2 downlink MIMO schemes are presented for 4m antenna spacing and compared with 0.3m antenna spacing and SISO systems.

In addition, the error performance results of wider antenna separation (up to 10m) is presented to determine the optimum antenna spacing for the selected multi-antenna scheme algorithms.

Chapter 5 presents the error performance of spatial diversity and multiplexing MIMO techniques used in 25GHz and 60GHz RoF systems. The experimental setup for the systems are described, and the measurement results at different transmit antenna separation distance and receive antenna locations follow. Further, the EVM results of the 25/60GHz spatial diversity and multiplexing are compared with the EVM result of a SISO system.

Chapter 6 presents the overall conclusions drawn from the investigations and recommendations for future research.

REFERENCES

[1] "Cisco Visual Networking Index: Global Mobile Data Traffic Forecast Update 2016-2021", 2017.

[2] T. Norman, "Research forecast report - Wireless network traffic 2010-2015: forecasts and analysis," Analysys Mason, Tech. Rep., 2010.

[3] M. Tolstrup (2008): Indoor Radio Planning: A Practical Guide for GSM, DCS, UMTS, HSPA and LTE, John Wiley & Sons.

[4] IEEE 802.16m, "IEEE 802.16m System Description Document (SDD)", Rev. IEEE 802.16m-09/0034r2, September 2009

[5] S.A. Mahmud, G.M. Khan, H. Zafar, K. Ahmad, N Behttani, "A Survey on Femtocells: Benefits Deployment Models and Proposed Solutions," Journal of Applied Research and Technology, Volume 11(5), pp. 733-754, 2015

[6] K. Elleithy and V. Rao, "Femto Cells: Current Status and Future Directions," International Journal of Next-Generation Networks (IJNGN), Vol.3(1), pp. 1 - 9, 2011.

[7] O.A Akinlabi, B.S. Paul, M. Joseph and H.C. Ferreira, "A Review of Femtocell," The International MultiConference of Engineers and Computer Scientists (IMECS), Hong Kong, pp. 1 - 7, 2014.

[8] R. Pabst et al., "Relay-based deployment concepts for wireless and mobile broadband radio," in IEEE Communications Magazine, vol. 42(9), pp. 80-89, 2004.

[9] Technowizz (2010): Femtocells & Relays in Advanced Wireless Networks, Available: https://technowizz.wordpress.com

[10] N. J. Gomes, P. P. Monteiro, and A. Gameiro, Next Generation Wireless Comunications Using Radio over Fiber: John Wiley & Sons, Inc., 2012.

[11] G. S. D. Gordon, M. J. Crisp, R. V. Penty, and I. H. White, "Experimental Evaluation of Layout Designs for 3 x 3 MIMO-Enabled Radio-Over-Fiber Distributed Antenna Systems," IEEE Trans on Veh. Technol., pp. 643 - 653, 2014.

[12] T. Alade, H. Osman, and M. Ndula, "In-Building DAS for High Data Rate Indoor Mobile Communication," presented at the IEEE 75th Veh. Technol. Conf., Yokohama, 2012. pp. 1-5

[13] E.M. Vitucci, L. Tarlazzi, F. Fuschini, P. Faccin, and V. Degli-Esposti, "Interleaved-MIMO DAS for Indoor Radio Coverage: Concept and Performance Assessment," IEEE Trans. on Antennas and Propag., vol. 62, pp. 3299 - 3309, 2014.

[14] A. Chowdhury, H. Chien, S. Fan, J. Yu, and G. Chang, "Multi-Band Transport Technologies for In-Building Host-Neutral Wireless Over Fiber Access Systems," J. Lightwave Technol, vol. 28, pp. 2406 - 2415, 2010.

[15] D. Wake, M. Webster, G. Wimpenny, and K. Beacham, "Radio over fiber for mobile communications," IEEE International Topical Meeting on Microwave Photonics, pp. 157 - 160, 2004.

[16] A. Das, A. Nkansah, N. J. Gomes, I. J. Garcia, J. C. Batchelor, and D. Wake, "Design of Low-Cost Multimode Fiber-Fed Indoor Wireless Networks," IEEE Trans. on Microw. Theory and Techn, vol. 54, pp. 3426 - 3432, 2006.

[17] A. Attar, H. Li, and V. C. M. Leung, "Applications of Fiber-connected Distributed Antenna Systems in Broadband Wireless Access," Proc. Int. Conf. on Computing, Networking and Commun. Maui, HI. pp. 623 - 627, 2012.

CHAPTER 2

BACKGROUND STUDY AND LITERATURE REVIEW

2.1. Introduction

Chapter 1 briefly discussed distributed antenna systems (DASs) and their benefits in providing wireless services to areas of poor coverage, especially in indoor environments. It was also mentioned that even though coaxial cable and other electrical cables can be used to connect the central unit (CU) to the remote antenna units (RAUs), radio-over-fibre (RoF) links are the most preferred in terms of low-loss and high bandwidth.

In this Chapter, a more detail background of in-building DAS is presented, followed by a description of RoF link configurations, modulation types and metrics for evaluating the performance of the link. In addition, the principles of multiple-input, multiple-output (MIMO) technology used by current and emerging wireless systems are presented together with their performance metrics. Finally, the performance of the integration of RoF-DAS and MIMO system reported in previous works is reviewed to determine the improvement in capacity, throughput and coverage it offers over a DAS supporting only a SISO configuration.

2.2. In-building Distributed Antenna System

Improving the wireless coverage inside a building could require multiple access points (APs) deployed around the building, to ensure uninterrupted wireless service as the user moves around. A co-located antenna system (CAS) where the transmitting antennas are co-located inside the AP, and placed on each floor in a multi-storey building to provide wireless services to all users in the coverage area is shown in Fig. 2.1a. CAS cannot guarantee complete coverage throughout the building especially as

the wireless user gradually moves away from the coverage area of the AP; here, the user will experience weak signals since it is far from the reach of the serving AP. In addition, current and emerging wireless networks need a scalable and complete solution for addressing coverage and capacity challenges.

DASs have the ability to provide higher quality coverage, lower interference and higher capacity throughout a building compared to CASs. A typical DAS deployment is shown in Fig. 2.1b, where RAUs are geographically mounted on the celling in every part of the building; it can use RF splitters to split the wireless signal from the CU to the RAUs. Since the RAUs are geographically distributed, the radio transmission distance from the user is reduced, the channel capacity is also increased as a result of higher signal-to-noise ratio (SNR) and the transmission power is reduced since each RAU covers a specific area.
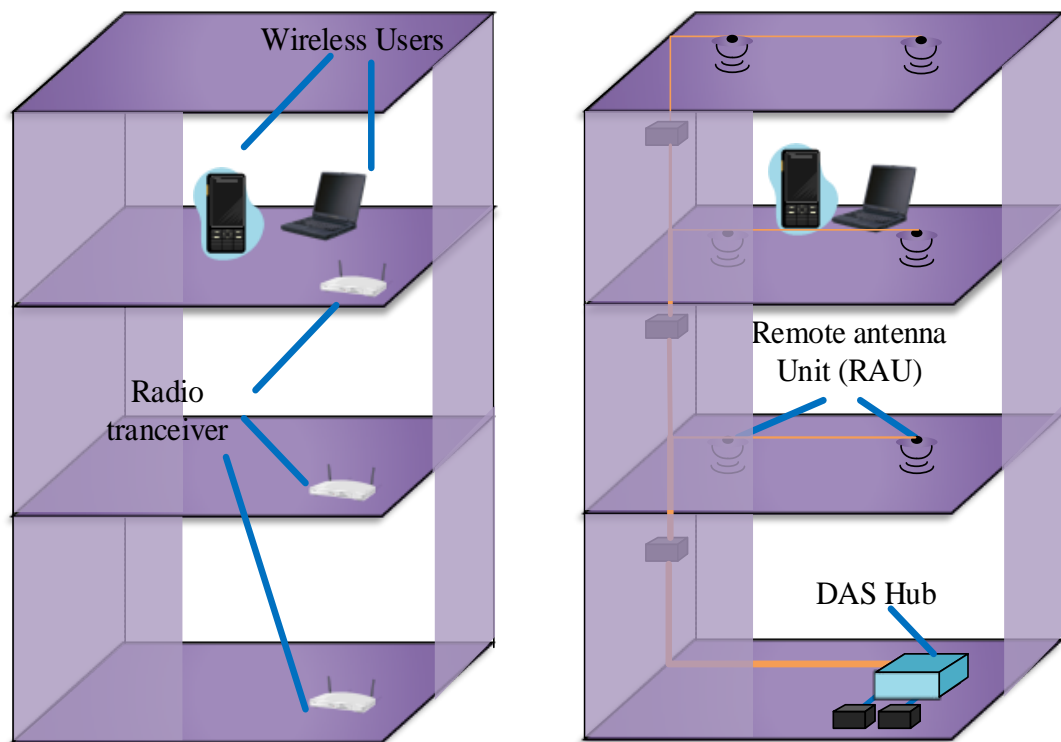
Figure 2.1 (a) Conventional co-located antenna system (CAS) (b) Distributed antenna system (DAS)

Many operators and neutral-host providers have widely deployed in-building DASs, for example, in Bristol Airport, UK, a data centre in Asburn, USA, a convention

centre in Dublin, Ireland, Hotel San Antonio, Texas, USA, football stadium in London, UK, to mention just a few [1]. In many of these applications, the DAS uses RoF links to distribute the wireless signals to the RAUs.

2.2.1. RoF Link configurations

The RoF link may be considered a subsystem in a larger RF system as shown in Fig. 2.2; it is used to transport radio signals over fibre optic cable in order to improve transmission of signals from a base station to remote antennas [2].
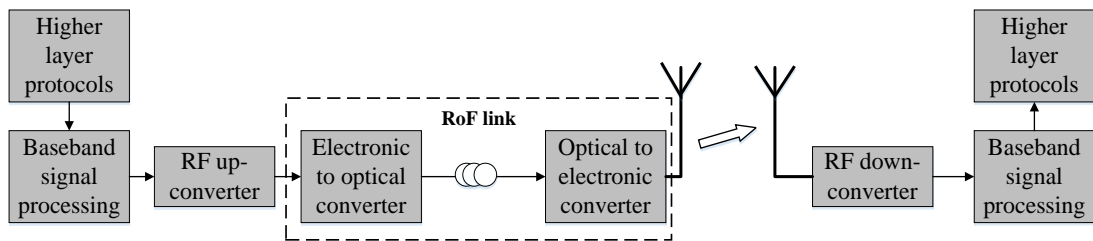
Figure 2.2 Radio-over-fibre link.

The data from the higher-layer protocols is passed down for baseband signal processing where functions such as modulation and coding takes place. The baseband signal is up-converted to produce the RF signal, which is applied to the RoF link using an electronic to optical converter (usually a laser diode) and the resultant optical signal is transmitted over optical fibre cable to an optical to electronic converter (usually a photodiode) at the receiving end to recover the signal before wireless transmission. The receiver unit (a mobile phone, laptop etc.) receives the RF signal and down-converts it to baseband signal for further processing before passing it to higher-level protocols.

There are different RoF link configurations; the simplest among them is the RF-over-fibre link where the RF signal is used to modulate a laser transmitter and the resultant optical signal is transmitted over a fibre optic cable to a PD receiver as shown in Fig. 2.3. The RF signal is recovered by the PD and amplified for wireless transmission.
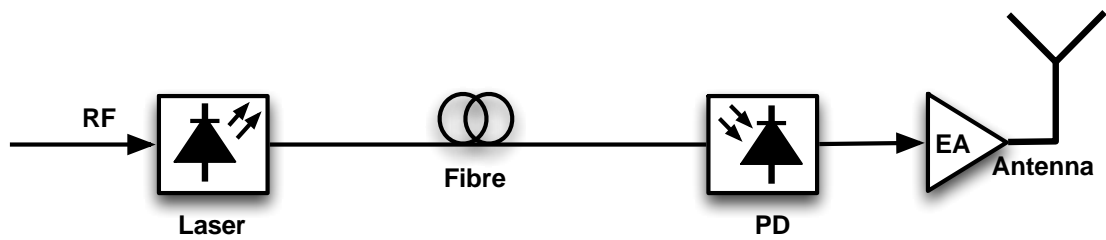
Figure 2.3 RF-over-fibre link.

The advantage of the RF-over-fibre link is that, apart from signal amplification and optoelectronic conversion at the RAU, all other functions are carried out in the CU, which allows easy maintenance and upgrade procedures. The major drawback of RF-over-fibre link is the high noise and distortion of the analogue transmission, especially at high frequencies (beyond 3GHz), as sometimes it is difficult to obtain RF/optical components that have low noise and distortion at these frequencies.

The IF-over-fibre link is an alternative to the RF-over-fibre link; it is mostly considered when operating in a high frequency domain where the RF signal is converted to a lower frequency, or intermediate frequency (IF) and used to modulate a laser transmitter. The optical signal is transported through the optical fibre to the PD receiver where the IF signal is recovered, then it is up-converted back to its RF signal frequency before wireless transmission as shown in Fig. 2.4.
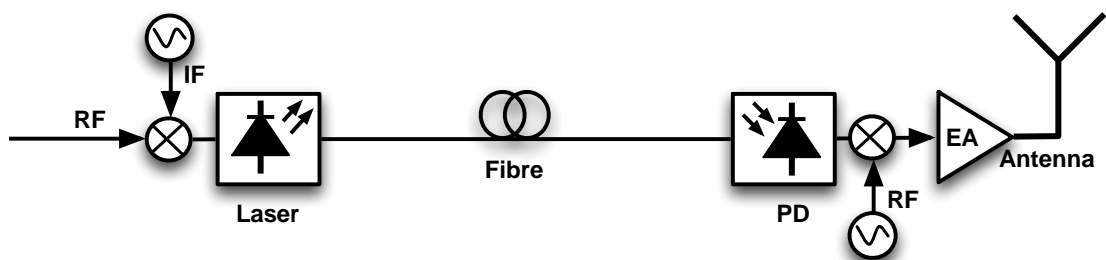
Figure 2.4 IF-over-fibre link.

The advantage of the IF-over-fibre link is that it allows the use of simple intensity modulation direct detection (IM-DD) transmission and a semiconductor laser diode

transmitter at low frequency [3], although at the additional cost of local oscillators and mixers used in the IF/RF conversions.

Fundamentally, in RoF transmission, the RF signal is usually transmitted as an analogue waveform, and used to modulate an optical source to a receiver. However, the RF signal can be digitized before using it to modulate an optical source, and transmitted over an optical fibre. At the receiver, the digital RF signal is recovered by the PD, and converted to an analogue signal before amplifying it for wireless transmission as shown in Fig. 2.5. This RoF link configuration is referred to as a Digitized-RF-over fibre link.
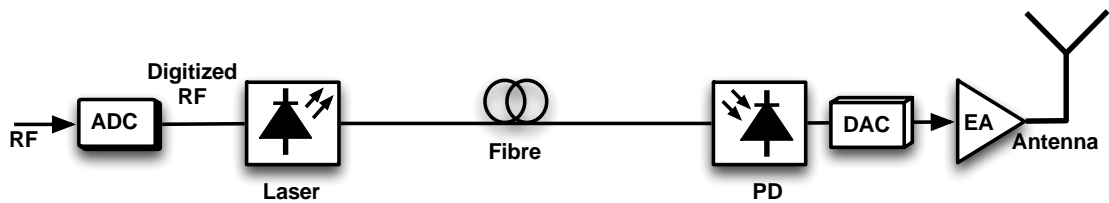
Figure 2.5 Digitized-RF-over-fibre link.

The digitization of the RF signal is performed by an analogue-to-digital converter (ADC) prior to the laser transmitter and a digital-to-analogue converter (DAC) is used after the PD receiver, to convert the digital RF signal back to its analogue form. The advantage of the Digitized-RF-over-fibre link is that the nonlinearity in analogue transmission can be avoided since the digitized signal can maintain its dynamic range independent of the fibre transmission distance until the received signal goes below the link sensitivity [4]. However, the locations of the component are distributed between the CU and RAU, which increases the complexity of the link compared to other configurations.

2.2.2. Types of modulation for RoF links

The simplest and most straightforward modulation for RoF link is "direct modulation", where the RF signal is directly modulated onto the laser light-wave. The modulating device for direct modulation, the semiconductor laser, is commercially available at low-cost for frequencies up to 3GHz but beyond this frequency, lasers become expensive and the modulation response, depending on the laser, could fall-off rapidly anywhere between 2 and 20 GHz. Direct modulation also causes an undesirable wavelength shift in the output of a laser-diode, resulting in excessive chromatic dispersion [5], and this too is more severe for higher frequency modulation. Therefore, the RoF link needs to use "external modulation" where the light-wave generation and RF signal modulation are done separately to reduce the wavelength shift while performing intensity modulation. However, external modulation does not remove dispersion at high frequencies, other techniques such as optical single-sideband or double-sideband-suppressed carrier are employed to reduce the effect of dispersion.
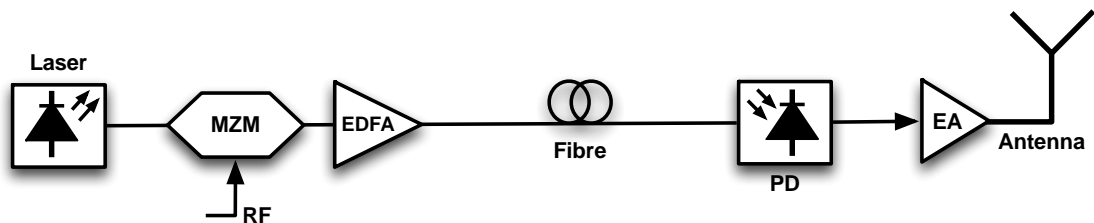
Figure 2.6 Diagram showing RoF link using external Mach Zehnder modulator.

Fig. 2.6 shows the RoF link using an external Mach Zehnder modulator (MZM) to modulate the intensity of the optical carrier using the RF signal. The resultant optical signal power from the MZM can be boosted using an erbium-doped fibre amplifier (EDFA) before entering the fibre optic cable. The optical signal is received by the PD and down-converted to RF signal for amplification before wireless transmission. The advantage of external modulation is that it removes the laser diode related problem such as the wavelength chirp, and the slope efficiency scales with

continuous-wave laser power [6]. However, using external modulators are at the cost of greater complexity for the RoF link.

2.2.3. Performance Metrics for RoF links

There are some specific metrics that can be used to determine the performance of an RoF link. The link gain is one of such performance metric, and when examining the RoF link gain, it is necessary to relate the RF output power from the PD to the RF input power to the laser.

The formula to calculate the gain for a direct modulated RoF link G_d is given by [2]:

$$G_d = \frac{P_o}{P_i} = \frac{\eta^2{}_{LD}\ R^2}{L^2{}_{opt}} \frac{Z_{out}}{Z_{in}} \tag{2.1}$$

where P_o is the output RF power, P_i the input RF Power, η_{LD} is the laser diode slope efficiency (W/A), R is the photodiode responsivity (A/W), L_{opt} is the loss of the optical link, Z_{out} and Z_{in} are the input and output impedance respectively.

The formula to calculate the gain for an MZM external modulated RoF link G_e is [2]:

$$G_e = \left(\frac{P_{opt}\ \eta_M\ R}{L_{opt}\ L_M} \right)^2 \frac{Z_{in}}{Z_{out}} \tag{2.2}$$

where P_{opt} is the input optical power to the modulator, η_M is the slope efficiency of the modulator at the operating point and L_M is the optical insertion loss.

From equations (2.1) and (2.2) it is clear that the RoF link gain is dependent on the slope efficiency of the laser or modulator and photodiode responsivity.

The linear operating region of a laser can be determined by plotting the output power vs. injection current (P-I) curve as shown in Fig. 2.7. This is achieved by increasing the input current to the laser and obtaining the output power, in order to determine

the spontaneous emission, stimulated emission and saturation regions. The current between zero and the threshold is dominated by the spontaneous emission of the laser while there is nonlinearity mainly around the threshold. The linear increase from the threshold is dominated by the stimulated emission, and the laser goes to its saturation when there is a loss of efficiency at high current resulting in nonlinearity.
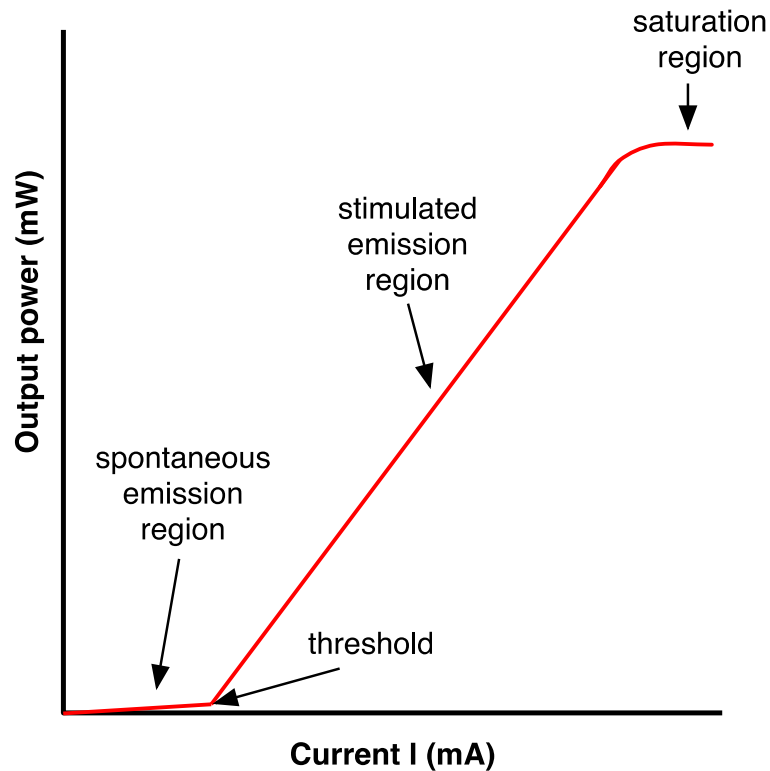
Figure 2.7 Laser P-I curve.

Noise contributes to the performance degradation of a RoF link, and there are three sources of noise in the link, these being: relative intensity noise (RIN), thermal noise and shot noise. RIN and thermal noise quantifies the noise of the optical source (laser) and the receiver (photodiode) respectively, while shot noise is a result of the quantum nature of the light, which varies with detected optical power [7]. It is also important to note that additional amplifiers used in the RoF link also contribute to the noise.

The noise figure (NF) is another metric used to determine the performance of the RoF link, and it can be defined in the user manual as the ratio of the output to input signal-

to-noise ratio, expressed in decibels. The expression of NF for a directly modulated RoF link NF_d is given by [2]:

$$NF_d = 10 \log \frac{N_o}{N_i G_d} \qquad (2.3)$$

where N_o is the total output noise power from the link, i.e. $N_o = \eta_{th} + \eta_{sh} + \eta_{rin}$ where η_{th} is the thermal noise power, η_{sh} is the shot noise power and η_{rin} is the RIN noise power, N_i is the input noise power, $N_i = k\,T\,B$, where k is Boltzmann's constant = 1.379×10^{-23} J/K, T is the temperature (e.g. 290 K), B is the noise bandwidth and G_d is the gain from equation (2.1).

The expression of NF for an external modulated RoF link NF_e is given by [2]:

$$NF_e = 10 \log \frac{N_o}{N_i G_e} \qquad (2.4)$$

where N_o is the total output noise power from the link, $N_o = \eta_{th} + \eta_{sh} + \eta_{rin} + \eta_{EDFA}$ where η_{th} is the thermal noise power, η_{sh} is the shot noise power, η_{rin} is the RIN noise power and η_{EDFA} is the EDFA noise power. N_i is the input noise power and G_e is the gain from equation (2.2).

The distortion is another contributor to the performance degradation of a RoF link, and it occurs as a result of nonlinear performance of the link. For a narrowband system, the third-order intermodulation distortion (IMD3) is the most important form of distortion [8]. Intermodulation distortion occurs when two or more signals at different frequencies are fed into the link resulting into the creation of new frequencies. For example, using f_1 and f_2 as the input fundamental tones, the IMD3 products generated are at $2f_1 - f_2$ or $2f_2 - f_1$ and will thus likely lie within the usable bandwidth, causing interference with other RF signals at different frequencies. The level of distortion can be represented by plotting the RF output power against the RF input power for one of the fundamental tones and one of the IMD3 products, as shown in Fig. 2.8.
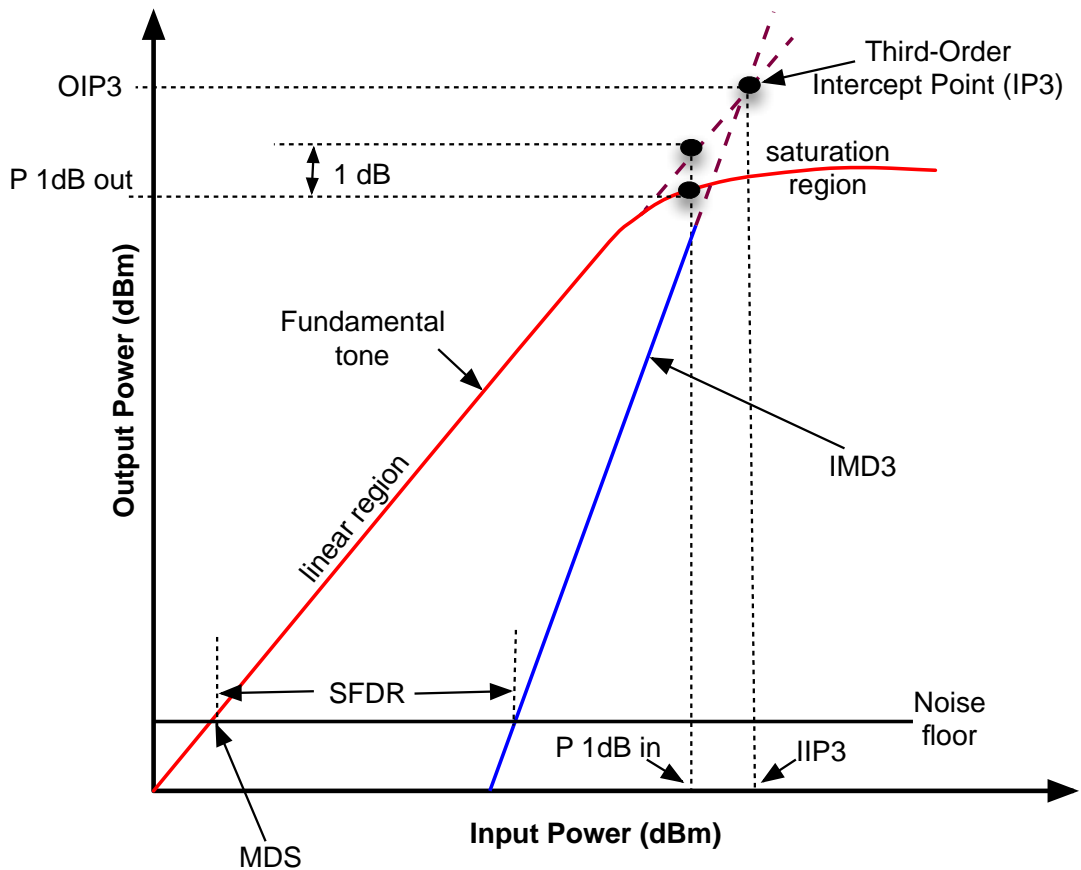
Figure 2.8 Typical plot of output power against input power for an analogue RF system, showing third-order intercept point, spurious-free dynamic range and 1-dB compression point.

Three important performance metrics can be obtained from Fig. 2.8, the first one is the third-order intercept point (IP3), where the linear extrapolations of the fundamental tone and IMD3 intercepts, which can be measured either at the input power (IIP3) or output power (OIP3). The second performance metric is the spurious-free dynamic range (SFDR), which defines the difference between minimum detectable signal (MDS) and the point at which IMD3 crosses the noise floor. Finally, the third performance metric is the 1-dB compression (P1dB) point, which determines the power that causes the gain of the fundamental tone to decrease by 1 dB from the linear extrapolation, and it can be measured either at the input power (P 1dB in) or output power (P 1dB out). The P1dB is often specified in the data sheet of the device and a further backoff of 8-10dB for the OFDM case, and 6-8 dB for the QAM16 single-carrier case is required [9].

2.3. Multiple-Input Multiple-Output (MIMO) systems

Since the IEEE 802.11a/b amendment was ratified, the wireless industry has released successive amendments for increasing WLAN access points (APs) capability to improve signal quality and data rates. Multi-carrier transmission with orthogonal frequency division multiplexing (OFDM) was introduced in the transition from IEEE 802.11b to 802.11g mainly to improve signal resistance to frequency selective fading compared to single carrier systems [10]. The IEEE 802.11a/b/g compliant APs were transmitting and receiving RF signal using single-input single-output (SISO) system, but in the IEEE 802.11n standard, the multiple-input multiple-output (MIMO) system was introduced to provide improvement in signal quality and data rates to keep pace with the rapidly growing desire for higher-speed networks.
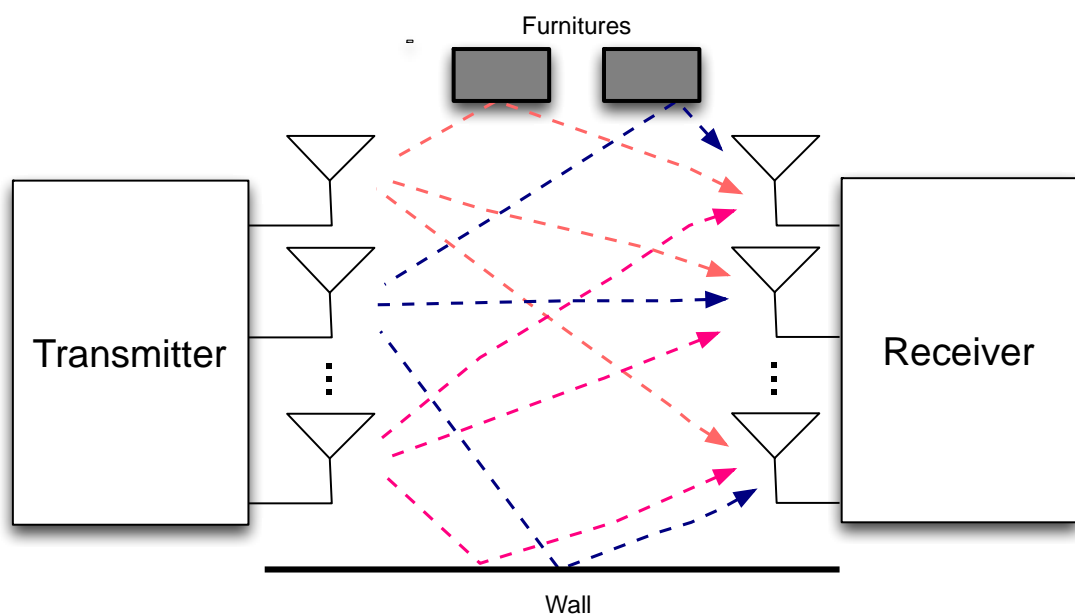
Figure 2.9 MIMO with multipath fading.

MIMO uses multiple antennas to transmit radio signals through a multipath wireless propagation channel as shown in Fig. 2.9, and the signals are received with multiple antennas before using advanced digital signal processing (DSP) techniques to retrieve the original transmitted signals. Almost every newly shipped WLAN product in the last eight years supports the IEEE 802.11n standard specification, with up to3 spatial streams (3×3 MIMO), a channel bandwidth of 40MHz and 64-QAM

modulation, to deliver a maximum theoretical data rate of 450Mbps [11]. Although IEEE 802.11n defines up to four spatial streams, there are few chips and APs using more than three streams [11]. Recently, there has been a dramatic increase in the shipment of WLAN products supporting IEEE 802.11ac specification which builds upon the previous 802.11n standard, and retaining support of three spatial streams, but with a leap from 40MHz channel bandwidth to 80MHz and 64-QAM modulation to 256-QAM, to deliver higher data rates of up to 1.3Gbps [11]. Other wireless communication standards like 4G/Long Term Evolution (LTE) also use MIMO, supporting up to 4 spatial streams (4x4 MIMO) [12].

MIMO systems can be broadly classified into spatial diversity (used to improve radio link reliability), spatial multiplexing (used to increase data rates) and beamforming (used to improve SNR) [13]. IEEE 802.11n APs operate in two MIMO modes, spatial diversity mode and spatial multiplexing mode. These modes are adaptive: depending on the signal-to-noise ratio (SNR), an AP switches dynamically between spatial diversity and spatial multiplexing modes [14]. For example, if the signal quality is very high the system uses spatial multiplexing, and if not, it automatically switches to spatial diversity mode or even to SISO mode. Transmit beamforming (TxBF) mode was introduced in IEEE 802.11ac as an optional feature [15].

2.3.1. Techniques used in MIMO systems

Spatial diversity is a technique used in MIMO systems to improve the radio link reliability, it does not increase the capacity of the system because the same data s_1 is sent from all antennas, but it can take advantage of the multipath phenomenon to improve the signal quality. The multipath phenomenon that was a problem with SISO systems helps the MIMO receiver see several versions of the transmitted signal and these signals can be combined in a gainful manner. Also, the transmitting antennas can be spatially separated to ensure that the independent signals are not faded simultaneously [16], and the odds of receiving the data is massively increased i.e., if any one path suffers fading, there is a high probability that the other paths do not, so the signal can still be received.

There are several spatial diversity techniques that can be used to transmit or receive data signals. These techniques can be grouped into three as shown in Fig. 2.10; receive diversity, transmit diversity and transmit/receive diversity techniques [13].
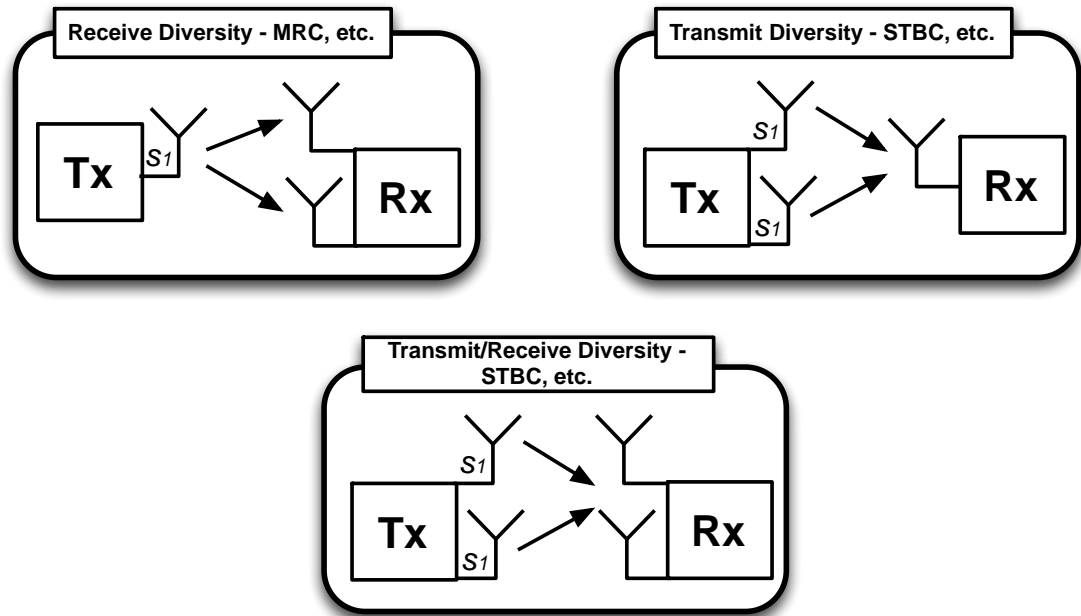
Figure 2.10 Techniques used in spatial diversity.

The receive diversity technique is used when there is one transmitting antenna and multiple receiving antennas. It is often referred to as a single-input, multiple-output (SIMO) scheme. The receiving antennas receives several versions of the transmitted signal, each experiencing a different multipath fading and these signals have to be combined efficiently. There are different combining algorithms that can be used in receive diversity: they include equal gain combining (EGC), selection combining (SC) and maximal ratio combing (MRC). These algorithms are discussed in detail in Chapter 4.

A drawback of the receive diversity technique is that most of the computation burden is on the receiver side and it incurs high power consumption for the receiver unit [17]. The transmit diversity technique can be employed to achieve diversity at the transmitter side. It uses multiple transmitting antennas and one receiving antenna, and it is often referred to as a multiple-input, single-output (MISO) scheme. There

are different algorithms that can be used in transmit diversity: these include Alamouti space-time block coding (STBC), transmit antenna selection (TAS) and delay diversity (DD) algorithms [18]. Receive diversity and transmit diversity techniques are SIMO and MISO schemes, respectively; MIMO scheme can also be used in spatial diversity with multiple transmitting antennas and multiple receiving antennas and using the Alamouti STBC algorithm [19]. This technique is referred to as transmit/receive diversity. Again, details of these algorithms are discussed in detail in Chapter 4.
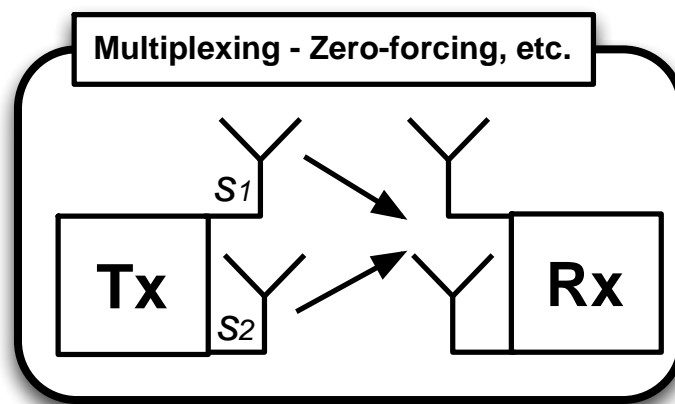
Figure 2.11 Spatial multiplexing technique.

Spatial multiplexing can be used in MIMO systems to achieve higher data rates by transmitting separate data s_1 and s_2, via multiple antennas at the same time to multiple receiving antennas, as shown in Fig. 2.11, and an algorithm/equalizer is used at the receiver to detect the independent data streams. The detection algorithms for spatial multiplexing-MIMO can be broadly classified into linear and non-linear algorithms. Some examples of linear algorithms are Zero-forcing, minimum mean square error (MMSE), etc. while some examples of nonlinear algorithms are maximum likelihood (ML), sphere detection algorithm, etc. Zero-forcing linear detection algorithm is the simplest algorithm to implement since it only removes the effect of inter-symbol interference (ISI), treating all transmitted signals as interference except for the desired signals from the target transmit antennas [20]; details of this algorithm is discussed in Chapter 4.

The spatial diversity and spatial multiplexing MIMO techniques requires the transmitting or receiving antennas to be physically separated to provide sufficient de-correlation for the channels, but in cases where this physical antenna separation is not possible, the beamforming technique can be used. Beamforming (BF) as shown in Fig. 2.12 works by concentrating the signals from multiple antenna elements toward a desired user instead of radiating out into the atmosphere in all directions [21]. BF is achieved by adaptively phasing the antenna elements to form a concentrated and directed beam pattern to the desired user, and it can be used at both the transmitter-side and receiver-side to provide significant antenna gains, thereby providing increased signal-to-noise ratio (SNR).
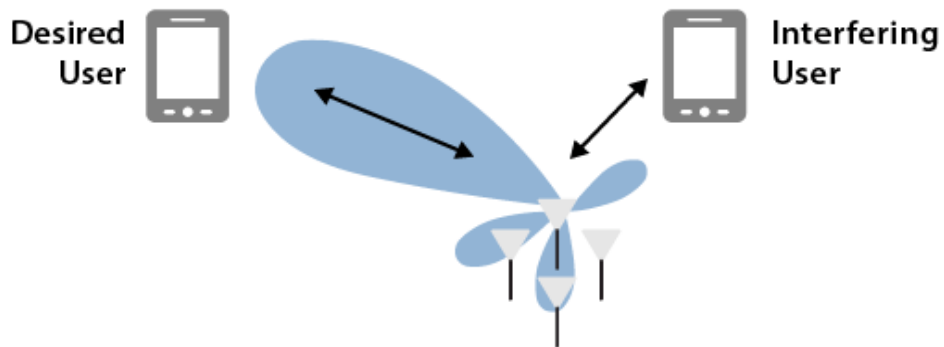
Figure 2.12 Smart antenna system - beamforming [22].

There are several BF techniques that have been reported in the literature, and they are implemented either in the analogue or digital domain [22]. Analogue BF is achieved by transmitting the same signal to the antenna array elements and then, by using analogue phase shifters (one per antenna element), the signal is focused in the direction of the user. The processing for digital BF on the other hand is done in baseband using the feedback of current channel state information from the receiver to adjust the signals to each transmit antenna, thereby focusing the signal in the direction of the user. When the correct amplitude and phase information is fed back to the transmitter and applied to the signal, the signal strength at the receive antenna is increased and SNR is improved such that higher modulation and coding scheme (MCS) can be used. In addition, the digital BF requires multiple RF chains to the antenna array (one per antenna element) for gain and phase control.

2.3.2. Performance metrics for MIMO system

The performance of a communication system can be measured by the amount of error in the received data, and in terms of the channel capacity that determines the rate at which data can be transmitted through the channel.

Error probability is a measure of the errors introduced into the communication system by the RoF link or wireless channel due to noise, interference, distortion, bit/symbol synchronization problems, attenuation, wireless multipath fading etc., that can alter the data as it is transmitted across the channel. These errors can be evaluated in terms of bit error rate (BER) or symbol error rate (SER); these metrics are estimated when the received errored bits/symbols are compared with the total number of bits/symbols, and provide accurate measures over a long time interval. BER/SER are unitless performance metrics and are measured after the QAM demodulation.
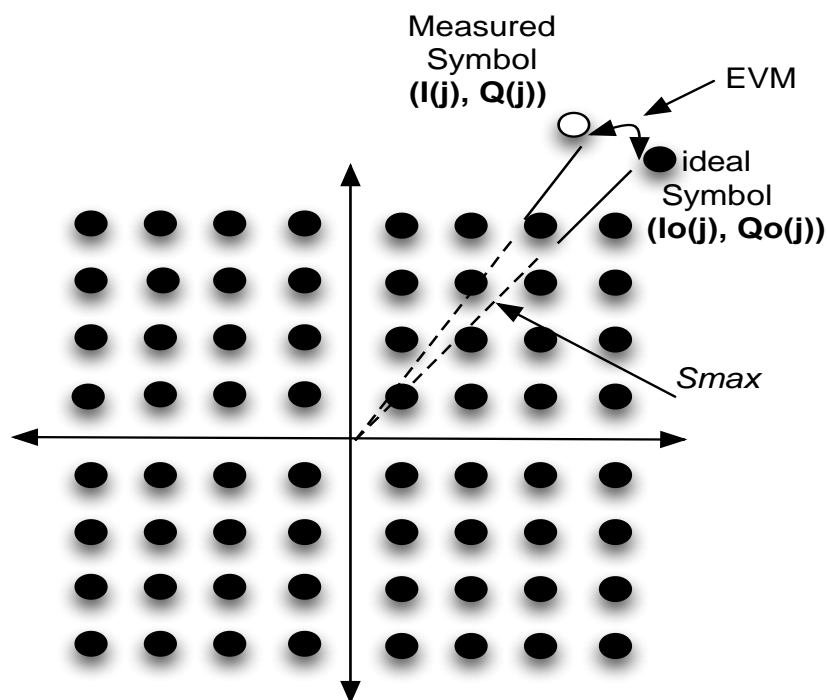
Figure 2.13 Constellation diagram of 64-QAM.

Error vector magnitude (EVM) is another performance metric used to quantify the performance of a communication channel; an ideal channel would have all the constellation vectors precisely at the ideal locations as shown in Fig. 2.13. However,

imperfections such as noise, interference, and distortion will cause the actual constellation vectors to deviate from the ideal, and EVM measures how far the vectors are from those ideal locations [23]. Fig. 2.13 shows the ideal vectors ($I_o(j)$, $Q_o(j)$) and measured vectors ($I(j)$, $Q(j)$); thus, the distance between the ideal constellation vector symbol and measured constellation vector symbol is the error vector.

EVM and carrier-to-noise ratio (CNR) are related, CNR represents a measurement parameter in the RF domain while EVM is a measurement in the baseband domain [24], and the relationship between them can be seen in the following equation [25]:

$$CNR = -(r + 20\log[EVM/(100\%)]) \qquad (2.5)$$

where r is the peak-to-average energy ratio of the QAM constellation, and is 3.7 dB for 64-QAM and 4.2 dB for 256-QAM [25]. The CNR requirement for a Ricean fading channel and a coding rate of 5/6 are 24 dB for 64-QAM and 30 dB for 256-QAM [26]. Using the equation (2.5), the EVM requirements become 6.5% for 64-QAM and 3.1% for 256-QAM.

Modulation error rate (MER) can also be used to measure the error in the received vector [25]; it is calculated as the ratio of average signal constellation power to average constellation error power, and it is often used to quantify the error performance of a communications system that uses digital modulation (such as QAM). MER and SNR can be used interchangeably, since MER is a measure of the SNR in a digital modulated signal [27]. The value of MER in dB is always lower (worse) than the SNR value, as the MER takes into account noise, interference, and distortion [28].

The capacity of a wireless system determines the maximum data rate at which reliable communication is possible in a wireless channel [29]. The channel capacity can be calculated from the complex channel matrix H obtained from channel state information (CSI) estimated at the receiver, using preamble symbols known to both transmitter and receiver. The complex channel matrix H for a 2x2 MIMO is represented as:

$$H \quad = \quad \begin{bmatrix} h_{11} & h_{12} \\ h_{21} & h_{22} \end{bmatrix} \tag{2.6}$$

and after H is estimated at the receiver, its singular values (σ_i) can be obtained from the singular value decomposition (SVD), which decomposes the channel matrix into two independent channels (in the case of a 2x2 MIMO). These values are used to calculate the channel capacity (C_{MIMO}) of the spatial multiplexing-MIMO scheme. This is given by an extended Shannon capacity equation as [29]:

$$C_{MIMO} = \log_2 (I_{NR} + \frac{\rho}{NT} \sigma_i^2) \qquad \text{bps/Hz} \tag{2.7}$$

where N_T and N_R are the number of transmit and receive antennas respectively, and ρ is the SNR. In this chapter, we use the measured modulated error rate (MER) as SNR because MER measures the noise in a communication system as well as interferecne and distortion effects, and in [30] MER/SNR has also been used interchangeably.

The MIMO capacity in equation (2.7) reduces to the following expression for SIMO capacity (C_{SIMO}) [31]:

$$C_{SIMO} = \log_2 (1 + N_R \rho) \qquad \text{bps/Hz} \tag{2.8}$$

Here, the MER ρ is multiplied by a factor of N_R representing the total received power accumulated in the single degree of freedom of the channel. The capacity of a MISO channel (C_{MISO}), is [30]:

$$C_{MISO} = \log_2 (1 + \rho) \qquad \text{bps/Hz} \tag{2.9}$$

The capacity equation for MISO in (2.9) is the same as SISO, but, the MER ρ for MISO is expected to be higher than that of SISO, due to the diversity gain.

The channel capacity calculation only gives the maximum theoretical data rate that can be transmitted with small probability of error; however, the practical maximum data rate is determined by a throughput measurement using a testing tool. For example, in Chapter 3, the throughput measurements were carried out using the commercial software Networx, and achieved by transferring large files between the Host PC and mobile laptops.

2.4. Performance of MIMO in RoF-DAS

Distributed antenna systems (DASs) were originally introduced to simply increase coverage and signal-to-noise ratio (SNR) in wireless communications [32], but due to its centralized architecture, it can enable joint processing functions such as co-channel interference cancellation, optimal resource allocation and signal delay management to improve the system performance [33-36]. DAS can also facilitate easy upgrade of existing services to emerging wireless services making it easier to adopt different techniques such as higher order modulation, orthogonal frequency-division multiplexing (OFDM), advanced coding schemes and, more recently, multiple-input multiple-output (MIMO) schemes to widely improve wireless access rates.

The integration of RoF-DAS and MIMO can bring about further improvements in performance of the wireless system, due to the increased channel decorrelation. MIMO requires high signal-to-noise ratio for the high orders of modulation schemes, such as 16-QAM and 64-QAM, also the wireless user needs to separate the multiple signals that overlap one another in frequency and time. RoF-DAS readily enables a wide MIMO antenna spacing that enables greater spatial decorrelation and SNR can be increased due to reduced distances. A MIMO-supported WLAN AP such as one based on IEEE 802.11n/ac standards, is readily accommodated in the RoF-DAS architecture as shown in Fig 2.14.
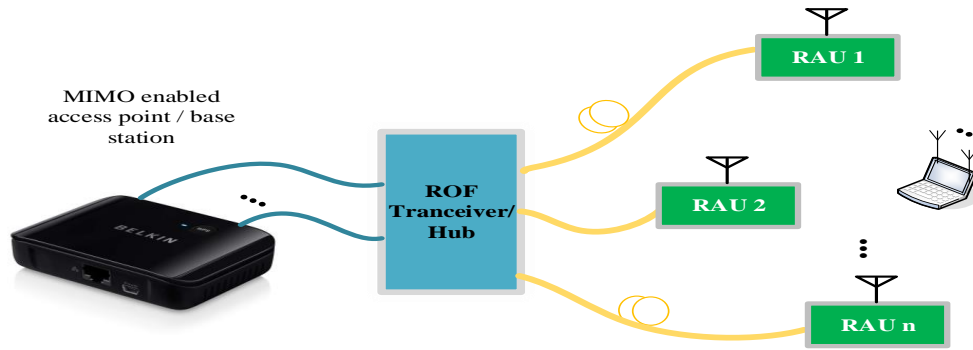
Figure 2.14 Diagram showing 2x2 MIMO over RoF DAS.

Several research works have examined the performance of MIMO systems in RoF-DAS architecture; most of them considered how capacity, throughput and coverage of a MIMO wireless system is improved.

2.4.1 Capacity performance of MIMO in RoF-DAS

The capacity of a 3×3 RoF-enabled MIMO system in an indoor line-of-sight (LOS) scenario was demonstrated in [37] for both conventional and distributed antenna arrangements. The experiment was carried out using a vector network analyser and a Zinwave 2700 DAS to provide RoF links over 30-m of OM1 multi-mode fibre (MMF). Measurements of the wireless channel were carried out over a 22MHz bandwidth and based on the measured values the MIMO system capacity was calculated using the expanded Shannon capacity expression in [29]. The results taken at 15 receiving locations revealed that there was improvement of 7.4% in average capacity with 2m antenna separation over the conventional MIMO antenna arrangement with approx. 0.06m antenna separation, and for a distributed transmitting antenna arrangement with 4m separation, the increase was 11.3% more than the conventional MIMO antenna arrangement.

A similar measurement to [37] was carried out in [38] for 3×3 RoF-enabled MIMO system but in a non-line-of-sight environment. The transmitting antennas were placed inside a laboratory while the receiving antennas were placed outside, along the corridor. Measurements were carried out when the transmitting antennas were

separated at 0.06m, 2m and 4m respectively and compared with the SISO system. For each transmitting arrangement and receiving location, the channel matrix *H* was measured with 1600 frequency bin samples in a 22MHz bandwidth, and was averaged over 16 sweeps in the time domain. The result of the calculated capacity from 12 receiving positions revealed that the conventional MIMO arrangement with closely spaced antennas had a mean capacity of 133 Mbps, i.e. 1.86 times that of SISO system (71.3 Mbps), while with MIMO DAS with 4-m antenna separation, the capacity increased to 192 Mbps.

The capacity performance of a 2x2 MIMO RoF system was demonstrated in [39], where a pair of Agilent vector signal generators (VSG) was used to generate two 16-QAM MIMO-OFDM streams occupying 16.6 MHz bandwidth at 2.4 GHz. The signal streams were injected into two separate RoF links and two vector signal analysers (VSAs) were used at the receiver side to decouple the two streams. The separation distance between the two transmitting antennas was varied from 0.1 to 4 meters while the receiving antennas were placed close to each other (~0.1 m separation). Also, a variable optical loss was introduced in one of the RoF links to study the system tolerance to optical power imbalance. The EVM and condition number (CN) values were measured to evaluate the system's capacity for each time instant. The results revealed that the optimum separation distance between the two transmit antennas was about one meter and the maximum tolerable optical power imbalance of the two RoF links was about 6dB.

2.4.2. Throughput and coverage analysis for MIMO in RoF-DAS

The throughput performance of a MIMO system in a RoF distributed antenna system was investigated in [40]. The host PC and access point (AP) were connected by a 100Mbps Ethernet cable, and the AP ports were connected to the RAUs using RoF links. The receiver unit consists of a PC connected with Draft[1] IEEE802.11n certified WLAN adaptor. The throughput measurements were taken when the two transmit

---

[1] The final IEEE 802.11n standard had not been finalised at the time this equipment was made

antennas were placed close to each other at a distance of 0.1m and when they are far apart at a distance of 4m, and the receiver unit was moved around other locations in the room. In the experiments 1 and 2, the Modulation and Coding Scheme (MCS) was set to level 12 with 16QAM, Coding Ratio 3/4, 2 spatial streams Data Rate: 86.7Mbps while for experiments 3 and 4 the MCS was set to level 4 with 16QAM, Coding Ratio 3/4, 1 spatial streams, Data Rate: 43.3Mbps.

The results of experiment 1 (when the antenna distance was 0.1m) and experiment 2 (when the antenna distance was 4m), using MCS level 12 where 2 spatial streams were transmitted at spatial multiplexing mode revealed that the throughput performance improved at 4m antenna distance since each spatial stream is propagated through increasingly different paths and the spatial correlation is reduced. Also, the results from experiment 3 (when the antenna distance was 0.1m) and experiment 4 (when the antenna distance was 4m), using MCS level 4 where 1 spatial stream is transmitted at spatial diversity mode reveals that the throughput performance also improved for 4m antenna separation since the spatial correlation is reduced which improves the diversity effect.

The throughput and coverage area performance of a 2x3 MIMO system was investigated in [41] for different transmit antenna separation distance in a RoF-DAS. The theoretical model and measurement data in [42], [43] were used to calculate the coverage area for a 30 x 30 m cell at different transmit antenna separations varying it from 0.1 m to 7 m. The results show a clear trend as the distance between the transmit antennas is increased, the coverage improves. Also, a MIMO WLAN AP with IEEE 802.11n (Draft 2)[1] standard was used as a signal source for the data throughput measurements in RoF-DAS. The result shows that the total throughput of the system increases with larger antenna spacing up to 5m.

In [44], an indoor deployment solution based on MIMO RoF-DAS was investigated to distribute the MIMO signals over a service area in order to improve the coverage and channel capacity. This was achieved using a 2x2 MIMO test bench for measuring the indoor propagation channel. The MIMO waveforms were generated by LTE signal

---

[1] The final IEEE 802.11n standard had not been finalised at the time this equipment was made

generation software and downloaded to the two Agilent MXG signal generators and an LTE signal analysis software running on the Master Agilent MXA signal analyser was used to perform the MIMO signal demodulation. The result of this experiment showed that the performance of MIMO-DAS in terms of path gain (which is related to the SNR at the receiver), CN, and capacity can be improved over the traditional co-located MIMO arrangement.

2.4.3. Performance of MIMO in millimetre-wave systems

The feasibility of MIMO in millimetre-wave systems was studied in [45] using an IEEE 802.11ad compliant wide-beam commercial off-the-shelf (COTS) wireless device, in a typical academic office building. The COTS Dell wireless device has an IEEE 802.11ad Wireless network interface card (WNIC), configured to use the unlicensed 57-64 GHz spectrum with three 2.16 GHz channels and it offers data rates between 385Mbps and 6.76Gbps. The wireless device is also equipped with 2x8 phased array antennas with relatively wide main beams (30°−40°).

The measurement setup consists of a laptop, connected to the IEEE 802.11ad COTS Dell wireless device through a Gigabit Ethernet interface to generate/receive TCP/UDP traffic, and a Dell laptop (Latitude E420) complaint with IEEE 802.11ad standard. The throughput measurement was carried out in two locations inside an academic building, to capture different scenarios that are likely to occur in an office environment. The first location was an open hall thinly populated by some desks and chairs and a staircase from the floor above, and the second location was a narrow Corridor (5ft wide) offering opportunities for reflection/multipath from the walls on the side. The result confirms that wide-beam antennas can provide high throughput for MIMO in mm-wave communication systems at various locations typical of an indoor environment and in addition, the signal strength does not drop consistently with distance.

In [46] the feasibility of a beamforming MIMO system in a LOS channel was investigated both numerically and experimentally. The numerical investigation was carried out by modelling a 2D geometrical beamforming MIMO channel derived under a pure LOS environment, and the behaviour was examined as the parameters

used for the array antennas were varied. The experimental investigation was carried out using a 28GHz MIMO beamforming prototype with two transmitting and receiving array antennas (2×2 beamforming MIMO transmission). The transmitting array antenna comprises 8 horizontal elements in the form of a uniform linear array (ULA), while the receiving array antenna comprises 4 horizontal elements in the form of a ULA. The experimental measurements were carried out in an outdoor LOS environment. The result of the numerical and experimental investigation shows that the condition number (used to characterize the LOS MIMO channel) is highly dependent on the number of arrays as well as the array spacing.

2.4.4. Performance of millimetre-wave-over-fibre systems

Optical generation and transmission techniques for mm-wave signal has been a topic of interest for many researchers. In [47], the nonlinearity and noise effects of a 25GHz millimetre-wave-over-fibre system was experimentally examined with multilevel quadrature amplitude modulation (QAM) data — IEEE 802.16 schemes — at 20MSps and an orthogonal frequency-division multiplexing (OFDM) 802.11g signal (54Mbps). The optical millimetre-wave signal was generated using an optical phase modulator (PM) along with a DWDM de-multiplexing filter, and the PM was driven by a 23.152GHz RF signal. A Vector Signal Generator (VSG) was used to generate the IEEE 802.16 modulation schemes and 54 Mbps WLAN 802.11g at an IF of 1.848 GHz. The IF data modulation was applied either to one (single) or to both (dual) wavelengths. For the single wavelength modulation, the optical carrier was data modulated using an MZM and coupled together with the unmodulated upper first order sideband were coupled together using a 3dB optical coupler. The resultant optical signal was fed into an EDFA and filtered by an optical DWDM filter of 50GHz channel spacing to reduce the Amplified Spontaneous Emission (ASE) noise before transporting it over 20km single mode fibre (SMF) to the RAU. For dual wavelength modulation, both the carrier and the upper first order sideband were data modulated using two MZMs biased at its quadrature point, and they were coupled together using a 3dB optical coupler. The resultant optical signal was fed into an EDFA and filtered by an optical DWDM filter of 50GHz channel spacing to reduce the ASE noise before transporting it over 20km SMF to the RAU.

The RAU had a PD, bandpass filter (BPF), low-noise amplifiers, and a directional horn antenna of 20dBi gain, which transmits the millimetre-wave signal wirelessly to the mobile unit. At the mobile unit a directional horn antenna of gain 20dBi was connected to a low-noise amplifier and to an Agilent Vector Signal Analyser (VSA). The VSA was connected to a laptop with Agilent VSA software for EVM measurements. The measured EVM result of both dual and single wavelength modulation techniques matches the wireless standards' requirements, and in the lower input RF power region, noise was the limiting factor, with the EDFA ASE noise being the dominant noise in the system. Also, in the higher input RF power region, either amplifier or MZM nonlinearity may dominate the system.

A 125GHz mm-wave signal was generated using a sideband generator comprising of an intensity modulator and a phase modulator, and its feasibility for 10Gbps wireless links was presented in [48]. The experimental setup comprises of a DFB laser, a sideband generator, and a 12.5GHz arrayed-waveguide grating (AWG). The sideband generator was used to achieve a number of continuous power-flattened sidebands with a frequency spacing of 12.5 GHz, and two sidebands with frequency spacing of 125 GHz were selected and coupled together. The generated 125GHz optical mm-wave signal was modulated using a 10Gbps non-return-to-zero (NRZ) format in a LiNbO3 intensity modulator and the signal was amplified by an optical amplifier before removing the ASE using an optical bandpass filter (OBPF). A uni-travelling carrier photodiode (UTC-PD) module with waveguide output was used for downconverting the optical signal to electrical signal, and the signal was demodulated by an envelope detection method. The result of the 10Gbps wireless link shows that a clear eye opening was observed and BERs under 10^{-10} were obtained.

In [49], a simple and cost effective approach for the optical generation and transmission of a data modulated 60GHz signal was presented using a direct modulated gain switched laser (GSL). The experiment was carried out using a commercial DFB laser biased at 43 mA and the gain was switched by an RF signal composed of a 15 GHz sinusoidal signal, coupled with 1.25Gbps data generated by using a pulse pattern generator synchronized with the 10MHz reference from the signal generator (SG). The generated gain switched spectrum is filtered by an optical

band stop filter (OBSF) in the form of a fibre Bragg grating with 0.28 nm to suppress three optical tones in the middle, and an optical band pass filter (OBPF) with bandwidth 0.485 nm was used to reject the outer sidebands. After filtering, the optical signal was amplified by using an EDFA and then transmitted over SMF to the RAU, and a PD was used to detect the optical signal and generate a data modulated 60 GHz mm-wave signal.

The mm-wave signal from the PD was boosted by an amplifier before transmitting the it wirelessly to the mobile unit via a 20dBi horn antenna. At the mobile unit, the mm-wave signal was received by an identical horn antenna, amplified, and mixed with a 60GHz LO to downconvert to a baseband signal. The signal was then filtered by using a low pass filter (LPF) and amplified again. The demodulated 1.25Gbps signal was detected by a bit error rate tester (BERT) and the eye diagrams were monitored by using a high digital speed sampling oscilloscope. The result shows that as the optical suppression for the sidebands increases, the system performance was improved and the lowest BER curve was obtained.

2.4.5. Performance of MIMO in millimetre-wave-over-fibre systems

The performance of a 2×2 OFDM-MIMO system employing a 60GHz RoF system was demonstrated in [50]. The in-phase and quadrature-phase (I/Q) components of the OFDM signal was generated using an arbitrary waveform generator with a sampling rate of 12 GS/s. The I/Q signal was mixed with a 25GHz carrier signal using an electrical I/Q mixer and the output 25GHz signal was combined with another 35.5 GHz carrier signal to produce a 60.5GHz OFDM signal. The optical source to the MZM was a DFB laser at 1550nm carrier, and it was modulated by the 60GHz signal. The optical signal at the output of the MZM was amplified using an EDFA and the resultant signal was split equally, one of the signals was transported to a 60GHz PD after 1km optical fibre to create a signal delay and the other signal was transported to the other 60GHz PD to imitate a 2x2 MIMO.

The measurement was performed in a typical laboratory and the transmitters were placed on two tripods. The receiver side had two antennas and they were separated

by a fixed distance of ~5 cm which was the minimum separation distance allowed by the horn antennas, while the transmitting antennas were separated by a fixed distance of 17 cm which was found after geometrical calculations to be the optimum transmit antenna separation. The result of the experiment shows that transmitting a wireless 2x2 MIMO signal at 60GHz, a data rate of 51Gbps can be achieved over 4m wireless distance using an optimal antenna separation of 17cm at the transmitter. Also, data rates higher than 51Gps were tested, but their performance was found to be above the forward error correction (FEC) coding threshold (1×10^{-3}).

A 60GHz OFDM-RoF system employing wireless 2×2 MIMO was also demonstrated in [51] using least mean squares (LMS) algorithm to estimate the MIMO channel coefficients that were used to compensate for the I/Q imbalance. In addition, a bit-loading algorithm was used to improve the spectral efficiency by optimizing the power weightings and modulation format allocations of the OFDM subcarriers. The 60GHz 2×2 MIMO RoF system experiment was carried out by generating OFDM I/Q signals with an arbitrary waveform generator (AWG), and mixed with a 25GHz carrier signal using an electrical I/Q mixer, then the output signal was combined with a 35.5GHz carrier signal to produce 60.5GHz OFDM signal.

The optical source to the MZM was a DFB laser, and it was modulated by the 60GHz signal. The optical signal at the output of the MZM was amplified using a 42dB gain EDFA and the resultant signal was filtered by a tunable optical band-pass filter to remove ASE noise. After 25km fibre transmission, the optical signal was split equally, one of the signals was transported to a 60GHz PD and the other signal was delayed by a 2km single-mode fibre before transporting it to the other 60GHz PD. The two 60GHz OFDM signals were then fed into two horn antennas with 24dBi gain. At the receiver side, the two OFDM signals were down-converted to two separate IF frequencies at 5GHz using an LO of 55.5GHz and captured by a real-time scope before an offline MATLAB program was employed to demodulate the MIMO signals for BER calculations. The result of the experiment shows that the performance of 16QAM and 32QAM OFDM signal transmissions were under the FEC threshold and a data rate of 76.3Gbps can be achieved using a bit-loading algorithm over 25km fibre transmission and 3.5m wireless transmission.

In [52] the performance of a wireless 2x1 60GHz RoF system was experimentally demonstrated using space-frequency block coding (SFBC) algorithm. The experiment used a software defined radio (SDR) platform to generate the 1.52GHz IF signals, and the signals were intensity-modulated onto a 58.48GHz optical carrier using a MZM on each link before transporting the signals over 100m fibre links to the 60GHz PD. The two transmitting antennas were separated at approx. 2.5m with each one having a 24° half-power beam width for coverage. After 5m wireless transmission, the signals were down-converted to IF using an envelope detector and another SDR platform was used to perform real-time baseband processing. The result of the experiment shows that using a wireless 2x1 60GHz RoF system the channel capacity can be increased due an increase in SNR compared to single antenna transmission.

2.5. Summary

A detailed background study on in-building DAS has been presented in this Chapter, comparing it with the CAS method of deployment. It was discussed that DAS provides better quality coverage and can deliver higher data rate than CAS. Also, RoF-based DAS was discussed with a particular focus on RoF link configurations, direct and external intensity modulation alternatives and the metrics for evaluating the performance of RoF links. The RoF link configurations discussed in this Chapter included RF-over-Fibre, IF-over-Fibre and Digitised-RF-over-Fibre links. It was discussed that RF-over-Fibre link is the simplest and cheapest to implement but it suffers from high noise and distortion especially at high frequencies (beyond 3GHz), while IF-over-Fibre and digitised-RF-over-Fibre links are alternatives, but their configurations are at the expense of additional devices. Also, direct modulation is the most straightforward type of modulation for RoF links, but its modulation and response at higher frequencies could be very poor and depending on the laser this could be from 2GHz. External modulation on the other hand is used for higher frequencies (certainly beyond 20GHz), where the RF signal, light-wave generation and intensity modulation needs to be done separately, and it can be used for frequencies up to 100 GHz.

In addition, the RoF link performance metrics were presented in this Chapter, and these include: the link gain and noise figure used for both direct and external modulation. Also, the performance metrics that reveal the distortion properties of the RoF link were discussed; these include the third-order intercept point (IP3), spurious-free dynamic range (SFDR) and the 1-dB compression (P1dB) point. The principle of MIMO systems used to improve the signal quality and increase data rates in a communication system has been discussed, and the algorithms used to achieve diversity, multiplexing and antenna gains. The performance metrics used to evaluate the performance of MIMO systems were also discussed, these include the Bit/symbol error rates, error vector magnitude (EVM) and channel capacity.

Finally, the performance reported in previous works on MIMO systems in RoF-DAS was reviewed to determine the improvement in capacity, throughput and coverage it offers over DAS supporting only a SISO configuration. The result from these works

shows that the capacity, throughput and error performance of a wireless MIMO systems in RoF-DAS can be improved significantly when compared to the performance of a SISO system. However, these works did not analyse the practical issues with the deployment of wireless MIMO in a RoF-DAS infrastructure, and since the works were based on commercial products, the specific algorithms used are unknown. Also, the performance reported in previous works on the feasibility of generating and transmitting mm-wave MIMO signals with small probability of error was reviewed. The performance analysis in these works was only been presented for a single user location and at a particular wireless distance, while in this thesis the analysis is for different user locations and different wireless distances. In addition, DWDM-RoF transport method is used in this thesis which has flexibility for wavelength selection/allocation to specific RAUs, and is useful especially when separate data streams are required to be transported through the RoF link.

REFERENCES

[1] E. Baumann (2011). The wireless world indoors. Available: www.zinwave.com

[2] N. J. Gomes, P. P. Monteiro, and A. Gameiro, Next Generation Wireless Communications Using Radio over Fiber: John Wiley & Sons, Inc., 2012.

[3] E. I. Ackerman and C. H. Cox, "RF fiber-optic link performance," IEEE Microwave Magazine, vol. 2, pp. 50 - 58, 2001

[4] C. Lim et al., "Fiber-Wireless Networks and Subsystem Technologies," in Journal of Lightwave Technology, vol. 28, no. 4, pp. 390-405, Feb.15, 2010.

[5] G. Losio "White Paper Modulation of Light," ProLabs, 2014, http://www.prolabs.com/wp-content/uploads/2016/06/White-Paper-Modulation-of-Light.pdf

[6] C. H. Cox and E. I. Ackerman, "A path to realizing high-performance 100-GHz analog links," , IEEE Avionics, Fiber-Optics and Photonics Conference (AVFOP), San Diego, CA, USA, pp. 1 - 3.

[7] M. Cvijetic and I. B. Djordjevic,"Advanced Optical Communication Systems and Networks," Artech House, 2013

[8] H. Al-Raweshidy and S. Komaki, Radio Over Fiber Technologies for Mobile Communications Networks: Artech House, 2002.

[9] IEEE 802.16 Broadband Wireless Access Working Group: Performance aspects of OFDM PHY proposal, available at http://ieee802.org/16

[10] IEEE Wireless LAN Medium Access Control (MAC) and Physical Layer (PHY) Specifications – Higher Speed Physical Layer Extension in the 2.4 GHz Band, IEEE Amendment 802.11b-1999, 1999

[11] Aruba Networks, Inc (2014). 802.11ac In-Depth.

[12] Agilent Technologies (2011). Application Note: Introducing LTE-Advanced.

[13] J. Mietzner, R. Schober, L. Lampe, W. H. Gerstacker and P. A. Hoeher, "Multiple-antenna techniques for wireless communications - a comprehensive literature survey," IEEE Communications Surveys & Tutorials, Vol. 11(2), pp. 87 - 105, 2009

[14] C. Kim and J. Lee, "Dynamic rate-adaptive MIMO mode switching between spatial multiplexing and diversity" EURASIP Journal on Wireless Communications and Networking, 2012:238.

[15] QUALCOMM. (2012) IEEE802.11ac: The Next Evolution of Wi-Fi Standards

[16] A. F. Molisch, "Wireless Communications" Wiley-IEEE Press, 2011

[17] V. Gangwar and D. Chandra, "Comparison of BER for BPSK & QAM modulation with Alamouti STBC," International Journal of Scientific & Engineering Research, Vol. 4(5) pp. 2337 - 2340, 2013

[18] N.S. Murthy, S. Sri Gowri, and J.N.V. Saileela, "Transmit Diversity Technique for Wireless Communication over Rayleigh Channels Using 16 QAM Modulation Schemes," Trends in Networksand Communications, Vol. 197, pp/ 127 - 137, 2011

[19] S. Alamouti, "A simple transmit diversity technique for wireless communications," IEEE Journal on Selected Areas in Communications, Vol. 16(8), pp. 1451 - 1458, 1998

[20] Y. Cho, J. Kim, W. Yang, and C. G. Kang, MIMO-OFDM Wireless Communications with MATLAB: John Wiley and Sons Ltd, 2010.

[21] Altera Corporation, Multiple Antenna Technology, https://www.altera.com/solutions/industry/wireless/applications/multiple-antenna-technology.html

[22] S. Sun, T. S. Rappaport, R. W. Heath, A. Nix and S. Rangan "Mimo for millimeter-wave wireless communications: beamforming, spatial multiplexing, or both?", IEEE Communications Magazine, Vol. 52(12),pp. 110 - 121, 2014

[23] C. D. Ziomek and M. T. Hunter. (2012). Extending the Useable Range of Error Vector Magnitude (EVM) Testing

[24] R. Hranac, Carrier-to-Noise Versus Signal-to-Noise: Cisco Systems, 2003.

[25] W. Music. (2001). TG3 measurement accuracy, IEEE P802.15 working group for wireless personal area networks. Available: http://www.ieee802.org

[26] Digital video broadcasting; Framing structure, channel coding and modulation for digital terrestrial television, 2008

[27] Rohde&Schwarz (2003), The right way to measure: SNR and MER of digitally modulated signals with additive noise.

[28] T.Li, "MER-an important indicator of digital cable TV transmission system", Cable TV Technology, no.193, 2006, pp.50-55.

[29] D. Tse and P. Viswanath, Fundamentals of wireless communication: Cambridge University Press, 2005.

[30] H. Tang, X. Wan, L. Hong, W. Chen and J. Yi, "Detection improvement by modified modulation error rate of reference signal in passive radar," 2014 XXXIth URSI General Assembly and Scientific Symposium (URSI GASS), Beijing, 2014, pp. 1-4.

[31] C.Langton and B.Sklar. (2011). Finding MIMO - Complex To Real. Available: complextoreal.com

[32] F. Cao and Z. Fan, "Joint proportional fair user scheduling for in-building distributed antenna systems," IET Communications, Vol. 7 (16), pp. 1802 - 1809, 2013.

[33] T. Alade, H. Zhu, and H. Osman, "The impact of antenna selection and location on the performance of DAS in a multi-storey building," IEEE Wireless Communications and Networking Conference (WCNC), Shanghai, China, 2013. pp. 3213 - 3218

[34] H. Zhu, "Performance Comparison Between Distributed Antenna and Microcellular Systems," IEEE Journal on Selected Areas in Communications, Vol. 29(6), pp. 1151 - 1163, 2011.

[35]   M. J. Crisp, S. Li, A. Watts, R. V. Penty and I.H. White "Uplink and Downlink Coverage Improvements of 802.11g Signals Using a Distributed Antenna Network," Journal of Lightwave Technology, Vol. 25(11), pp. 3388 - 3395, 2007.

[36]   A. Hekkala, M. Lasanen, I. Harjula, L. C. Vieira, N. J. Gomes, A. Nkansah, "Analysis of and compensation for non-ideal RoF links in DAS [Coordinated and Distributed MIMO]," IEEE Wireless Communications, vol. 17(3), pp. 52 - 59, 2010.

[37] K. Zhu, M. J. Crisp, S. He, and R. V. Penty, "MIMO system capacity improvements using radio-over-fibre distributed antenna system technology," Optical Fiber Communication Conference and Exposition and the National Fiber Optic Engineers Conference (OFC/NFOEC), pp. 1 - 3, Los Angeles, CA, 2011.

[38] K. Zhu, M. J. Crisp, H. Sailing, R. V. Penty, and I. H. White, "An experimental investigation of RoF-enabled MIMO DAS in a non-light-of-sight environment," CLEO:Laser Science to Photonic Applications, Baltimore, MD, 2011. pp. 1-2

[39] A. Kobyakov, M. Sauer , A. Ng'oma and J.H. Winters, "Effect of Optical Loss and Antenna Separation in 2x2 MIMO Fiber-Radio Systems," IEEE Transactions on Antennas and Propagation, Vol. 58, Iss. 1, pp. 187 - 194, 2009.

[40] T. Yamakami, T. Higashino , K. Tsukamoto and S. Komaki, "An experimental investigation of applying MIMO to RoF ubiquitous antenna system," International topical meeting on Microwave photonics and Asia-pacific microwave photonics conference. MWP/APMP, Gold Coast, Qld 2008. pp. 201 - 204

[41] M. Sauer and A. Kobyakov, "Fiber-radio antenna feeding for MIMO systems," Asia Optical Fiber Communication & Optoelectronic Exposition Conference, Shanghai, 2008. pp. 1-3

[42] A. Kobyakov, D.Thelen ; A.Chamarti ; M. Sauer and J. Winters, "MIMO radio signals over fiber in picocells for increased WLAN coverage," Optical Fiber communication/National Fiber Optic Engineers Conference, San Diego, CA, 2008. pp. 1-3

[43] J. Winters "On the Capacity of Radio Communication Systems with Diversity in a Rayleigh Fading Environment," IEEE Journal on Selected Areas in Communications, Vol. 5, Iss. 5, pp. 871 - 878, 2003.

[44] L. Tarlazzi, P. Faccin , E. M. Vitucci , F. Fuschini and V. Degli-Esposti, "Characterization of an Interleaved F-DAS MIMO indoor propagation channel," Antennas and Propagation Conference (LAPC),Loughborough,2010 . pp. 505 - 508

[45] S. K. Saha, V. V. Vira, A. Garg and D. Koutsonikolas, "A Feasibility Study of 60 GHz Indoor WLANs," 2016 25th International Conference on Computer Communication and Networks (ICCCN), Waikoloa, HI, 2016, pp. 1-9.

[46] Y. H. Cho and J. J. Kim, "Line-of-Sight MIMO Channel in Millimeter-Wave Beamforming System: Modeling and Prototype Results," 2015 IEEE 81st Vehicular Technology Conference (VTC Spring), Glasgow, 2015, pp. 1-5.

[47] J. James, P. Shen, A. Nkansah, X. Liang and N. J. Gomes, "Nonlinearity and Noise Effects in Multi-Level Signal Millimeter-Wave Over Fiber Transmission Using Single and Dual Wavelength Modulation," in IEEE Transactions on Microwave Theory and Techniques, vol. 58, no. 11, pp. 3189-3198, Nov. 2010.

[48] H. Suzuki, M. Fujiwara, K. Iwatsuki, A. Hirata and T. Nagatsuma, "Photonic millimetre-wave generator using intensity and phase modulators for 10 Gbit/s wireless link," in Electronics Letters, vol. 41, no. 6, pp. 355-356, 17 March 2005.

[49] H. Shams, P. M. Anandarajah, P. Perry and L. P. Barry, "Photonic generation and distribution of a modulated 60 GHz signal using a directly modulated gain switched laser," 21st Annual IEEE International Symposium on Personal, Indoor and Mobile Radio Communications, Instanbul, 2010, pp. 1032-1037.

[50] C.H. Ho, W.R. Jiang, R. Sambaraju, W.Y. Lee, T.H. Lu, C.Y. Wang et al., "Performance Evaluation of a 60 GHz RoF System Employing MIMO and OFDM Modulation", IEEE Journal on Selected Areas in Communications, vol. 31, no. 12, pp. 780-787, 2013.

[51] H. T. Huang et al., "2x2 MIMO OFDM-RoF System Employing LMS-Based Equalizer With I/Q Imbalance Compensation at 60 GHz," in IEEE Photonics Journal, vol. 6, no. 3, pp. 1-7, June 2014.

[52] L. Cheng, M.M.U. Gul, F. Lu, M. Zhu, J. Wang, M. Xu et al., "Coordinated Multipoint Transmissions in Millimeter-Wave Radio-Over-Fiber Systems", Journal of Lightwave Technology, vol. 34, pp. 653-660, 2016.

CHAPTER 3

ANALYSIS OF PRACTICAL ISSUES WITH COMMERCIAL MULTIPLE-INPUT MULTIPLE-OUTPUT ACCESS POINT IN DISTRIBUTED ANTENNA SYSTEM

3.1. Introduction

In the previous chapter, past research on RoF-DAS supported MIMO systems has been reviewed. These works examined the overall throughput and capacity performance of MIMO in RoF-DAS but did not examine practical issues that can cause deterioration in throughput performance when transmitting MIMO signals over RoF-DAS infrastructure. DAS operators give high priority to these issues and need to compensate for them to make the system perform more efficiently when it is deployed in the building [1]. In this Chapter, two practical issues with MIMO over RoF-DAS, fibre length difference and the received power imbalance are analysed, discussions on the practical issues, and description of the bi-directional MIMO-over-fibre DAS experiment are presented, followed by the measurement results and summary.

3.2. Practical issues with MIMO-DAS

Previous works [2], [3] have shown that the major issue with DAS when distributing WLAN signals is the effect of different fibre lengths connecting the CU to the RAUs, which causes the throughput to fall as the fibre length increase. This is because the DAS infrastructure increases the delay spread of the system as it amplifies and maintains the direct paths of the signals reaching every RAU [4], resulting in Inter-Symbol Interference (ISI). In [5], it was experimentally verified that using an IEEE

802.11g AP in a DAS infrastructure, the throughput halves with a fibre difference of 30m due to the stringent signal-to-noise ratio (SNR) and delay spread requirements specified in IEEE 802.11g standard as the data rate increases [6]. Therefore, at worse propagation conditions, the AP will switch to a lower data rate and the throughput falls. The majority of previous works on the effect of different fibre lengths in DAS have been analysed with non-MIMO APs.
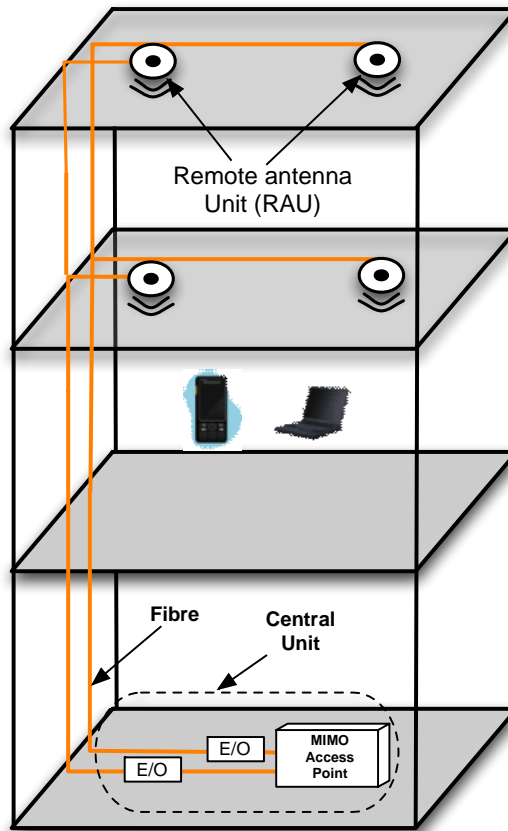
Figure 3.1 2x2 MIMO AP in RoF-DAS

MIMO requires multiple separate RF chains, and for a RoF-DAS infrastructure it means each RF chain from the CU should be connected to each RAU as shown in Fig. 3.1, and the received signals needs to be aligned at the user equipment (UE) before they are combined to improve signal quality and data rates. When the fibre link difference exceeds a certain distance, the differential delay increases and received signal cannot be aligned, hence the throughput drops rapidly due to severe ISI. Further, MIMO systems need spatial independence of the wireless channels, which generally requires an antenna separation of at least ¼ the radio signal

wavelength [7]. With optical feeding of the antennas, significantly larger antenna spacing can easily be accomplished, which opens up new possibilities for covering wider areas with MIMO [8-10]. Increasing distance between RAUs can not only extend the wireless coverage, but also improve the throughput performance by reducing the correlation between the different spatial streams [11], [12]. However, large antenna separation may lead to a received power imbalance problem that can reduce the throughput performance. This is because the signal strengths of the two received signals in MIMO should be relatively equal [13]. Recent standards employing MIMO techniques, such as LTE, can cope with up to 12-15 dB of power imbalance between different spatial streams at the UE [14]. Normally in a traditional co-located antenna system (CAS), MIMO antennas are always installed in the same device; hence, the received power at the UE would not exceed such a figure. However, MIMO-DAS systems cannot guarantee such similar power levels at each position in a real environment with large antenna separation. Hence, both reducing correlation and decreasing the received power imbalance should be considered when implement MIMO-DAS.

In this Chapter, an experiment has been carried out to investigate the throughput performance of IEEE 802.11n 2x2 MIMO AP and a spatial diversity-supported AP in a RoF-based DAS with different fibre lengths and power imbalance. The analysis of fibre length difference is examined for seven cases; five for MIMO-supported AP and two for spatial diversity-supported AP. The throughput measurement was carried out with wireless users at different locations in a typical office environment, and the fibre length difference was varied from 25m to 150m. The analysis of power imbalance effect is validated with a MIMO-supported AP and a spatial-diversity-supported AP. Although, the room the throughput measurements were carried out was not large enough to create path losses that will show the power imbalance effect, the effect was created artificially by using different transmit power levels at each RAU. The output power levels before the antennas used in the experiment was varied so that the UE can experience large power imbalance that can be seen in the experiment, contributed to by the different path loss.

3.3. Experimental Setup

Fig. 3.2 shows the bi-directional MIMO-over-fibre DAS experimental setup. The AP was connected to a host PC using a 1Gbps Ethernet cable. The parameters for MIMO-supported AP and spatial diversity-supported AP used in the experiment are shown in Table 3.1. In the downlink, the RF signals transmitted from the AP were attenuated to produce 2.5dBm at which point the distributed feedback (DFB) laser diode (LD) attains its best error vector magnitude (EVM) performance (as shown in Fig. 3.3) when converting the RF into optical signals. The resulting optical signals are transported over single-mode fibre (SMF) links to the RAUs. At the RAUs, the optical signals were detected by the photodiodes and an electronic amplifier was employed to boost the signal power level for transmission over the wireless path.
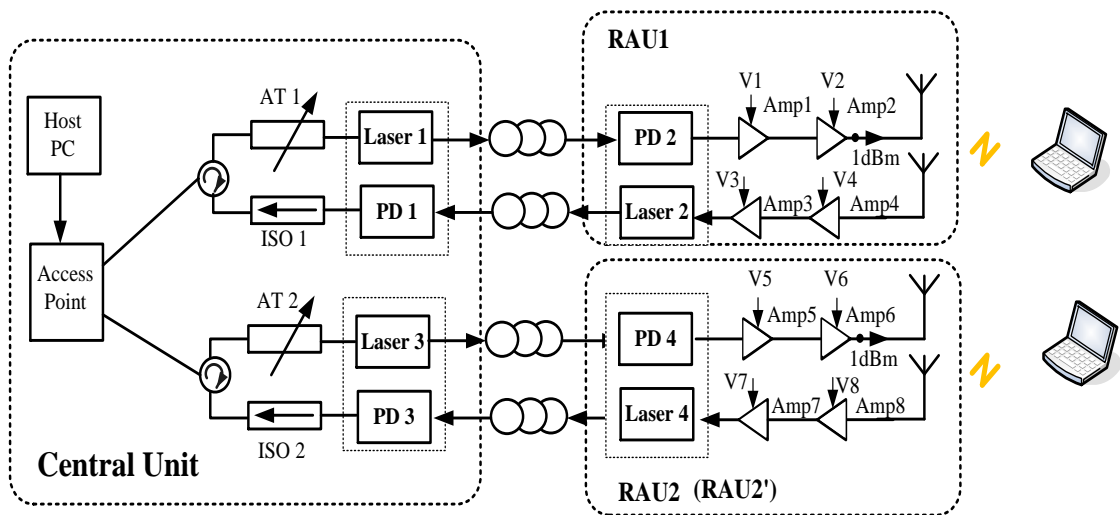
Figure 3.2 The experiment set-up. PD=Photodetector, AT=Attenuator, V=Voltage, ISO=Isolator, Amp=Amplifier.

In the uplink direction, the RF signals received from the antennas were amplified before up-converting them into optical signals at the RAUs. The optical signals were then transmitted through SMF links to the PDs in the CU where the signals are down-converted to RF signals. RF isolators were connected after the PDs to keep the signals flowing in one direction only. Also RF circulators were used in the CU to ensure the signal it receives from one port is transmitted from its next port only to isolate the

signal flow between the two directions (i.e. downlink and uplink). The output power to each downlink antennas was set at 1 dBm at which point the cascaded amplifiers were tested to be operating in it linear region. The AP antennas were used in the experiments and the gain of each antenna is approximately 9.5dBi.

Table 3.1 Parameters for MIMO-supported AP and spatial diversity-supported AP used in Experiment

AP Type	Parameter	Value
MIMO-supported AP Experiment	Modulation	OFDM-MIMO
	Radio Frequency Band	Draft 802.11n 2.0 : 2.4GHz
	Bandwidth	20/40MHz auto
	Measured Date Rate	96Mbps
	RoF Link Gain	-25dB
	RAU Transmit Power	1dBm
	Antenna Gain	9.5dBi
Spatial diversity-supported AP Experiment	Modulation	OFDM
	Radio Frequency Band	802.11b/g: 2.4GHz
	Bandwidth	20MHz
	Measured Date Rate	25Mbps
	RoF Link Gain	-25dB
	RAU Transmit Power	1dBm
	Antenna Gain	9.5dBi
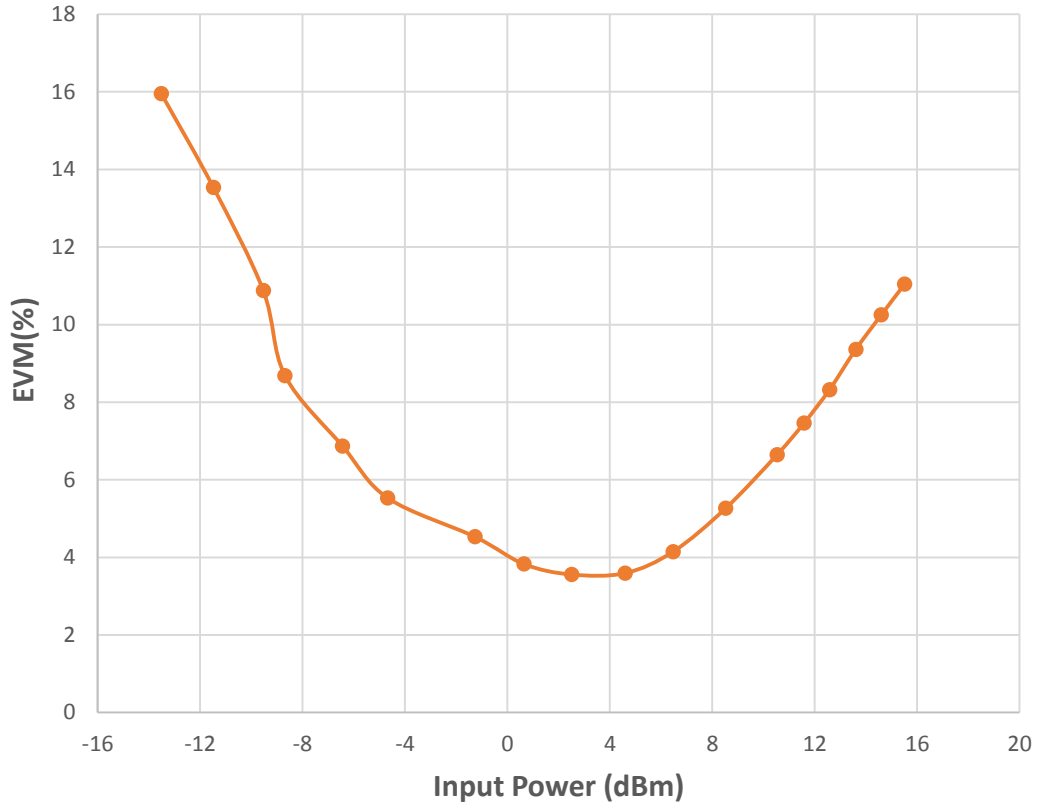
Figure 3.3 EVM vs. input power of a laser diode (LD) connected to a photodiode (PD)

The optimum input power to the RoF link was decided by an EVM measurement. The experiment was carried out by generating IEEE 802.11n signal from an Agilent WLAN software, and downloaded onto a vector signal generator (VSG). The signal was then transmitted through the RoF link to a vector signal analyser (VSA) and the measurement was obtained from an Agilent demodulation software running on a laptop connected to the VSA. The input power at the VSG was varied between -15dBm to 16dBm as shown in Fig. 3.3 and the best EVM (3.5%) was at 2.5dBm input power.
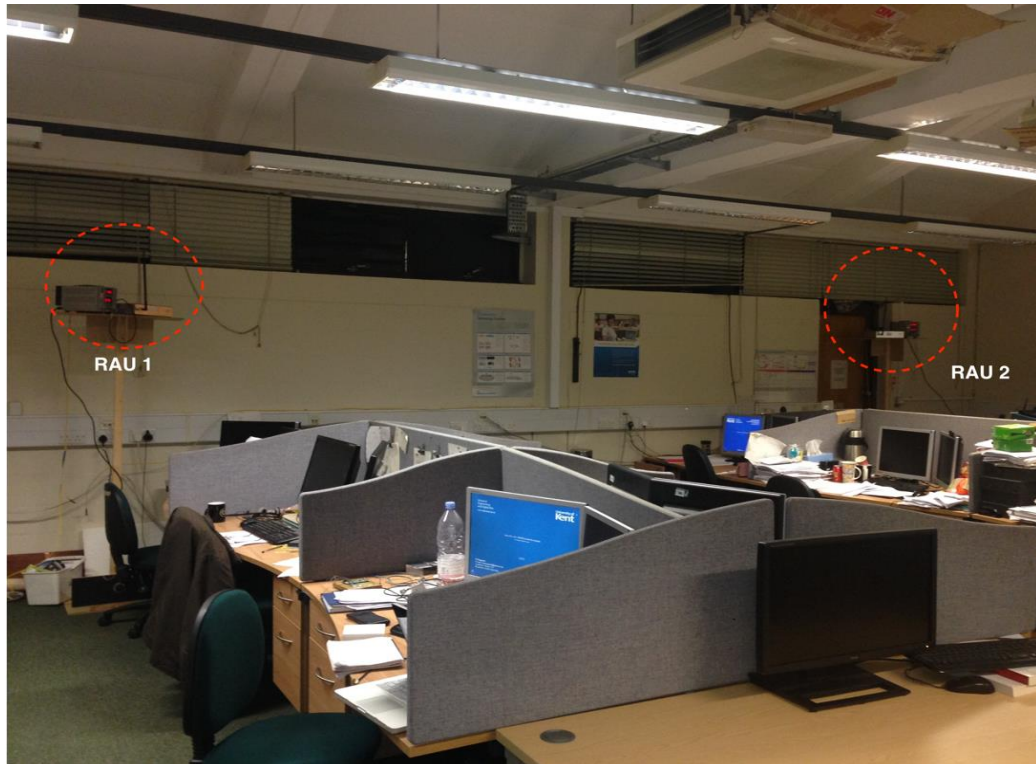
Figure 3.4 Experiment testing room

The CU and testing room were two separate rooms; the CU is a laboratory where the host computer, access point, downlink LDs and uplink PDs are placed while the testing room is a research office room with different furniture including desks, chairs and computers as shown in Fig. 3.4. The RAUs were placed on a wooden platform, so the signals were generally radiated above all furniture. Fig. 3.5 shows the layout of the testing room, A, B, C indicate a row number and 1, 2, 3 a column number used to identify the UE's positions at which measurements were carried out.

In the testing room, the distance between the two RAUs was set to 4.4m and 9m to observe the throughput at both antenna separations. The large antenna spacing was chosen to reduce the spatial correlation and provide higher received RF power for the UEs especially those closer to the RAUs, which is the specific benefit from the DAS architecture. The throughput measurements were carried out using the commercial software Networx, and achieved by transferring large files between the Host PC and mobile laptops.
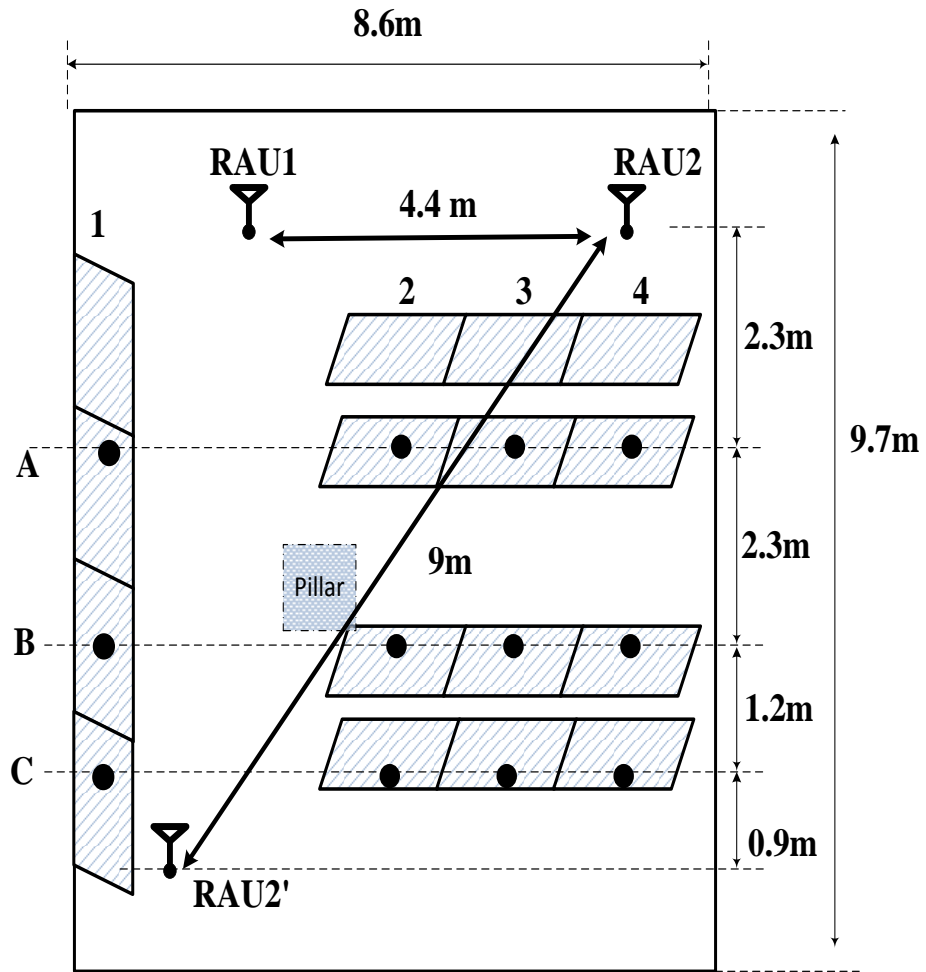
Figure 3.5 Experiment layout. The large black dots are the locations of the mobile devices.

3.4. Fibre length difference analysis results

In this experiment, the fibre lengths connecting the CU to the RAUs was varied according to Table 3.2, the two RAUs were placed in front of the testing room and separated at a distance of 4.4m. It must be noted that the output power for both RAUs were the same. In order to evaluate the throughput performance with fibre-length difference effects in the RoF-DAS, we consider both the MIMO-supported AP and spatial diversity-supported AP. Seven configurations were used in the experiment, as shown in Table 3.2, using different sets of fibre links. In all test Cases, i.e. Cases 1-7, the throughput in each user position shown in the layout of Fig. 5 was measured. At the CU, a Belkin IEEE 802.11n MIMO-supported AP is used in Cases 1-5, while a 3com spatial diversity AP is used in Cases 6 and 7.

Table 3.2 Configurations in Fibre length difference Experiment

	AP Type	FL[1]-RAU1(m)	FL-RAU2(m)
Case1		25	25
Case2		75	25
Case3	MIMO	125	25
Case4		175	25
Case5		125	125
Case6	Spatial Diversity	25	25
Case7		175	25

[1] FL: Fibre length.

3.4.1. Single user measurements

Figs. 3.8 - 3.10 shows the normalized downlink throughput measurement results; these are normalized by the maximum throughput each mode can reach. The maximum throughput for these APs was measured in the laboratory before connecting it to the RoF links (i.e. the antennas were connected directly to the AP ports). For the spatial diversity-supported AP (shown in Fig. 3.6), the maximum throughput it could reach is 25Mbps while for the MIMO-supported AP (shown in Fig. 3.7) it is 96Mbps due to the use of MIMO techniques and the bandwidth is twice that of the spatial diversity-supported AP. The measurements were carried out in the positions shown in Fig. 3.5 with the different sets of fibre lengths for Cases 1-7.
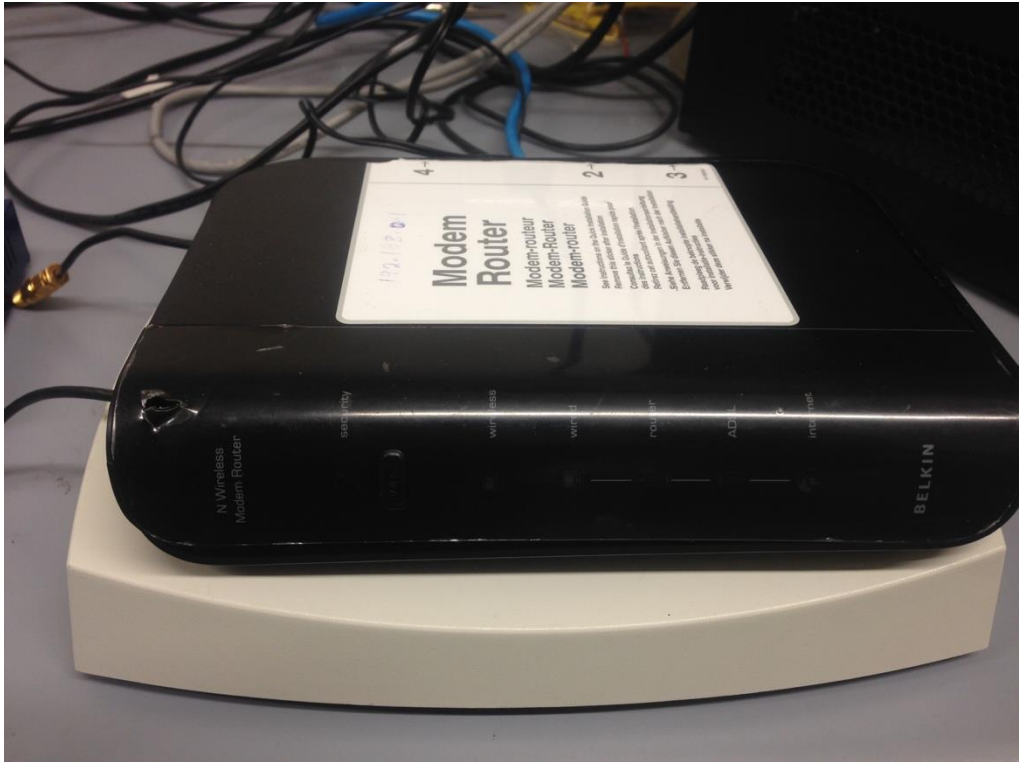
Figure 3.6 MIMO-supported AP

Figure 3.7 Spatial diversity- supported AP
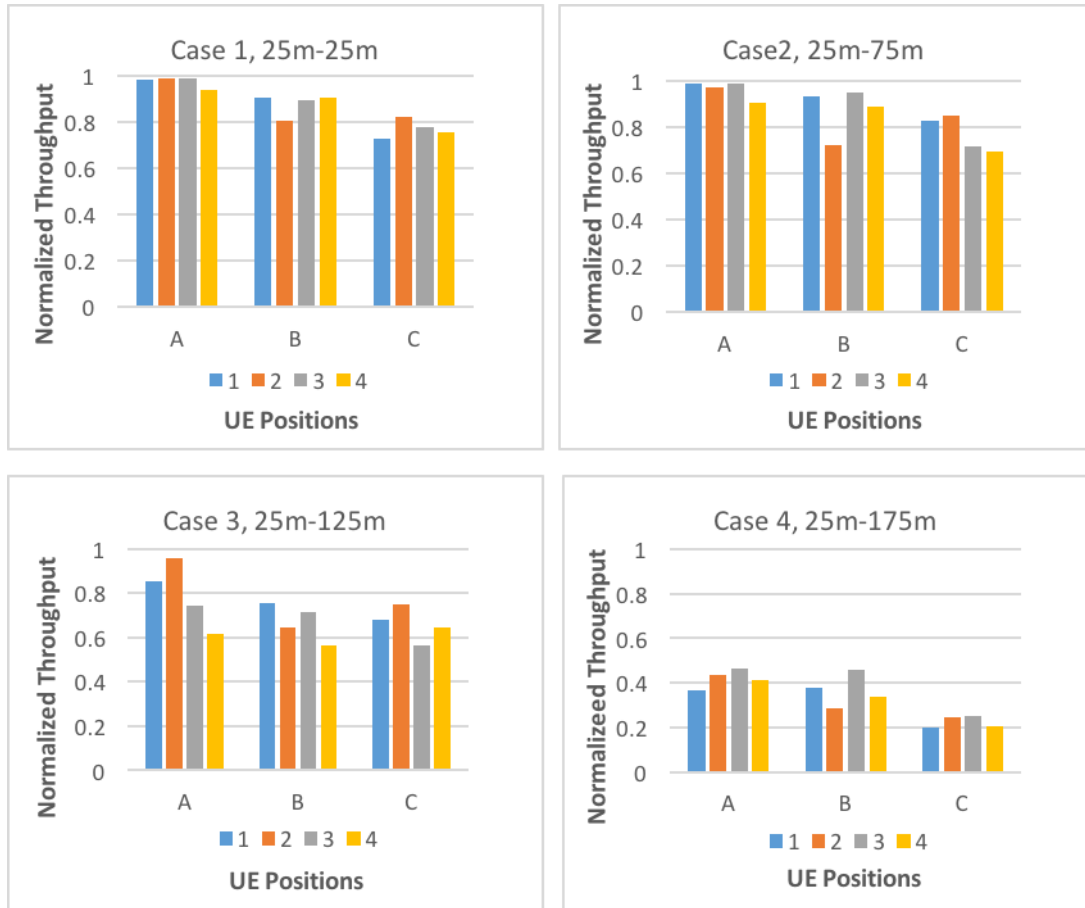
Figure 3.8 MIMO-supported downlink throughput with different fibre links (a) Case 1, 25m-25m (b) Case 2,25m-75m (c) Case 3,25m-125m (d) Case 4, 25m-175m.

Fig. 3.8 shows the normalized throughput for Cases 1-4, for Cases 2-4, the throughput dropped gradually as the fibre-length difference increased. This decrease is mostly because of the severe ISI, as the fibre length difference increases, it introduces large delay between the received signals from the two RAUs. This verifies the discussion in session 3.2 that when the fibre link difference exceeds a certain distance, the differential delay increases and the received signal cannot be aligned, hence the throughput drops rapidly due to severe ISI. It can be observed from Fig. 3.8a that the normalized throughput performance for Case 1 was almost the same for all measured positions since the fibre links were equal.
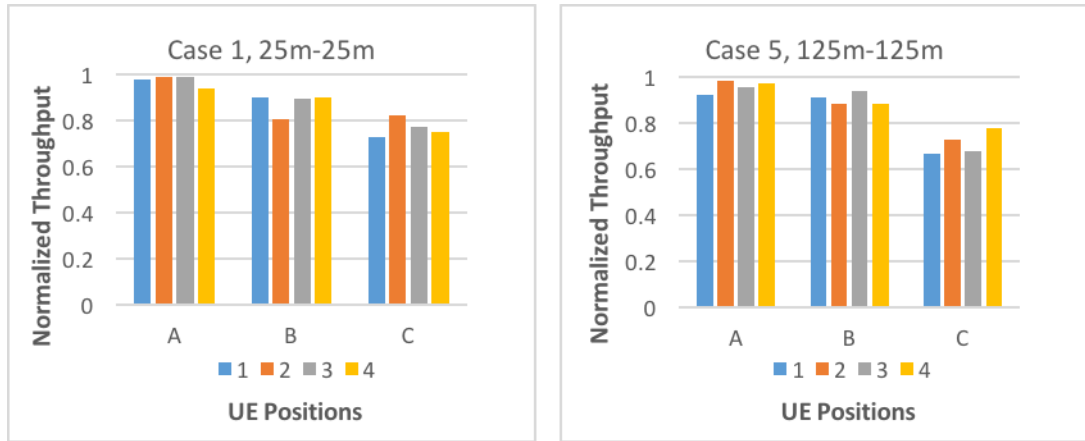
Figure 3.9 MIMO-supported downlink throughput with the equal fibre link lengths (a) Case 1, 25m-25m (b) Case 5, 125m-125m

In Case 5, where both RAUs had equal lengths but longer fibre i.e. RAU1 125m and RAU2 125m, the throughput does not reduce much due to the extra fibre delay compared to Case 1, as shown in Fig. 3.9, as the fibre delays are approximately equal; only a small performance decrease is observed due to the protocol overhead (e.g., longer wait times for acknowledgments). This verifies that the throughput decrease observed in Fig. 3.8 is not caused by the fixed fibre delay, but because the differential delay increased.
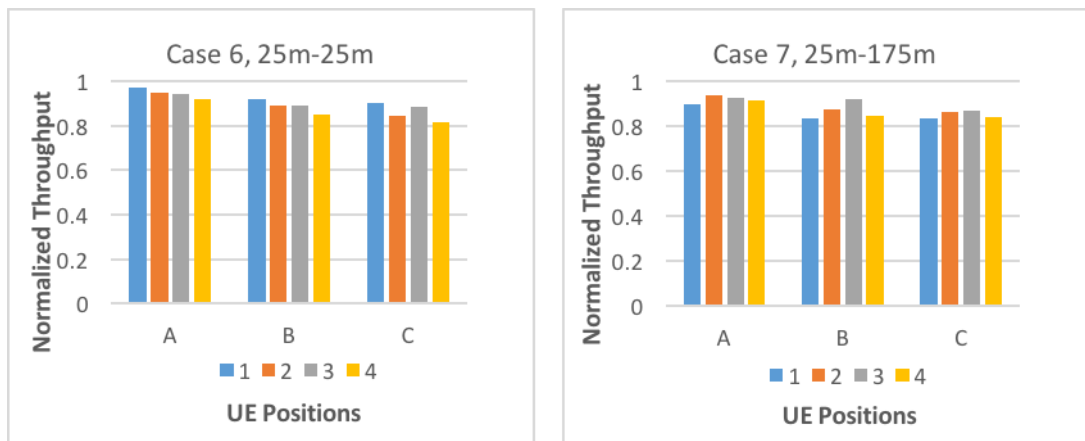
Figure 3.10 Spatial Diversity-supported downlink throughput with different fibre link lengths (a) Case 6, 25m-25m (b) Case 7, 25m-175m

Fig. 3.10 shows the result of throughput measurement with the spatial diversity AP. In such an AP, only one antenna port is employed at a time. It can be observed that the normalized throughput only shows very small changes between Case 6 and Case 7. This is simply because only the antenna which receives higher power or SNR is selected, meaning that the antenna with poor channel conditions does not significantly affect the whole system performance.

3.4.2. Multiple user measurements

An additional UE was added to determine the effects of multiple users accessing the AP from both antenna ports. The same model laptops with similar Network Interface Cards (NIC) were used to avoid any inequalities of throughput distribution, as different manufacturers often implement different MAC configurations, which may cause extremely variable contention performance. Additionally, the MIMO-supported AP was in 802.11n mode only, and no 802.11b&g users were allowed to access the network. For the 802.11g diversity AP, no 802.11b users were present within the association radius of the AP; thus, we can ensure the maximum throughput could be obtained.
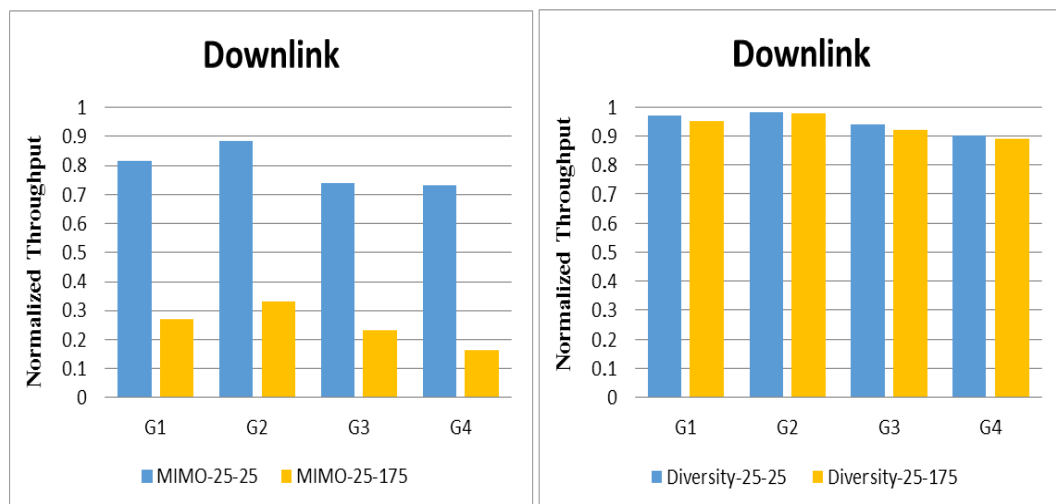
Figure 3.11 Multiple users downlink throughput comparison for MIMO AP and Diversity AP respectively with the fibre links 25m-25m and 25m-125m.
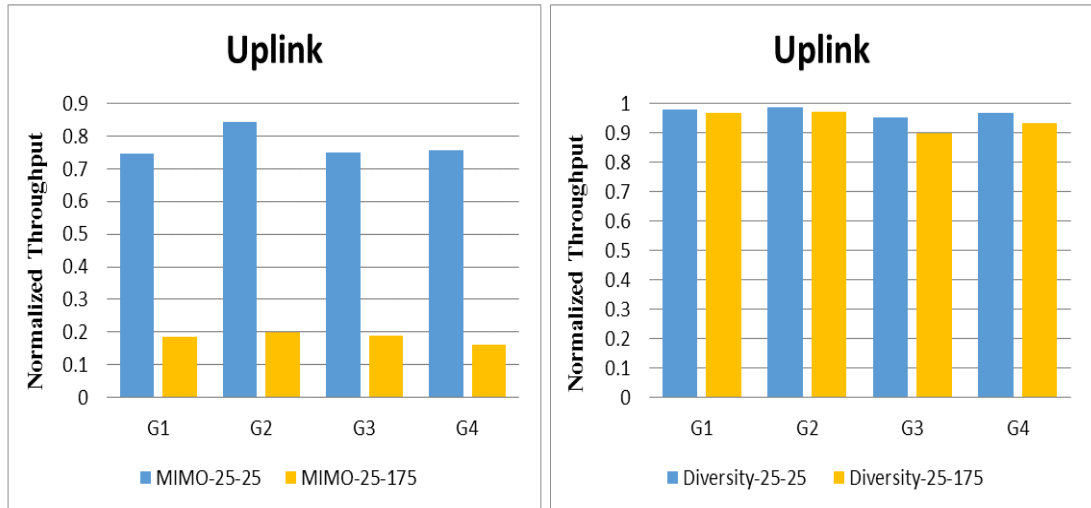
Figure 3.12 Multiple users uplink throughput comparison for MIMO AP and Diversity AP respectively with the fibre links 25m-25m and 25m-125m.

The multiple user experiment was carried out with RAU1 and RAU2 placed at different positions according to the experiment layout in Fig. 3.5. G1 means that both of the laptops are in position A1 (A is the row number and 1 is the column number), G2 means both are in A2, G3 both in B4, and G4 means 1 laptop in A1, and the other one in B4. The data recordings were collected at the same time, and after the throughput of the two laptops reached an equilibrium level. Downlink and uplink normalized throughput performance of the 2-laptop situation are shown in Fig. 3.11 and Fig. 3.12. Similar to the single-user situation, it can be observed from Figs. 3.11 and 3.12 that there is an obvious drop of the normalized throughput for both downlink and uplink with the MIMO AP in the 25m-175m configuration compared to the 25m-25m configuration. However, only a slight decrease in normalized throughput was observed with the diversity AP, as only one antenna is working at a time.

3.5. Power imbalance analysis results

The room in which the tests were carried out was not large enough to create path losses which would validate the power imbalance effect due to different antenna separation, therefore, the effect was created artificially by using different transmit

59

power levels at each RAU. The output power levels before the antennas used in the experiment are listed in Table 3.3.

Table 3.3 Configurations in Power imbalance Experiment

	Set 1	Set 2	Set 3	Set 4	Set 5	Set 6
Output Power in RAU 1 (dBm)	2.3	-3.4	-1	1	-5.5	-2.6
Output Power in RAU 2 (dBm)	-5.9	-9.2	-9.2	-9.2	-16.6	-16.6
Output Power Difference (dB)	8.2	5.8	8.2	10.2	11.1	14

The amplifiers were biased at different voltages to produce different output power for each transmit antenna and this output powers were grouped in sets. Sets 1 and 3 have the same output power difference but different transmit power from each antenna while sets 2 and 4 have low and high output power difference respectively. Sets 5 and 6 both have different high output power difference. By employing these different output powers, a larger received power imbalance can be seen in the experiment, contributed to by the initial output power difference and by different path loss.

The ITU indoor path loss model was used to predict the path loss in the tested area to calculate the received power imbalance, the path loss is given by [15]:

$$L_{path}=20\times\log_{10}(f) + N\times\log_{10}(d) + L_f(n) - 28\text{dB} \tag{3.1}$$

where N is the distance power decay index, f is the frequency in MHz, d is the distance in meters ($d>1$ m), $L_f(n)$ is the floor penetration loss factor and n is the number of floors between the transmitter and the receiver. In this case, the testing area is in a

single floor, $L_f(n)=0$. Following the validation of this model in [15], a value of $N=28$ for the typical office area was used. Hence, the path loss of each of the two spatial streams was predicted and the received power imbalance for each position calculated.

The relationship between MIMO-DAS throughput performance and received power imbalance for the different combination of sets are shown in Figs 3.13, 3.14 and 3.15. In these Figures, S represents Throughput, Pi represents Power Imbalance (dB). The experiment was conducted with a single user at the positions defined in Fig. 3.5 and the two RAUs were separated at a distance of 9m achieved by moving RAU 2 to the other end of the room shown in Fig. 3.5 as RAU 2'. A1, B1, C1 are positions close to RAU 1 and 2', A2, B2, C2 are positions further away from the RAUs and A3, B3, C3 are positions further away from RAU 1 and RAU 2' and positions A2, B2, C2. The throughput performance has been normalised by the maximum throughput each mode can reach, as described in 3.4.1 (96Mbps for the MIMO AP and 25Mbps for the spatial diversity AP).
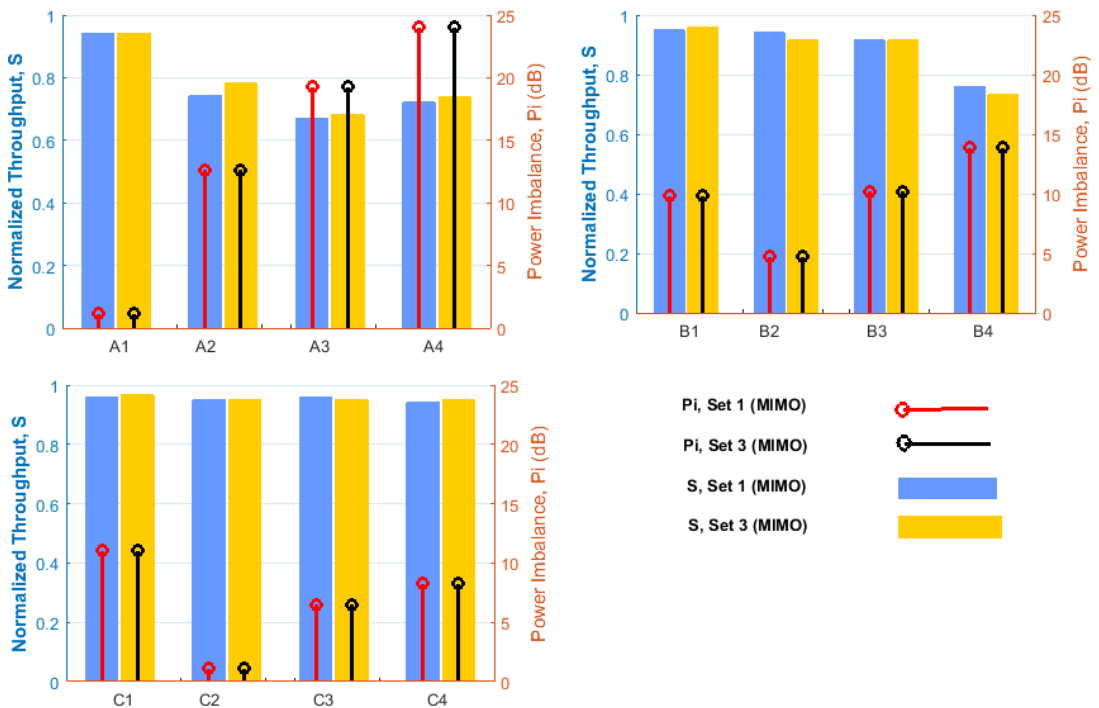
Figure 3.13 Throughput S and power imbalance Pi results of MIMO using set 1 and set 3

Fig. 3.13 shows a comparison of the throughput and power imbalance results of sets 1 and 3 where both RAUs have the same output power difference (8.2dB) but different output powers for each RAU. The result shows that the throughput drops in positions where power imbalance is above 12dB. Also, both sets exhibit similar behaviour despite different output power for each RAU, this reinforce the indication that the drop in throughput is not because of low received power, but due to the imbalance.
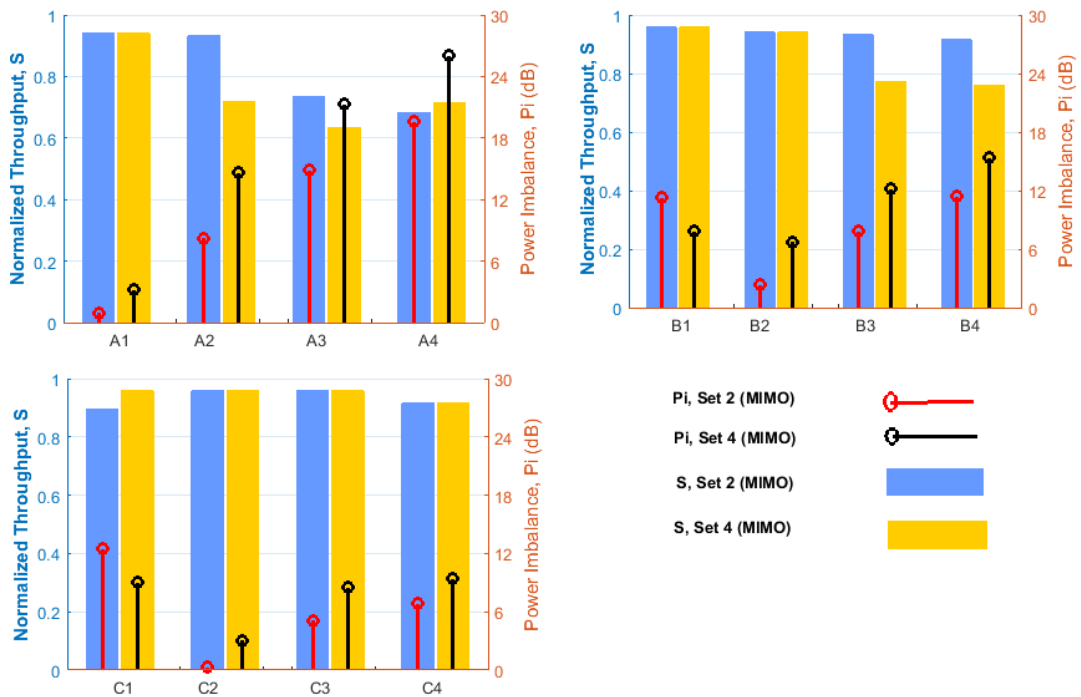
Figure 3.14 Throughput S and power imbalance Pi results of MIMO using set 2 and set 4

Fig. 3.14 shows a comparison of the throughput and power imbalance results of sets 2 and 4 where the output power difference of RAU1 is low (5.8dB) and RAU2' is high (10.2dB). The throughput drops in only few positions where power imbalance is above 12dB at the lower output power difference, while at higher output power difference, the throughput drops in more positions where power imbalance is above 12dB.

Fig. 3.15 compares the throughput performance of MIMO-supported AP with that of spatial diversity-supported AP when both APs are using set 6 with 14dB output

power difference. It can be observed from the results in Fig. 3.15 that the throughput of MIMO-supported AP drops has many positions when the power imbalance is above 12dB especially positions further away from the RAUs. However, for the spatial diversity-supported AP, the power imbalance problem does not affect the throughput performance since the diversity method does not combine the signals from the two antennas. It simply selects the antenna with the highest signal power and ignores the signal from the other antenna based on the selected signal path. Therefore, high throughput was obtained as long as there is at least one good link within its coverage.
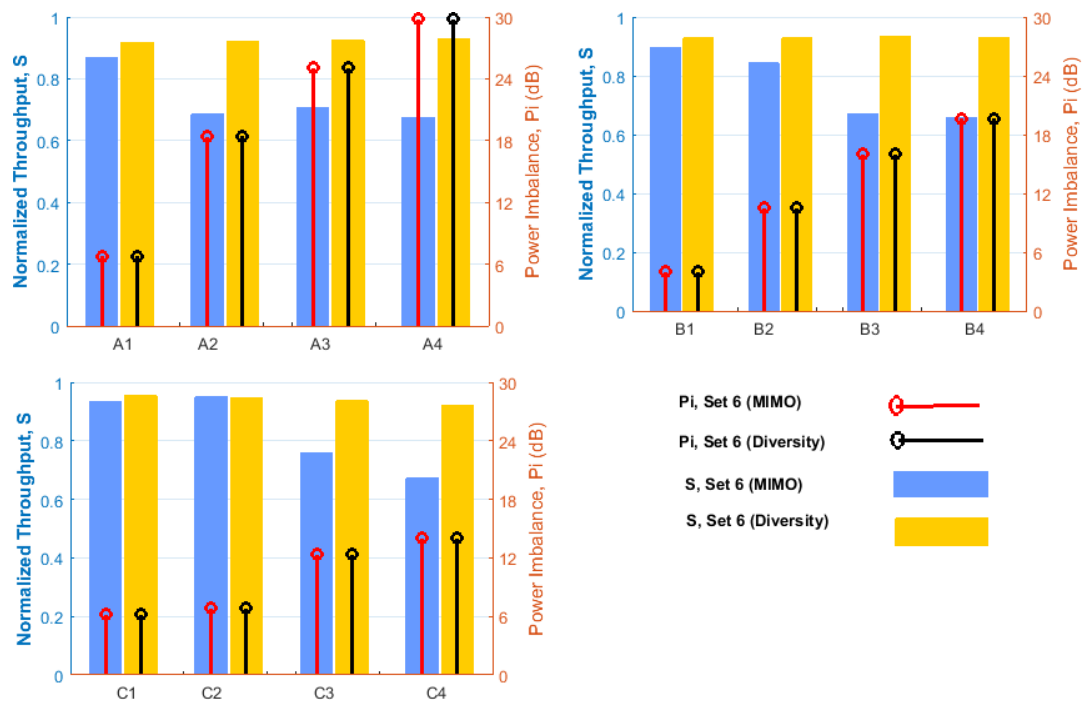
Figure 3.15 Throughput S and power imbalance Pi results of MIMO using set 6 and spatial diversity using set 6.

From Figs 3.13 to 3.15, it can be seen that the throughput dropped in the positions where the received power imbalance exceeds around 12dB. Also, it can be observed that the throughput performance does not fall any further than around 0.65 to 0.7, even when the received power imbalance problem becomes much more severe. For example, in Position A4, the power imbalance is as high as 30 dB in Set 6 and 19 dB

in Set 2, but the normalized throughput for the two Sets are not very different, both being around 0.67.

The predicted received power from each RAU is shown in Tables 3.4, 3.5 and 3.6, obtained from the ITU path loss model in (3.1). In the Tables, *S* represents Throughput, *Pr1* and *Pr2* represents Received Power (dBm) from RAU1 and RAU2 respectively, and Pi represents Power Imbalance (dB) and the positions the received power imbalance exceeds 12dB is indicated by the grey shading.

Table 3.4 Experimental Results (Set 1 and Set 3)

		Set 1				Set 3			
		1	2	3	4	1	2	3	4
RowA	*S*	0.942	0.742	0.669	0.721	0.942	0.785	0.681	0.738
	Pr1 (dBm)	-51.35	-43.30	-38.97	-36.39	-54.65	-46.60	-42.27	-39.69
	Pr2 (dBm)	-52.48	-55.95	-58.24	-60.41	-55.81	-59.25	-61.54	-63.71
	Pi (dB)	1.13	12.65	19.27	24.02	1.13	12.65	19.27	24.02
RowB	*S*	0.95	0.941	0.916	0.760	0.958	0.916	0.916	0.733
	Pr1 (dBm)	-52.81	-47.58	-45.82	-45.09	-56.11	-50.88	-49.12	-48.39
	Pr2 (dBm)	-42.96	-52.33	-56.02	-58.13	-46.26	-55.63	-59.32	-61.43
	Pi (dB)	-9.85	4.75	10.20	13.84	-9.85	4.75	10.20	13.84
RowC	*S*	0.958	0.950	0.958	0.941	0.967	0.950	0.950	0.950
	Pr1 (dBm)	-52.55	-49.96	-48.82	-48.39	-55.85	-53.26	-52.12	-51.69
	Pr2 (dBm)	-41.49	-51.03	-55.33	-55.82	-44.79	-54.33	-58.63	-59.12
	Pi (dB)	-11.06	1.07	6.51	8.23	-11.06	1.07	6.51	8.23

Table 3.5 Experimental Results (Set 2 and Set 4).

		Set 2				Set 4			
		1	2	3	4	1	2	3	4
RowA	S	0.941	0.933	0.734	0.683	0.941	0.717	0.634	0.715
	$Pr1$ (dBm)	-56.75	-51.00	-46.67	-44.09	-52.65	-44.60	-40.27	-37.69
	$Pr2$ (dBm)	-55.81	-59.25	-61.54	-63.71	-55.81	-59.25	-61.54	-63.71
	Pi (dB)	-0.94	8.24	14.87	19.61	3.16	14.65	21.27	26.02
RowB	S	0.958	0.941	0.933	0.916	0.958	0.941	0.772	0.760
	$Pr1$ (dBm)	-57.05	-53.28	-51.51	-50.79	-54.11	-48.88	-47.12	-46.39
	$Pr2$ (dBm)	-46.26	-55.63	-59.31	-62.23	-46.26	-55.63	-59.32	-61.43
	Pi (dB)	-11.26	2.35	7.80	11.44	-7.85	6.75	12.2	15.38
RowC	S	0.896	0.958	0.958	0.916	0.958	0.958	0.958	0.916
	$Pr1$ (dBm)	-57.25	-55.65	-54.52	-54.01	-53.85	-51.26	-50.12	-49.69
	$Pr2$ (dBm)	-44.79	-54.32	-58.63	-59.92	-44.79	-54.33	-58.63	-59.12
	Pi (dB)	-12.46	-0.33	5.12	6.83	-9.06	3.07	8.51	9.43

Table 3.6 Experimental Results (Set 6 MIMO and Set 6 Diversity).

		Set 6 MIMO				Set 6 Diversity			
		1	2	3	4	1	2	3	4
RowA	S	0.867	0.686	0.708	0.676	0.918	0.921	0.925	0.928
	$Pr1$ (dBm)	-56.25	-48.20	-43.87	-41.29	-56.25	-48.20	-43.87	-41.29
	$Pr2$ dBm)	-63.18	-66.64	-68.94	-71.10	-63.18	-66.64	-68.94	-71.10
	Pi(dB)	6.79	18.44	25.07	29.81	6.79	18.44	25.07	29.81
RowB	S	0.896	0.843	0.671	0.657	0.928	0.928	0.934	0.931
	$Pr1$ (dBm)	-57.71	-52.48	-50.72	-49.99	-57.71	-52.48	-50.72	-49.99
	$Pr2$(dBm)	-53.65	-63.03	-66.72	-69.63	-53.65	-63.03	-66.72	-69.63
	Pi (dB)	-4.06	10.55	16.00	19.64	-4.06	10.55	16.00	19.64
RowC	S	0.933	0.95	0.758	0.672	0.954	0.947	0.936	0.921
	$Pr1$ (dBm)	-57.45	-54.85	-53.72	-53.29	-57.45	-54.85	-53.72	-53.29
	$Pr2$ (dBm)	-51.29	-61.72	-66.03	-67.32	-51.29	-61.72	-66.03	-67.32
	Pi (dB)	-6.16	6.87	12.32	14.03	-6.16	6.87	12.32	14.03

The relationship between the received power and throughput is examined, it should be noted that the receiver sensitivity for 64QAM is -63dBm to -61dBm for different coding rates in 802.11n [16]. It can be observed from Tables 3.4, 3.5 and 3.6 that the

received powers from both RAUs are mostly above -63 dBm. Therefore, the drop in throughput at these positions where the received powers are above -63 dBm is due to power imbalance. Also, for other positions where one of the received power is lower than -63dBm, see set 6 (Table 3.6), in particular, the throughput remains at a similar level to other larger power-imbalance positions. For example, at position C4, the received powers are -53.29dBm from RAU1 and -67.32dBm from RAU2', and position A4, the received powers are -41.29dBm from RAU1 and -71.10dBm from RAU2'. There is no trend of reduced throughput as one of the received power levels falls. Therefore, we can deduce that the drop in throughput is not because one of the received powers is low but because of the large power imbalance. When the laptops cannot process the data with two streams in MIMO mode, it can still receive one stream with good quality and the AP switches dynamically to single-input single-output (SISO) or spatial diversity modes, according to the current channel state [17].

3.6 Summary

In this chapter, two practical issues with commercial MIMO access point in DAS, the effects of fibre length differences and power imbalances have been analysed. The experiment was carried out using commercial MIMO- supported AP and spatial diversity-supported AP.

The analysis of fibre length different was measured for a single-user and multiple-user client and the results show that MIMO signals can maintain high throughput performance when the fibre length difference between the two RAUs was under 100m but fell quickly when the fibre length difference was greater than 100m. This was because when the fibre link difference exceeds 100m, the differential delay increases and the throughput drops rapidly due to severe ISI. For the spatial diversity signals, the high throughputs was maintained even when the fibre link difference was 150m. This is because only one antenna port is transmitting at a time i.e. the one with the highest received power or SNR.

In addition, the analysis of power imbalances was measured to observe the relationship between MIMO-DAS throughput performance and received power imbalance, and the relationship between received power and throguhput. The results show that the throughput performance drops in specific positions when the received power imbalance was above 12dB and it was shown that the drop in throughput was not due to low or insufficient received power since most of the positions were above the receiver sensitivity but the throughput drop was mainly due to power imbalance.

Finally, it should be noted that any real environment would lead to receive powers that are different to the results of a wireless propagation model. Also, there is no exact value that can be defined as a limitation for power imbalance for a 2×2 MIMO system. These results simply match the LTE standard indicated limit range of 12-15dB.

REFERENCES

[1] M. Tolstrup, Indoor Radio Planning: A Practical Guide for GSM, DCS, UMTS, HSPA and LTE, Second Edition: John Wiley & Sons, Inc., 2011.

[2]   A. Hekkala, M. Lasanen, I. Harjula, L. C. Viera, N. J. Gomes, A. Nkansah, et al., "Analysis of and compensation for non-ideal RoF links in DAS [Coordinated and Distributed MIMO]," IEEE Wireless Communications, vol. 17, pp. 52 - 59, 2010.

[3]   H. Boelcskei, D. Gesbert, C. B. Papadias, and A.J. van der Veen, "Space-time wireless systems: from array processing to MIMO communications", Cambridge University Press, 2006.

[4] P. Assimakopoulos, A. Nkansah, and N. J. Gomes, "Use of commercial access point employing spatial diversity in a distributed antenna network with different fiber lengths," IEEE Int. Top. Meet. on Microw. Photon. and 9th Asia-Pacific Microw. Photon. Conf (MWP/APMP), Gold Coast, Australia, 2008. pp. 189 - 192

[5] M.J. Crisp, S. Li, A. Watts, R. V. Penty, and I. H. White, "Uplink and Downlink Coverage Improvements of 802.11g Signals Using a Distributed Antenna Network' Journal of Lightwave Technology Vol. 25(11) pp. 3388-3395 (2007)

[6] "IEEE Std. 802.11g/D1.1-2001", Part 11: Wireless LAN Medium Access Control (MAC) and Physical Layer (PHY) Specifications: Further Higher-Speed Physical Layer Extension in the 2.4 GHz band., 2003.

[7] H. Boelcskei, D. Gesbert, C. B. Papadias, and A.J. van der Veen, "Space-time wireless systems: from array processing to MIMO communications", presented at Cambridge University Press, 2006.

[8]   M. Sauer, and A. Kobyakov, "Fiber-radio antenna feeding for MIMO systems," Asia Optical Fiber Communication & Optoelectronic Exposition & Conference, Shanghai, China, 2008. pp. 1 - 3

[9]   A. Kobyakov, D. Thelen, A. Chamarti, M. Sauer, and J. Winters, "MIMO radio signals over fiber in picocells for increased WLAN coverage," Conference on

Optical Fiber communication/National Fiber Optic Engineers Conference, OFC/NFOEC, San Diego, USA, 2008, pp. 1 - 3

[10]   G. S. D. Gordon, M. J. Crisp, R. V. Penty, and I. H. White, "Experimental evaluation of layout designs for 3×3 MIMO-enabled Radio-Over-Fiber distributed antenna systems," IEEE Trans. Vehicular Technol., vol. 63, pp. 643-653, 2014.

[11] K. Zhu, M. J. Crisp, H. Sailing, R. V. Penty, and I. H. White, "MIMO system capacity improvements using radio-over-fibre distributed antenna system technology," presented at the Opt. Fiber Commun. Conf. and Exposition and the National Fiber Opt. Engineers Conf., Los Angeles, CA, 2011.pp. 1-3

[12]   T.Yamakami, T.Higashino, K.Tsukamoto, S.Komaki, "An experimental investigation of applying MIMO to RoF ubiquitous antenna system," IEEE Int. Top. Meet. on Microw. Photon. and 9th Asia-Pacific Microw. Photon. Conf (MWP/APMP), Gold Coast, Australia, 2008. pp. 201 - 204.

[13] W.C.Y. Vertical vs. Horizontal Separations for Diversity Antennas. Available:http://www.commscope.com/docs/antenna_separation_article_ta

[14]   E. M. Vitucci, L. Tarlazzi, F. Fuschini, P. Faccin, and V. Degli-Esposti, "Interleaved-MIMO DAS for indoor radio coverage: concept and performance assessment," IEEE Trans. Antennas and Propagation., vol. 62, pp. 3299-3309, 2014.

[15]   T. Chrysikos, G. Georgopoulos, and S. Kotsopoulos, "Site-specific validation of ITU indoor path loss model at 2.4 GHz," IEEE International Symposium on a World of Wireless, Mobile and Multimedia Networks & Workshops, Kos, Greece, 2009. pp. 1 - 6

[16]   "Coverage or capacity – making the best use of 802.11 n," Juniper Networks

[17] C. Kim and J. Lee, "Dynamic rate-adaptive MIMO mode switching between spatial multiplexing and diversity" EURASIP Journal on Wireless Communications and Networking, 2012:238.

CHAPTER 4

EXPERIMENTAL VERIFICATION OF MULTI-ANTENNA SCHEMES IN RADIO-OVER-FIBRE DISTRIBUTED ANTENNA SYSTEM

4.1. Introduction

In Chapter 2, experimental works on wireless MIMO performance through the use of radio-over-fibre distributed antenna systems (RoF-DAS) have been reviewed, with a particular focus on those using widely separated antennas. Also, in Chapter 3, two practical issues encountered when transmitting MIMO signals in a RoF-DAS, the fibre lengths difference and the power imbalance effects, have been analysed. However, these works were based on commercial products and the specific MIMO algorithms used within these products were unknown. Several works have used specific multi-antenna algorithms in RoF-DAS, for example, a precoding algorithm was demonstrated in [1] to show that centralized joint/cooperative processing could provide significant gains when compared to non-cooperative transmission. In [2], a space-frequency block coding (SFBC) algorithm was used in multiple-input single-output (MISO) scheme to show improved performance over single antenna transmission.

In this Chapter, specific single-input multiple-output (SIMO), MISO and MIMO algorithms are compared in an experimental RoF-DAS using user-defined processing functions for the signals. The benefits of selection combining (SC), equal gain combining (ECG) and maximal ratio combining (MRC) algorithms are experimentally investigated in a RoF-DAS uplink with a transmitting mobile unit placed at different locations in a typical office environment and the OFDM signals gathered through two RAUs and brought back to the central unit for processing (a 1x2 SIMO scheme). Also, the benefit of Alamouti space time block coding (STBC),

delay diversity (DD) and transmit antenna selection (TAS) algorithms are experimentally investigated in the RoF-DAS downlink where signals from two transmitting RAUs are encoded and sent to one receiving mobile unit (2x1 MISO scheme). Then, the effect of the greater channel decorrelation with two separated RAUs in a RoF-DAS each transmitting independent streams of data to one mobile unit with two receiving antennas (2 x 2 MIMO scheme) using the zero-forcing (ZF) algorithm to remove intersymbol interference (ISI) while the two independent data streams are multiplexed is investigated. In addition, the benefit of transmit/receive diversity for a 2x2 MIMO scheme using Alamouti STBC and DD-MRC are also investigated. Finally, the effect of wide antenna separation in RoF-DAS with MRC, Alamouti STBC and zero-forcing algorithms are investigated. All these algorithms are discussed in detail in the next section.
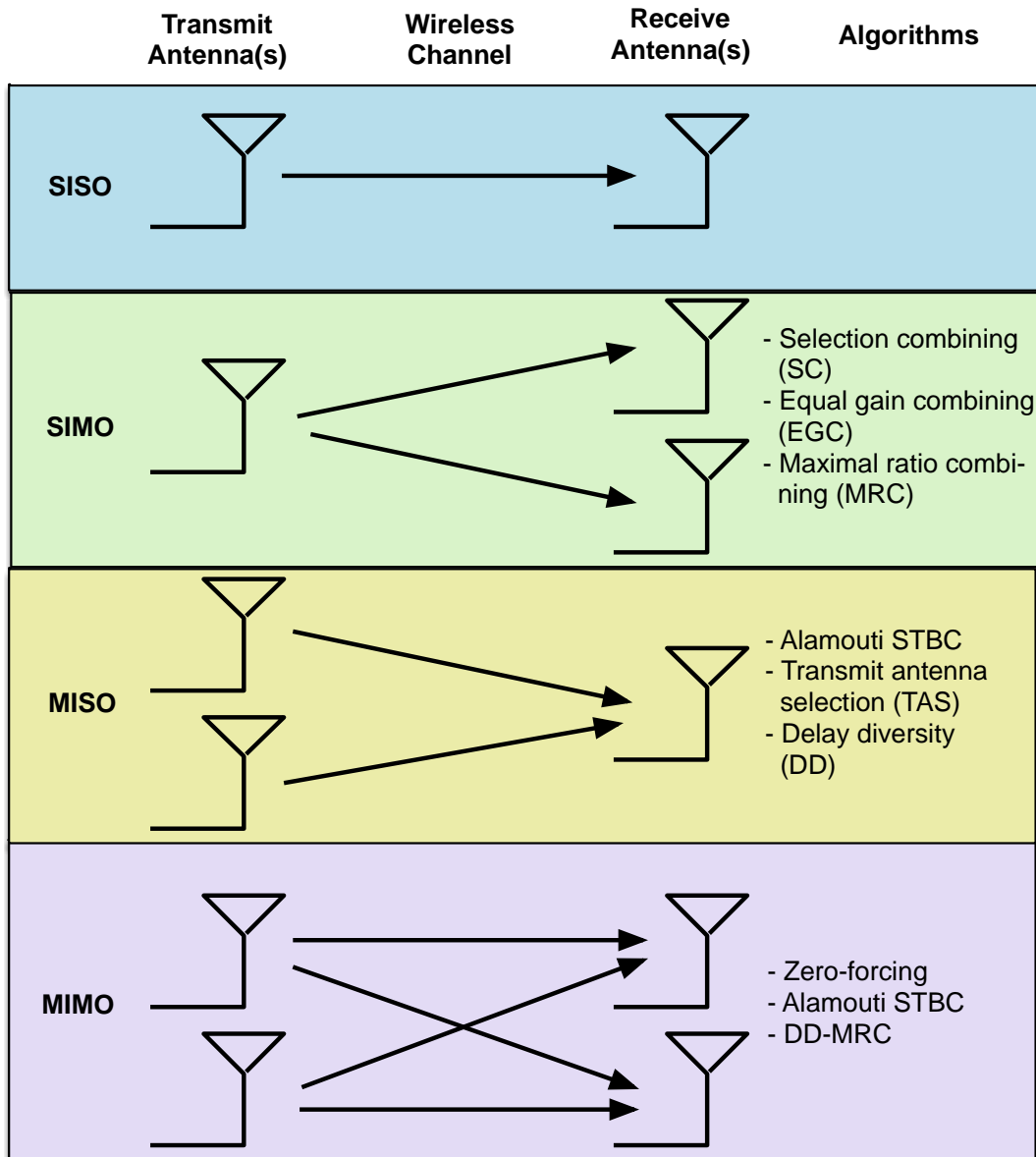
Figure 4.1 Description of SISO system and Multi-antenna configurations

4.2. Selected multi-antenna scheme algorithms

Multi-antenna schemes as shown in Fig. 4.1 comprise different transmit and receive antenna configurations used to enhance the performance of a wireless system compared to single-input single-output (SISO) systems. These schemes use different coded algorithms to process their data and they are discussed as follows.

4.2.1. Single-input multiple-output (SIMO) scheme algorithms

The SIMO scheme can be classified as a receive spatial diversity technique; it is often used in cellular uplinks, where the mobile device has one antenna but there is receive diversity at the base station [3]. There are several receive diversity combining algorithms that can be used for SIMO scheme, the most popular ones being selection combining (SC), equal gain combining (EGC) and maximal ratio combining (MRC) algorithms. SC works by selecting the receive antenna with the highest signal power and ignores the signal from the other antenna to perform detection based on the selected signal path. Using EGC, the estimated channel phase is applied to the received signal to adjust its phase in order to produce the best possible signal. SC is less complex than EGC algorithm in terms of hardware complexity, since it only utilizes one RF chain. MRC on the other hand has more hardware complexity than SC but its performance is better. The estimated channel amplitude and phase are applied to the received signal using (4.1) to maximize the post-combining signal-to-noise ratio (SNR) [4].

$$x = (\ |h_{11}|^2 * y_1) + (|h_{21}|^2 * y_2) \tag{4.1}$$

where h_{11} and h_{21} are the estimated channel co-efficient and y_1 and y_2 are the received signals from the first and second receivers respectively. Using MRC, the better signal from the multiple diversity antennas are amplified while the poorer signal is attenuated to achieve the best performance compared to SC. EGC is similar to MRC but its performance is slightly inferior, since it only applies the estimated channel phase to the received signals ignoring the amplitude. However, the hardware complexity for MRC is higher than EGC. MRC requires co-phasing, weighting and summing circuits resulting in complicated implementation compared to EGC that only requires co-phasing and summing circuits [5]. The performance of these three receive diversity combining algorithms have been analysed in [6-9] to show improved performance compared to a SISO system but not in an experimental DAS or RoF-supported system.

4.2.2. Multiple-input single-output (MISO) scheme algorithms

The MISO scheme can be classified as a transmit spatial diversity technique where most of the hardware complexity and computation burden is on the transmitter side in order to reduce power consumption at the receiver side. Alamouti Space-time block coding (STBC), transmit antenna selection (TAS) and delay diversity (DD) are algorithms that can be used to achieve diversity gain in MISO scheme.

STBC is an attractive algorithm in the MISO scheme, used in the downlink to encode signals transmitted from multiple antennas to a single (or multiples) receive antenna, and it is an optional feature in IEEE 802.11n/ac. Alamouti coding [10] is the most attractive STBC algorithm because it is simple and does not require feedback of channel state information to the transmitter. The encoded signals using Alamouti STBC are transmitted from two transmit antennas over two symbol periods. The first period has two symbols x_1 and x_2, simultaneously transmitted, while during the second period, these symbols are transmitted again but as $-x_2^*$ from the first antenna and x_1^* from the second antenna. The Alamouti STBC decoder restores the transmitted symbol periods using (4.2) and (4.3):

$$x_1 = h_{11}y_1 + h_{12}y_2 \qquad\qquad (4.2)$$

$$x_2 = -h_{11}y_2^* + h_{12}y_1^* \qquad\qquad (4.3)$$

where y_1 and y_2 are the received signals from the two transmit antennas over two-symbol periods and h_{11}, h_{12} represent the channel co-efficients estimated from the transmitted preamble symbols. Higher diversity order can be achieved when there is less spatial correlation between the transmitting antennas making their channels independent for the receiver to decode [11].

Delay diversity is another simple MISO scheme that can achieve diversity gain at the receiver without changing the SISO receiver structure. It is used to reduce the impact of possible unwanted signal cancellation that can occur if the same signal is transmitted from multiple antennas. In delay diversity, the original symbol is transmitted from the first antenna while the second antenna transmits a delayed replica of the original symbol. A 180° phase shift is usually introduced to achieve

this delay when the number of transmit antennas are two in order to position the signals on the peak of the frequency response that results from the addition of a delay [12].

Similar to selection combing (SC) receive diversity discussed in 4.2.1, transmit antenna selection (TAS) is the transmit diversity version of SC used at the transmitter side. Unlike SC, TAS requires a feedback path from the receiver to the transmitter. The feedback provides the transmitter with knowledge of the transmit antenna with the highest equivalent receive SNR so that the transmitter can switch off the transmit antenna with the low SNR and transmit only from antenna with the high SNR. These MISO scheme algorithms have been demonstrated in [13-16] to reduce error performance in an unstable wireless fading channel and improve performance over a SISO system, but they have not been demonstrated in an experimental RoF-DAS.

4.2.3. Multiple-input multiple-output (MIMO) scheme algorithms

A MIMO scheme uses multiple antennas at the transmitter and receiver to improve the wireless system reliability through spatial diversity and/or increasing data rates through spatial multiplexing. A spatial multiplexing MIMO scheme, transmits separate data on multiple antennas at the same time to multiple receive antennas. The challenging task for the receiver is to detect the separate data. Simple linear detection algorithms can restore the separate data. Such algorithms treat all transmitted signals as interference except for the desired signals from the target transmit antennas. Zero-forcing (ZF) linear detection algorithm nullifies the interfering signal by the following weight matrix [17]:

$$\mathrm{W}_{ZF} = (\mathrm{H}^H \mathrm{H})^{-1} \mathrm{H}^H \qquad (4.4)$$

where $(.)^H$ denotes the Hermitan transpose operation used to invert the effect of the channel. An evaluation of some detection schemes in [18] has shown that the zero-forcing linear detection algorithm, which is the simplest algorithm for MIMO, can produce similar error rate performance to the Vertical-Bell Laboratories Layered Space-Time (V-BLAST) detection algorithm that is adopted for MIMO in many

recent standards. The integration of MIMO schemes and RoF-DAS can further bring about improvement in throughput performance taking advantage of the largely separated multiple RAUs.

Spatial diversity gains can also be achieved in MIMO schemes using the Alamouti STBC algorithm. This technique is referred to as transmit/receive spatial diversity. The signal processing and coding at the transmitter for MIMO Alamouti STBC is the same as that of MISO scheme. The additional processing is the receive diversity gain as a result of the additional antenna at the receiver side. MIMO Alamouti STBC decoder uses the channel coefficients (h_{11}, h_{21}, h_{12}, h_{22}) estimated from the transmitted preamble symbols with the received symbol to decode the two symbol periods. It is represented as:

$$x_1 = h_{11}y_1 + h_{12}y_2{}^* + h_{21}y_1 + h_{22}y_2{}^* \qquad (4.5)$$

$$x_2 = -h_{11}y_2{}^* + h_{12}{}^*y_1 - h_{22}\,y_2{}^* + h_{21}\,y_1{}^* \qquad (4.6)$$

Delay diversity and MRC algorithms were discussed in MISO and SIMO schemes respectively to achieve transmit and receive diversity gains. These algorithms can be combined in a MIMO scheme, i.e. DD at the transmitter-side and MRC at the receiver-side to provide spatial diversity gain over conventional SISO system.

4.3. Experimental Setup

The experimental setup for downlink (MISO and MIMO schemes) and uplink (SIMO scheme) are similar but the arrangements are different and these will be discussed in this section.

4.3.1. Downlink experimental setup

Fig. 4.2 shows the downlink multi-antenna scheme experiment setup. The baseband signal was processed offline at the transmitter side using MATLAB/Simulink software. Pseudo-random data symbols of 88.614MSps were generated and converted to parallel sets of symbols for the 16-QAM-OFDM processing. The OFDM signal processing includes 512 IFFT size, 8 pilot subcarriers for phase tracking, 112 guard bands (zero padding) including 1 DC subcarrier, and 1/8 CP size; 304 OFDM symbols were transmitted including 1 OFDM preamble symbol used for channel estimation (other parameters are given in Table 4.1).
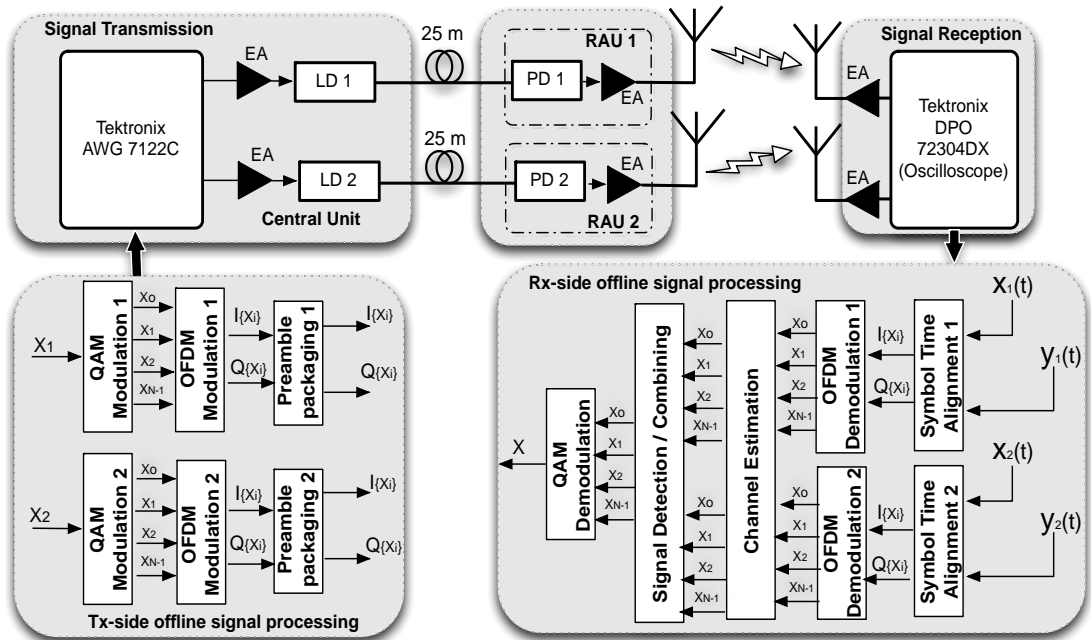

Figure 4.2 The downlink Experimental setup for 2x2 MIMO over Fiber EA= Electric amplifiers PD=Photodetector, LD=Laser diode, RAU=Remote antenna unit

Table 4.1 OFDM signal parameters

Parameters	Values
Carrier Frequency	2.4GHz
IFFT Length	512
Guard bands (zero padding)	111
DC subcarrier	1
Number of Pilots	8
CP size	1/8
Bandwidth	152MHz
DL transmit power	+11dBm
UL transmit power	+3 dBm
Antenna Gain	9dBi
RoF link gain	-25dB
Symbol rate	88.614MSps
Sample period (XDelta)	5.12e-6 ms

The I/Q samples were downloaded onto the Tektronix Arbitrary Waveform generator (AWG) 7122C channels (channel 1 and 2) using RFXpress software running on the AWG. The sample rate was set to 195.31 MHz (1/XDelta) and the signal was upconverted to radio frequency (RF) at a carrier frequency of 2.4GHz. The amplitude of the signal from the AWG was set to 0.112Vp-p (equivalent to -15dBm) to ensure the signal was operating in the linear region of the connected Mini-Circuit amplifiers (ZX60- 2522M+) with a further 10dB power back off due to the peak-to-average power ratio (PAPR) OFDM requirement. The amplifiers were biased to produce 20dB gain and the RF signal was directly modulated onto a distributed feedback (DFB) laser diode.

The laser diode used for the setup was an uncooled 1310 nm Emcore DFB laser diode [19] with a built-in isolator in a coaxial package and with a slope efficiency of 0.25 W/A and a threshold current of 10 mA. The RF signal was used to modulate the DFB

laser diodes and the resultant optical signals were transmitted over 25m length single mode fibres (SMF) from the central unit to a separate testing room, as shown in Fig. 4.3. The RAUs placed in the testing room consist of Appointech 2.5 GHz pin module [20] photodiodes (PDs) with a responsivity of 1 A/W at a wavelength of 1310 nm, which were biased at -5V for direct detection. The PDs were connected to Mini-Circuits amplifiers (ZX60-2531M+), biased to produce 28dB gain, increasing the signal level before wireless transmission. The transmit power before the antenna was +8dBm and the antenna gain is approximately 9dBi.
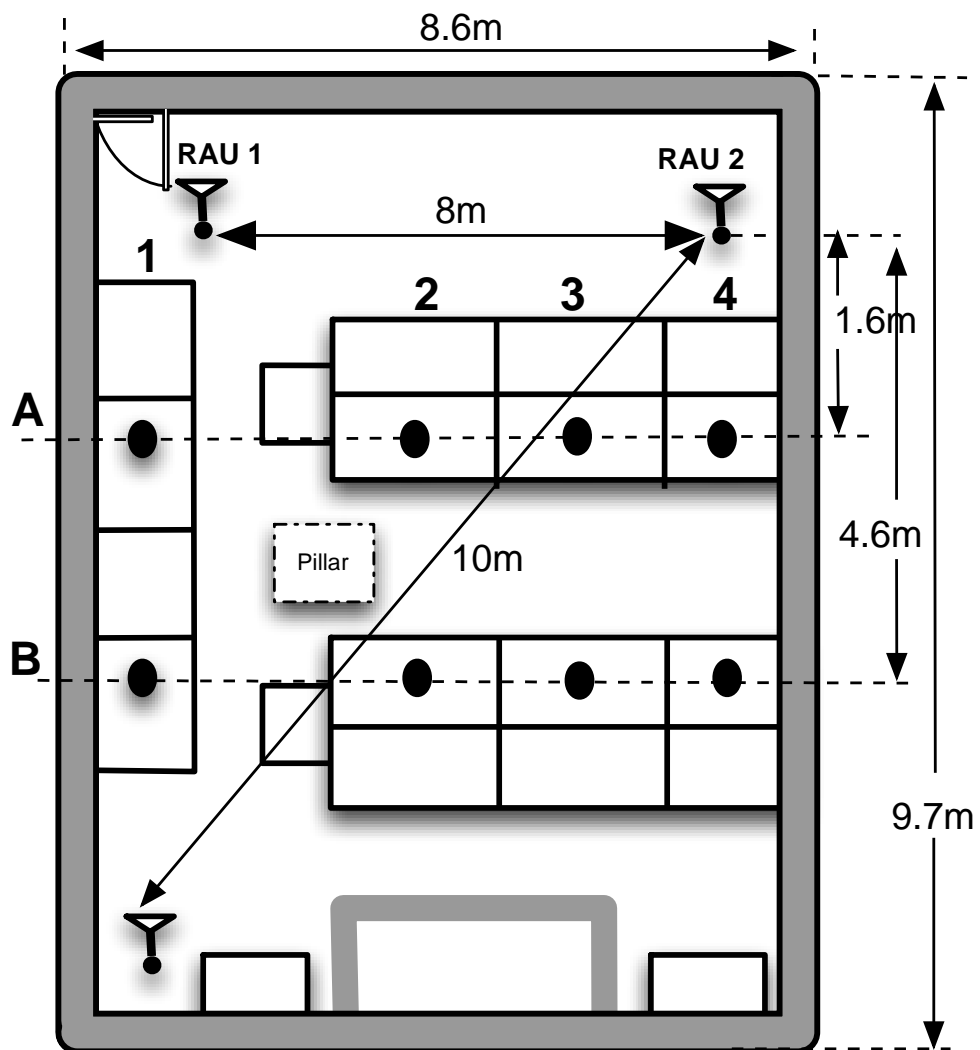

Figure 4.3 Testing room layout, an open plan office. A, B (1-4) represent the positions of the mobile user (the Oscilloscope/AWG)

The testing room layout in Fig. 4.3 represents a typical office, fitted with common office furniture (desks, chairs, shelves) and computers, which causes multipath fading as the signals are being transmitted from the RAUs. The room is 9.7 by 8.6 m enabling large antenna separation and different receive antenna positions. The RAUs were placed on a wooden platform extension in the front of the room so that the signals were generally radiating above the desktops. The receiver, a Tektronix DPO 72304DX (Oscilloscope) was moved around the room to capture the OFDM signal at different positions (A1 to A4 were positions close to the RAUs while B1 to B4 were positions further away from the RAUs). The received OFDM signals were then amplified with low noise figure RF amplifiers to boost the signal strength before saving the signals in MATLAB format for receiver side offline processing.

The receiver-side offline processing of the baseband complex signal captured at the Oscilloscope is shown in Fig. 4.2; it includes a MATLAB script written to perform OFDM symbol time alignment to detect the starting point of each OFDM symbol, followed by OFDM demodulation involving the removal of the CP, guard bands (zero padding) and DC subcarrier, leaving the pilot and data symbols for channel estimation and detection. The preamble symbol was used for least square (LS) channel estimation and the pilot subcarriers for phase tracking. The signal combining/detection (depending on the multi-antenna scheme algorithm) was done before the QAM demodulation.

4.3.2. Uplink experimental setup

Fig. 4.4 shows the uplink experimental setup, this setup was used for the 1x2 SIMO scheme experiment and it is the reverse of the downlink setup. The transmitted signal was processed using the same steps and parameters as the downlink but the Tektronix AWG 7122C was now at the mobile unit positions in the testing room. The amplitude of the signal from the AWG was set to 0.035Vp-p (equivalent to -25dBm) to ensure the signal was operating in the linear region of the connected Mini-Circuits amplifier (ZX60-2531M+). The amplifier was biased to produce 28dB gain and the transmit power before the antenna was +3dBm and the antenna gain is approximately 9dBi.
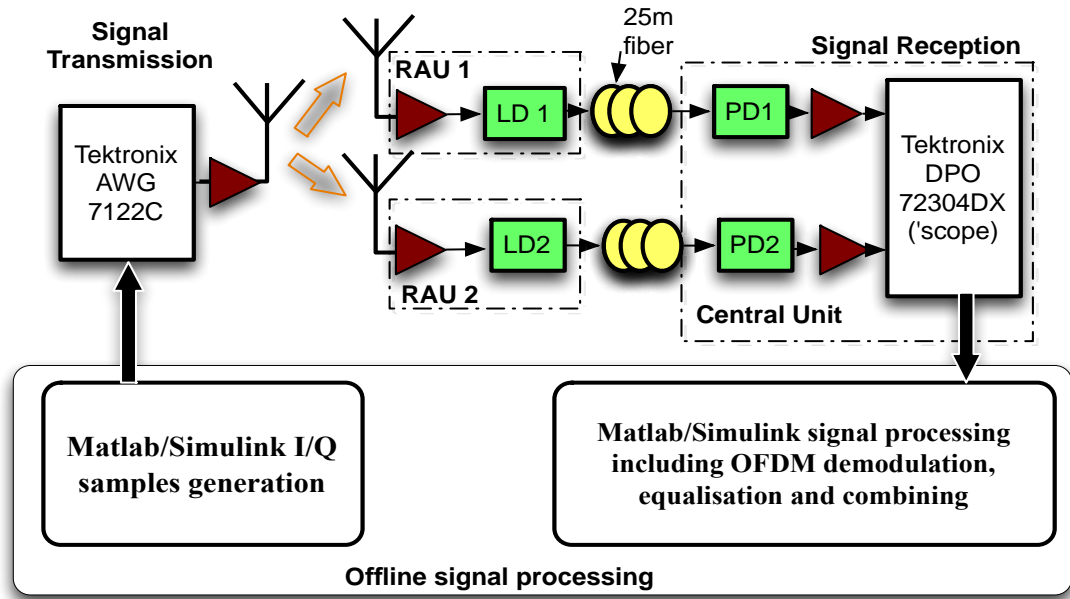
Figure 4.4 The uplink experimental setup for 1x2 SIMO over Fibre

The transmitted RF signals were received at the RAUs, where once again, amplifier gains were set to use the linear region of the laser diode and at the point where the received signal would experience less noise and distortion. Both laser diodes were connected to 25m lengths of single mode fibre (SMF) and then to the photodiodes in the CU. The RoF link, consisting of the direct modulated laser, optical fibre and direct detection Photodiode (PD) had a loss of 25dB, therefore low noise figure Mini-Circuits amplifiers (ZX60-242GLN+) were used before the oscilloscope (now in the CU) to boost the received signal power level. The received signals are saved in MATLAB format in the oscilloscope so that they can be demodulated offline and combined using SIMO scheme algorithms.

4.4. Error performance results

The result in Fig. 4.5 shows EVM measurements for the SISO system with the mobile unit placed at position A3, the closest position to the RAU. The experimental setup for downlink and uplink are different as shown in Fig. 4.2 and 4.4, which is typical for most bi-directional RoF links, [21], [22], therefore they both require separate optimization and the imperfect part of the uplink curve in Fig. 4.5 is due to linearity

issues with the amplifier. From Fig. 4.5, it can be seen that the lowest downlink EVM of 11.7% is achieved at +11dBm transmit power, and the lowest uplink EVM of 10% is achieved at +3dBm transmit power. To compare the multi- antenna schemes with SISO, the overall transmit power is kept the same.
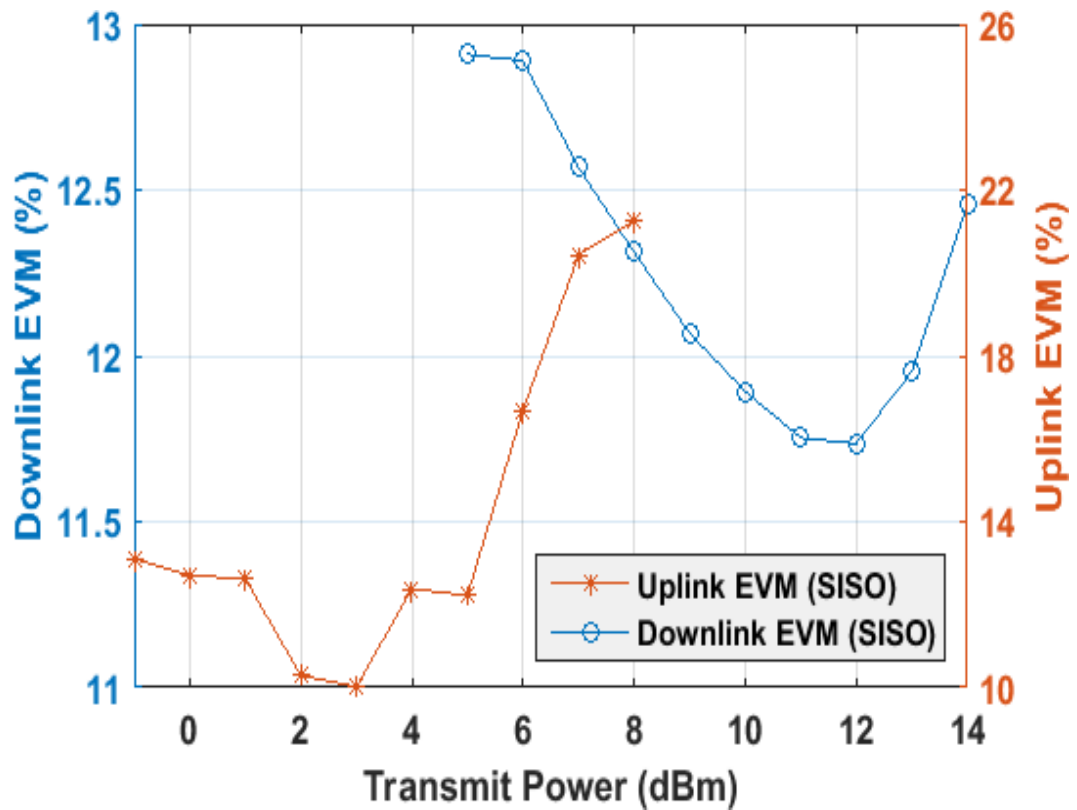
Figure 4.5 EVM of downlink and uplink signal transmitted from the RAU as the transmit power is increased to determine the optimum transmit power for measurement.

4.4.1. 1x2 SIMO scheme uplink results

The EVM and SER of selection combining (SC), equal gain combing (EGC) and maximal ratio combining (MRC) algorithms used to process the results of 1x2 SIMO scheme uplink experiment, are shown in Figs. 4.6, 4.7 and 4.8. The algorithms were written as MATLAB scripts based on description in 4.2.1 to combine the baseband signals received by two RAUs. Specifically, the MRC is a modified script in program 10.1 of [17] (as shown in Appendix A) where each received signal branch is

multiplied by a weight factor. The measurements were taken when the inter-RAU distance was approximately 0.3m and 4m to examine the performance of the schemes with close and large antenna separation. The results were obtained as the mobile unit was moved around the testing room (shown in Fig. 4.3) to the different positions indicated.

The result in Figs. 4.6, 4.7 and 4.8 shows that the EVM and SER are reduced in all transmitter's positions compared to the SISO system when the RAUs were placed closely together (0.3m separation) and processed with their respective algorithms. However, with 4m antenna separation, the EVM and SER performance of SC algorithm slightly reduced in some measured positions when compared with 0.3m antenna separation while for EGC and MRC algorithms, there was a consistent reduction in EVM and SER performance in all transmitter's positions.

Figure 4.6 SER and EVM of uplink **1x2 SC-SIMO** measured at inter-RAU distance of 0.3m and 4m at different positions compared to **SISO**
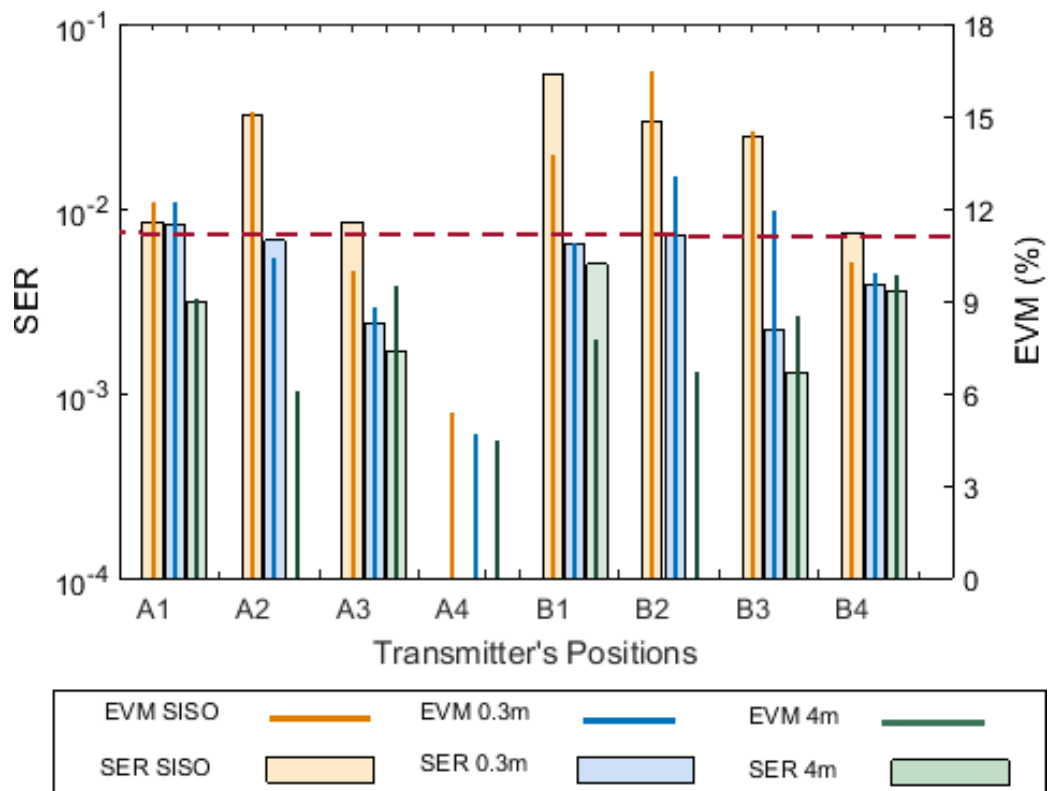
Figure 4.7 SER and EVM of uplink **1x2 EGC-SIMO** measured at inter-RAU distance of 0.3m and 4m at different positions compared to **SISO**.

Figure 4.8 SER and EVM of uplink **1x2 MRC-SIMO** measured at inter-RAU distance of 0.3m and 4m at different positions compared to **SISO**.

Fig. 4.9 compares the results of the three different combining algorithms, SC, EGC and MRC used to process 1x2 SIMO scheme uplink results when the inter-RAU separation was 4m. MRC algorithm provides the optimum EVM performance compared to other algorithms. This confirms the discussion in 4.2.1 that MRC achieves the best performance in the sense that it maximizes the post-combining SNR.
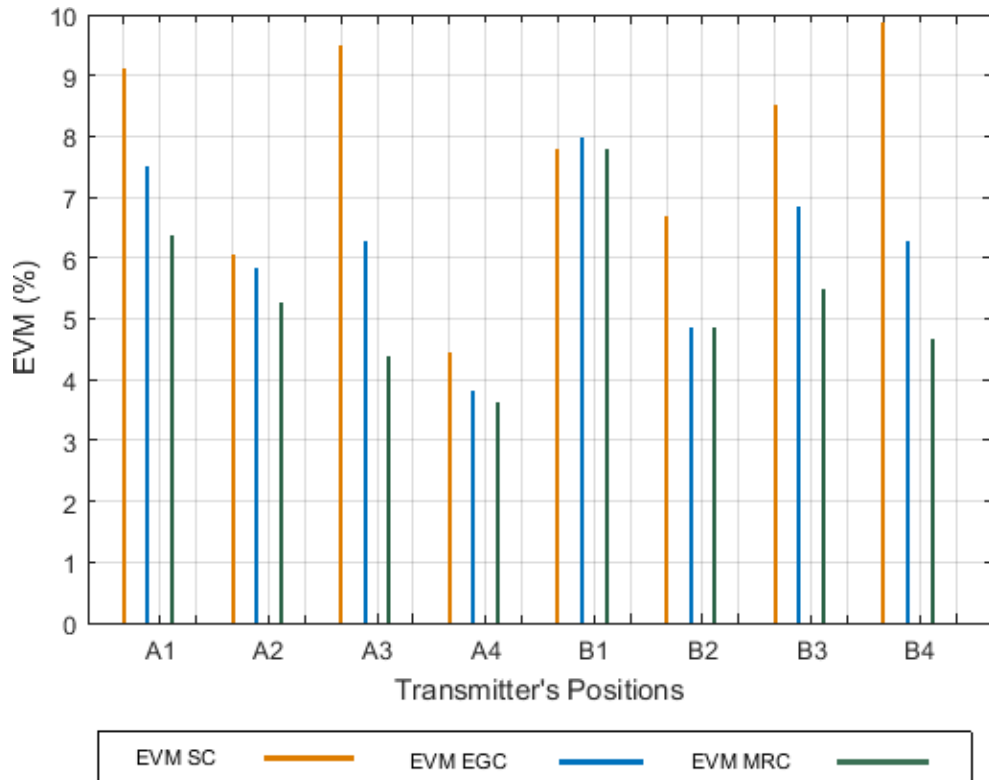
Figure 4.9 EVM of **SC**, **EGC** and **MRC** SIMO scheme measured at inter-RAU distance 4m at different positions A, B (1-4)

4.4.2. 2x1 MISO scheme downlink results

Figs. 4.10, 4.11 and 4.12 shows the measurement results for 2x1 MISO scheme downlink using Alamouti STBC, transmit antenna selection (TAS) and delay diversity (DD) processing algorithm respectively. Alamouti STBC encoding/decoding was done using the orthogonal space-time block code (OSTBC) encoder in the MIMO library of the MATLAB/Simulink communication system toolbox [23] to encode the input data and the OSTBC decoder to extract the symbols

that were encoded while TAS was achieved by transmitting the same signals from the two RAUs, and the strongest signal was determined by the highest MER obtained from the demodulated signals. This information was fed back to the transmitter and the RAU with the lower MER was switched off leaving the RAU with the high MER to transmit. DD was achieved by introducing 180° phase shift in baseband to the second OFDM symbol branch before sending it to the AWG while the first OFDM symbol branch was sent without phase shift.

Figure 4.10 SER and EVM of downlink **2x1 Alamouti STBC-MISO** measured at inter-RAU distance of 0.3m and 4m at different positions compared to **SISO**

Fig. 4.10 shows the EVM and SER results of 2x1 MISO scheme using Alamouti STBC algorithm, it can be observed that the performance improves when the RAUs are at 0.3m antenna separation compare to SISO. However, some of the receiver's positions were still above the 11.2% limit for 16-QAM (shown with the red dash line). When the RAUs were further separated at 4m, the EVM and SER reduces significantly in all receiver's positions and below the 11.2% limit.
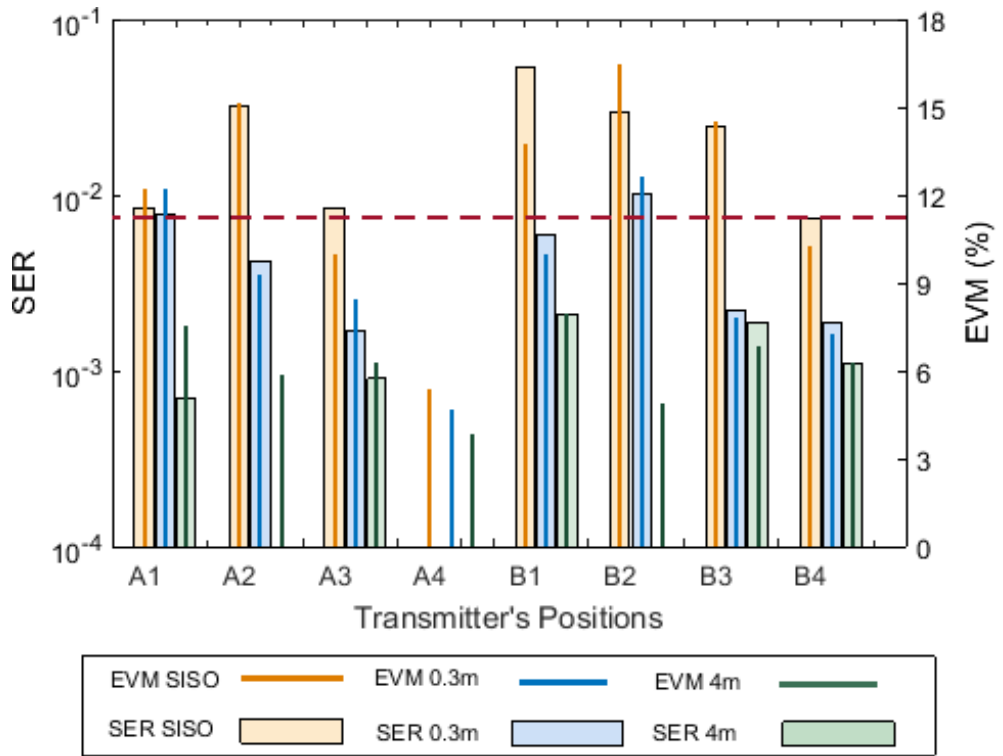
Figure 4.11 SER and EVM of downlink **2x1 TAS-MISO** measured at inter-RAU distance of 0.3m and 4m at different positions compared to **SISO**.
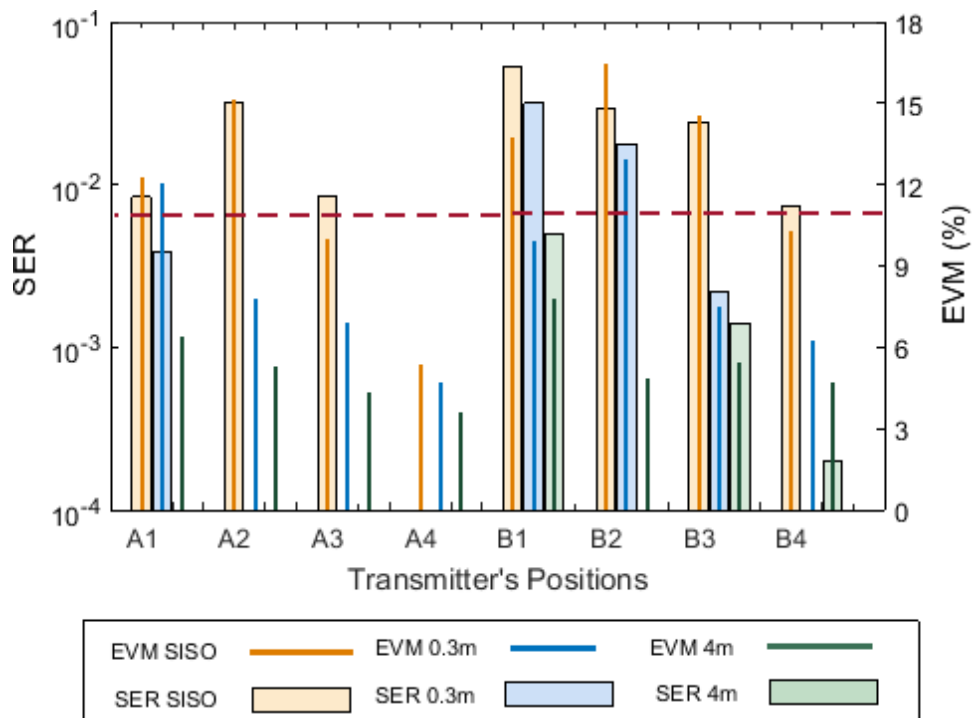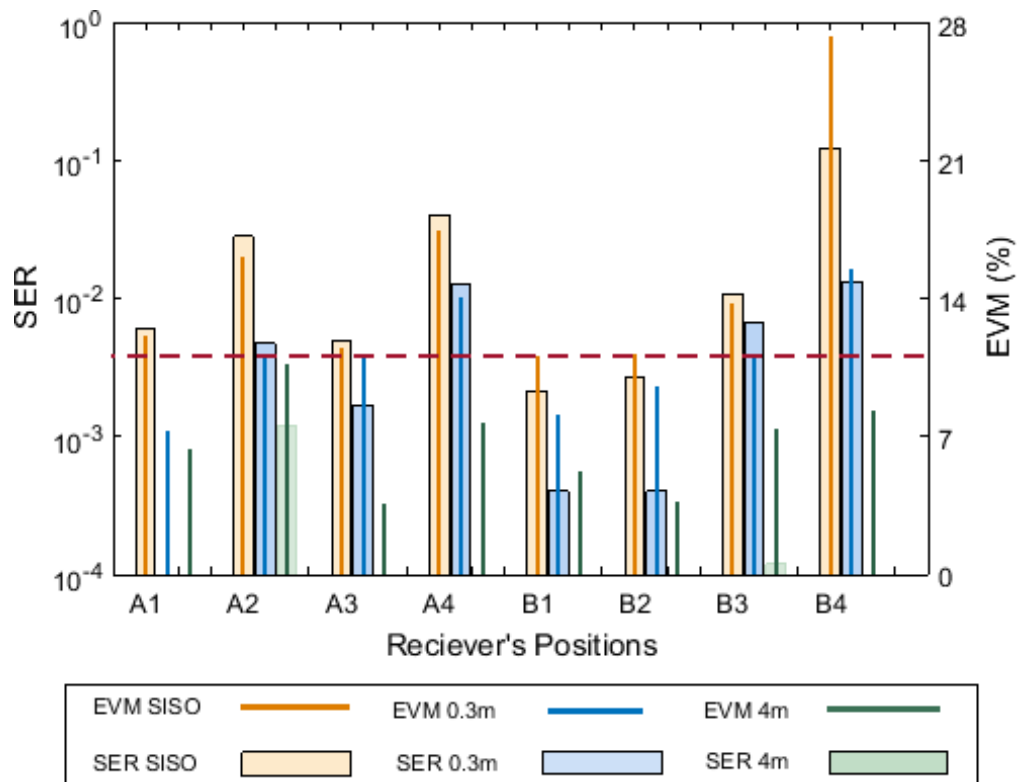

Figure 4.12 SER and EVM of downlink **2x1 DD-MISO** measured at inter-RAU distance of 0.3m and 4m at different positions compared to **SISO**

Figs. 4.11 and 4.12 shows the EVM and SER results using TAS and DD algorithms respectively, it can be observed that at 0.3m antenna separation, the performance improves slightly in most of the receiver's positions when compared to SISO while at 4m antenna separation, the EVM and SER further reduces slightly below the 11.2% limit in most of the receiver's positions.
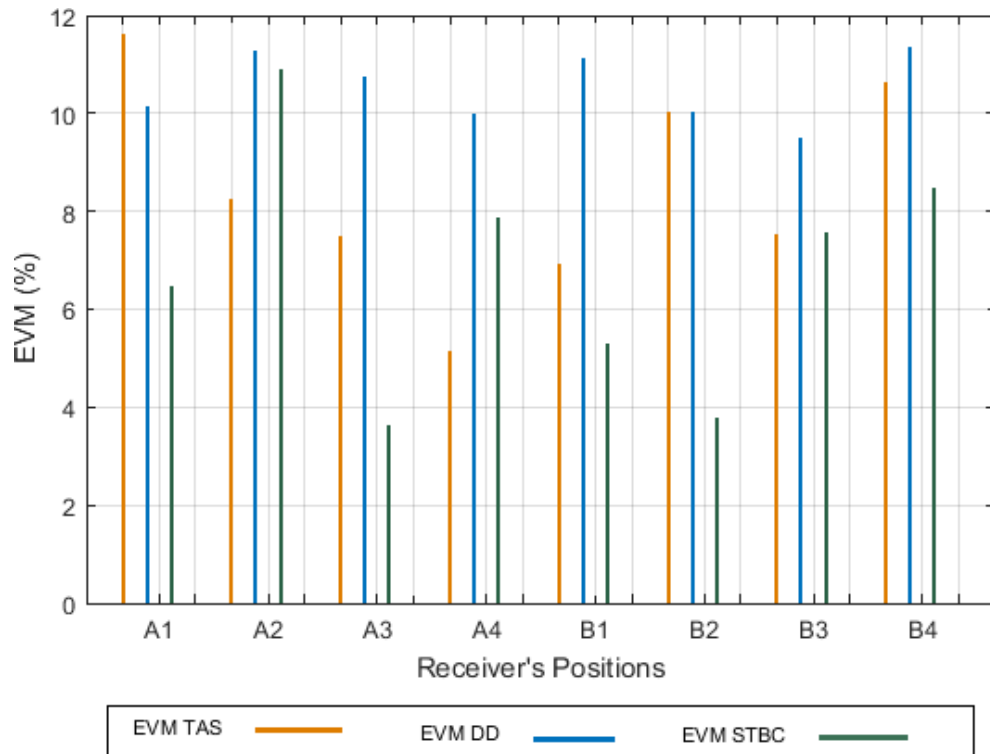
Figure 4.13 EVM of **TAS**, **DD** and **Alamouti STBC-MISO** scheme measured at inter-RAU distance 4m at different positions A, B (1-4)

In Fig. 4.13, the EVM of Alamouti STBC, TAS and DD algorithms are compared when the inter-RAU separation was 4m. It can be observed that the performance of Alamouti STBC algorithm was generally better than other algorithms because it can achieve its full diversity gain with linear processing at the receiver.

4.4.3 2x2 MIMO scheme downlink results

Generally, SIMO and MISO are diversity schemes designed to improve the error performance of conventional SISO wireless links. Spatial multiplexing-MIMO, on the other hand, is used to increase the data rate of the system. The performance of a wireless 2x2 MIMO scheme using zero-forcing algorithm (written as MATLAB script (as shown in Appendix B) based on description in 4.2.3) in a RoF-DAS infrastructure with inter-RAU distances of 0.3m and 4m is shown in Fig. 4.14 in terms of EVM and SER. These results show that when the RAUs are placed close together, EVM and SER are worse than for SISO in most receiver's positions. When the inter-RAU distance is 4m, the EVM is reduced in all receiver positions, below the required 11.2% limit for 16-QAM modulation. It can be seen, therefore, that obtaining any improvement with MIMO is very dependent on the channel decorrelation.

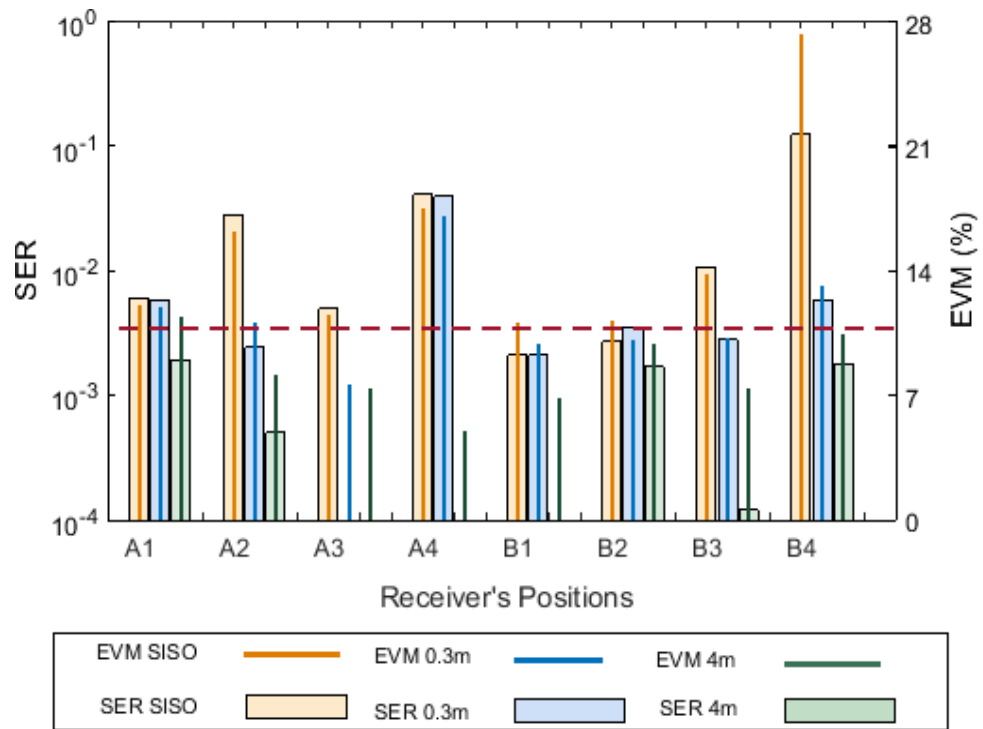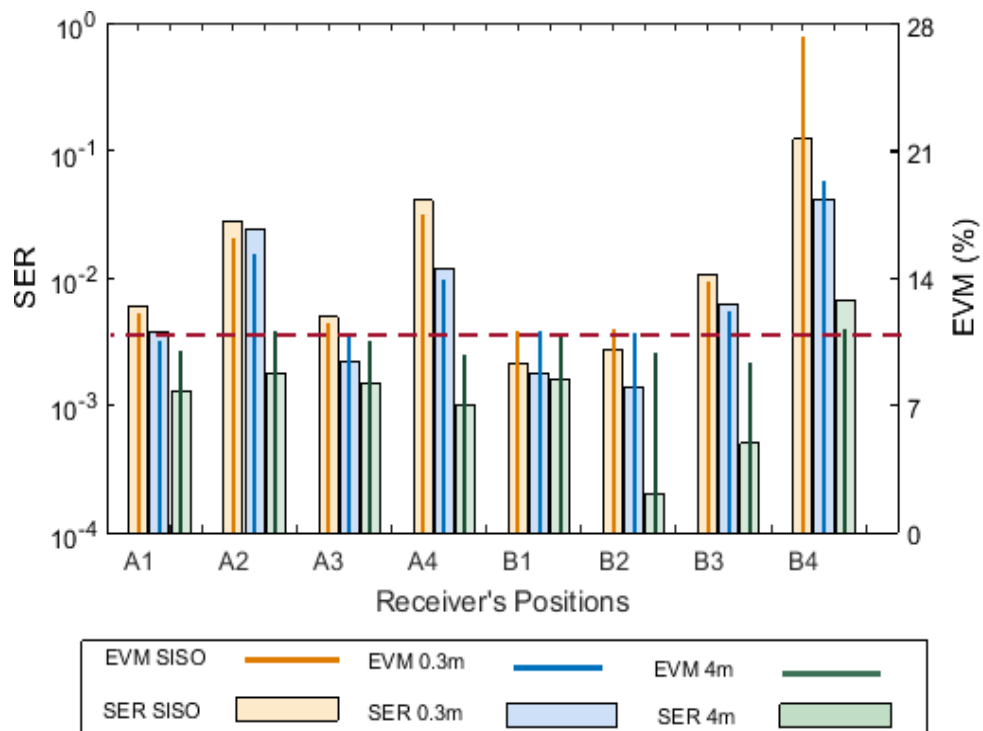Figure 4.14 SER and EVM of downlink **2x2 ZF-MIMO** measured at inter-RAU distance of 0.3m and 4m at different positions compared to **SISO**.

Figure 4.15 SER and EVM of downlink **2x2 Alamouti STBC-MIMO** measured at inter-RAU distance of 0.3m and 4m at different positions compared to **SISO**.

Apart from using a MIMO scheme to increase data rate, it can also be used to increase the reliability of the wireless system. Fig. 4.15 shows the EVM and SER results of the Alamouti STBC algorithm used in a spatial diversity-MIMO scheme when the inter-RAU separation distance was 0.3m and 4m. It can be observed that the EVM and SER performance reduced when the inter-RAU distances was 0.3m and further reduces at 4m antenna separation.

In Fig. 4.16, the EVM of SISO, Alamouti STBC-MISO and Alamouti STBC-MIMO algorithms are compared when the inter-RAU separation was 4m. It can be observed that the EVM and SER reduction using Alamouti STBC algorithm in spatial diversity-MIMO scheme is much greater than when using the Alamouti STBC in a MISO scheme. This is because of the additional antenna in the receiver, which provides receive diversity gain.
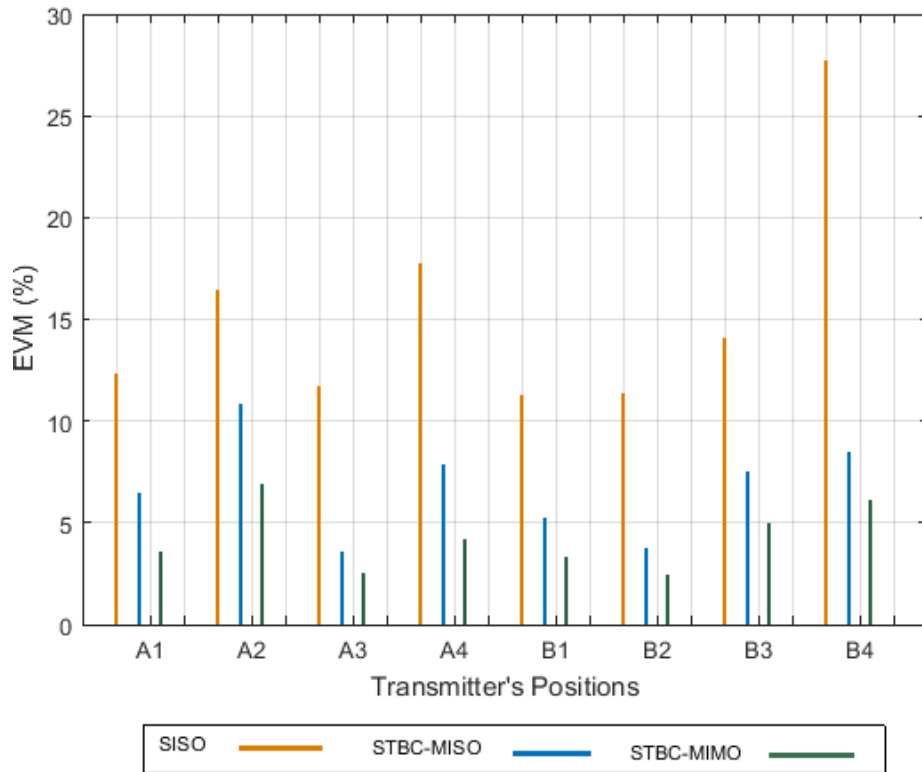
Figure 4.16 EVM of **SISO**, **Alamouti STBC-MISO** and **Alamouti STBC-MIMO** scheme measured at inter-RAU distance 4m at different positions A, B (1-4).
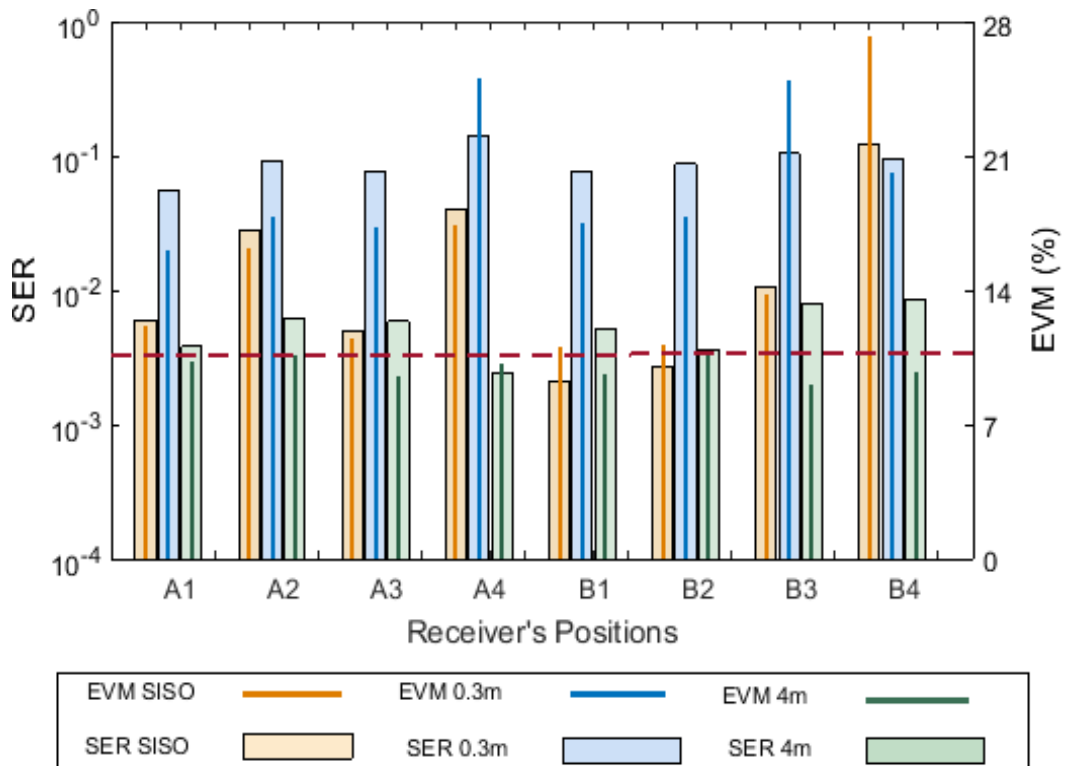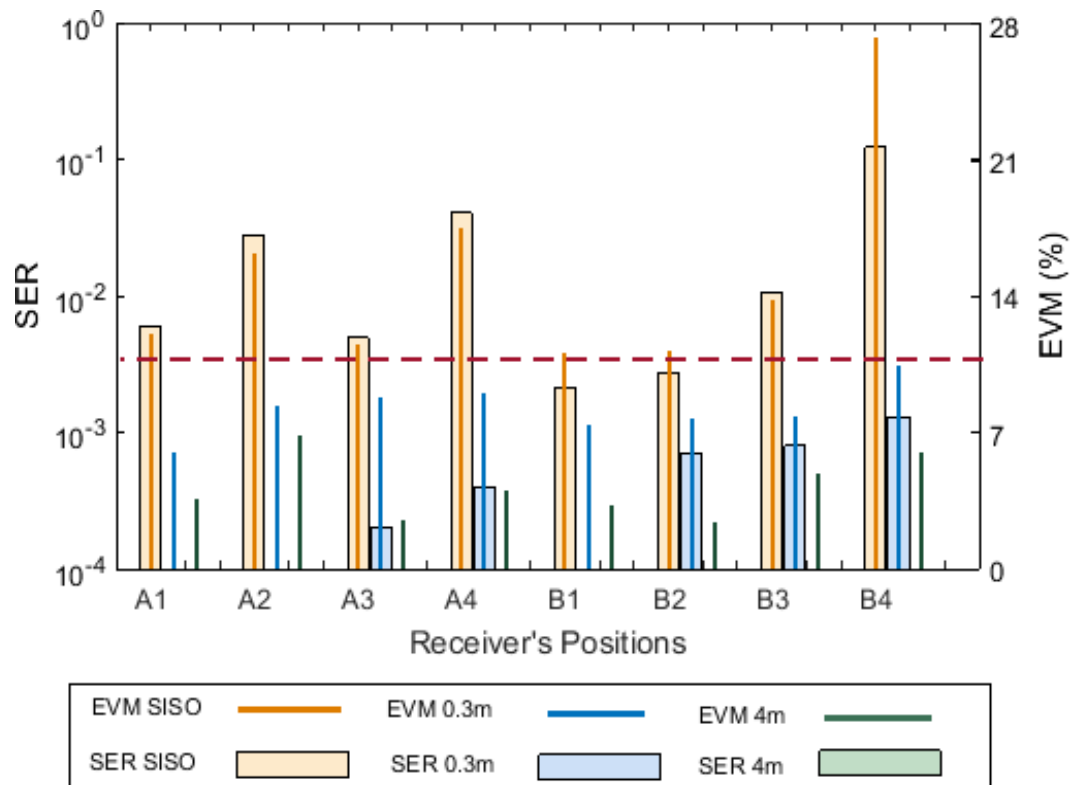

Figure 4.17 SER and EVM of downlink **2x2 DD/MRC-MIMO** measured at inter-RAU distance of 0.3m and 4m at different positions compared to **SISO**.

Fig. 4.17 shows EVM and SER results when DD was used at the transmitter and MRC at the receiver to combine the received signals. The EVM and SER result for 0.3m inter-RAU antenna separation distance when using the combined DD-MRC algorithm reduced slightly when compared to the SISO system but there was a consistent reduction when the antenna separation was 4m.

Figure 4.18 EVM of **Alamouti STBC-MISO**, **MRC-SIMO** and **ZF-MIMO** measured at inter-RAU distance 4m at different positions A, B (1-4).

For comparison purposes, in Fig. 4.18, EVM results at 4m RAU spacing for the optimum algorithms in SIMO and MISO scheme (MRC and STBC Alamouti algorithms) are compared with the MIMO scheme using the ZF algorithm noting that the overall transmit power was the same. Due to the total transit power constraints in Alamouti STBC-MISO scheme i.e. the total power splits into each antenna, the EVM performance of SIMO-MRC was generally better since it provides a power combining in the receiver.

The EVM result for zero-forcing-MIMO scheme shows generally higher EVM than the other schemes due to a trade-off between diversity gain and multiplexing gain for

multi-antenna schemes, the algorithms that maximize one of these can hardly maximize the other simultaneously. Also, zero-forcing, only removing inter symbol interference (ISI), and it is ideal only in noiseless channels since it does not consider noise in data detection. However, it is often used in MIMO schemes since it is the simplest algorithm to implement and is suitable for a RoF-DAS infrastructure when signal-to-noise ratio (SNR) can be increased due to lower path loss. The main objective of the algorithm is increased data rate, which is discussed in the next section.

4.5. Capacity performance results

Figure 4.19 Capacity and MER of downlink **2x1 Alamouti STBC-MISO** measured at inter-RAU distance of 0.3m and 4m at different positions compared to **SISO**.

The result in Fig. 4.19 shows the MER and corresponding capacity, MER was calculated after the signal combining, and the capacity is from equation (2.9), of the downlink Alamouti STBC-MISO scheme. Small improvements in capacity corresponding to the improvements in MER are evident for 2x1 Alamouti STBC-

MISO compared to SISO, and when the RAU separation was increased. As capacity has a logarithmic dependence on SNR (MER), the increases are not as significant as the linear EVM and SER reductions shown in Fig. 4.10.
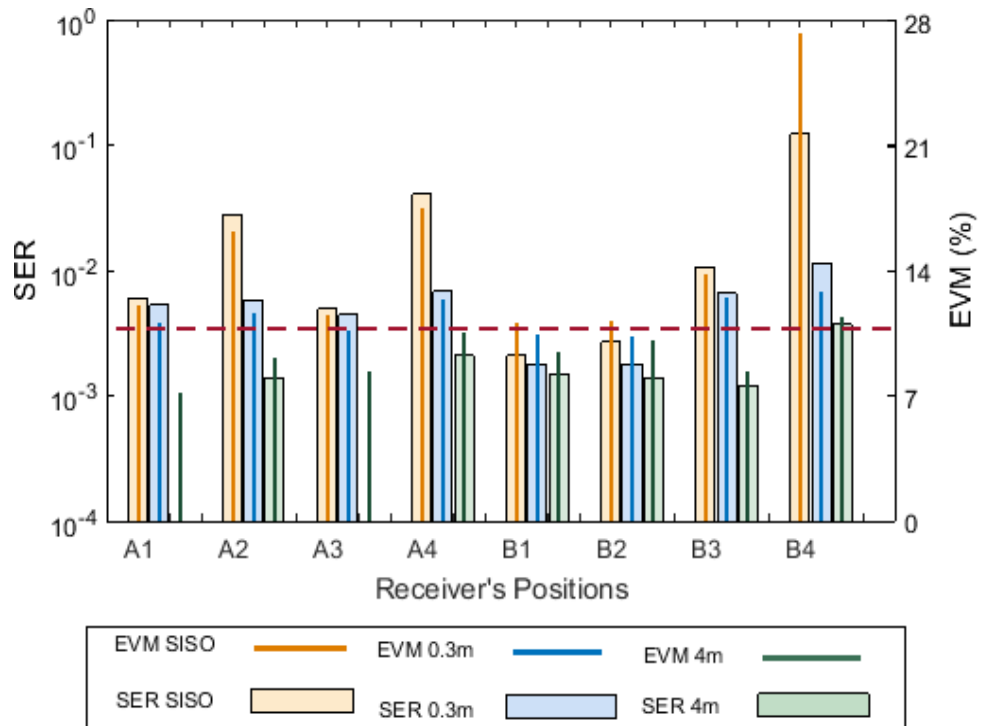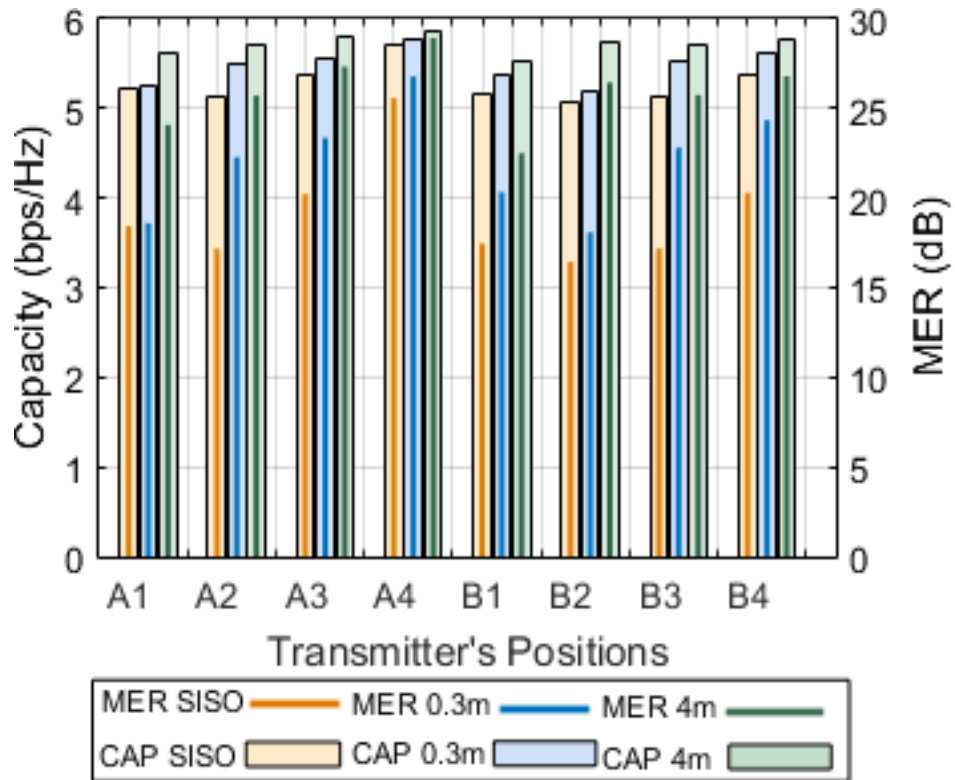

Figure 4.20 Capacity and MER of downlink **1x2 MRC-SIMO** measured at inter-RAU distance of 0.3m and 4m at different positions compared to **SISO.**

Fig. 4.20 shows the MER and capacity, using equation (2.8), of the uplink 1x2 SIMO MRC scheme. Again, small but consistent improvements in capacity can be seen for the SIMO compared to the SISO system, using equation (2.9), especially with the larger RAU separation. However, this is still a logarithmic gain, and to improve the capacity linearly, we examine the 2x2 MIMO scheme that is expected to provide pure multiplexing gains.
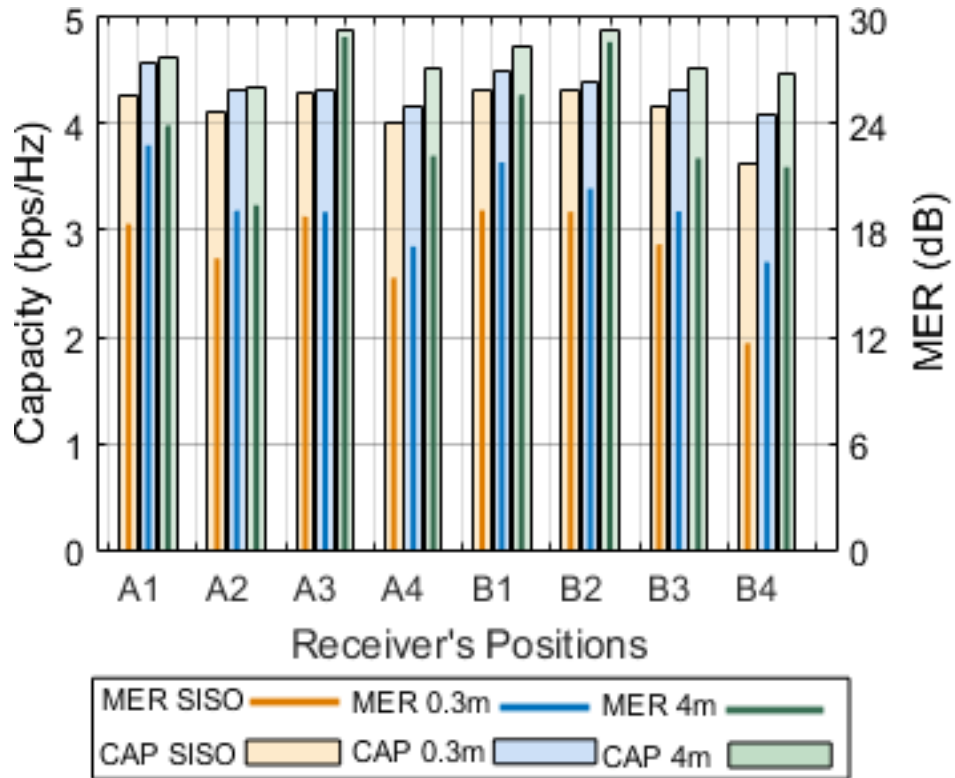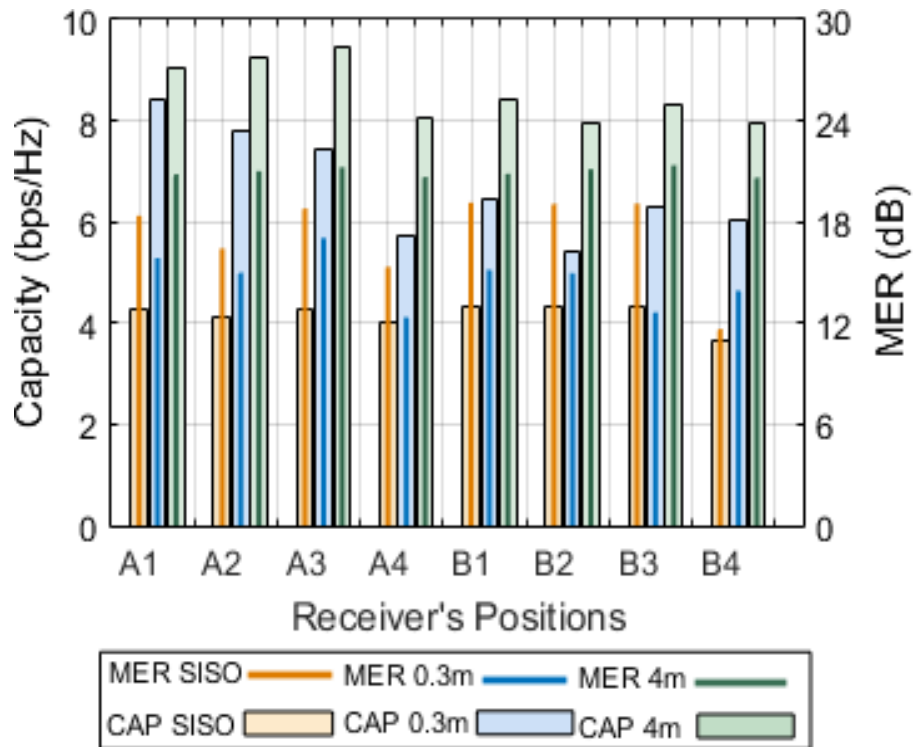
Figure 4.21 Capacity and MER of downlink **2x2 ZF-MIMO** measured at inter-RAU distance of 0.3m and 4m at different positions compared to **SISO**.

The MER and resultant capacity, using equation (2.7), for 2x2 spatial multiplexing-MIMO using the zero-forcing algorithm and compared to SISO are shown in Fig. 4.21. The capacity of SISO results from a lower MER than in the MIMO case, as in the latter case there is often a nearer RAU to increase the performance for each link, as well as the enhancement from the multiplexing gain, which increases for greater RAU separation. It can be observed, from some of the 0.3m separation results, at least, that capacity increase can be achieved even with lower SNR (MER) than in the SISO case, because of the spatial multiplexing gain.

Fig. 4.22 compares the MER and capacity results for all three schemes when the inter-RAU distance is 4-m, again noting that overall transmit power is the same. The capacity for SIMO is higher than that for MISO in all positions, even in positions where the MER is inferior, due to the improvement of effective SNR by the multiple receiving antennas. MIMO offers the highest capacity due to its spatial multiplexing.
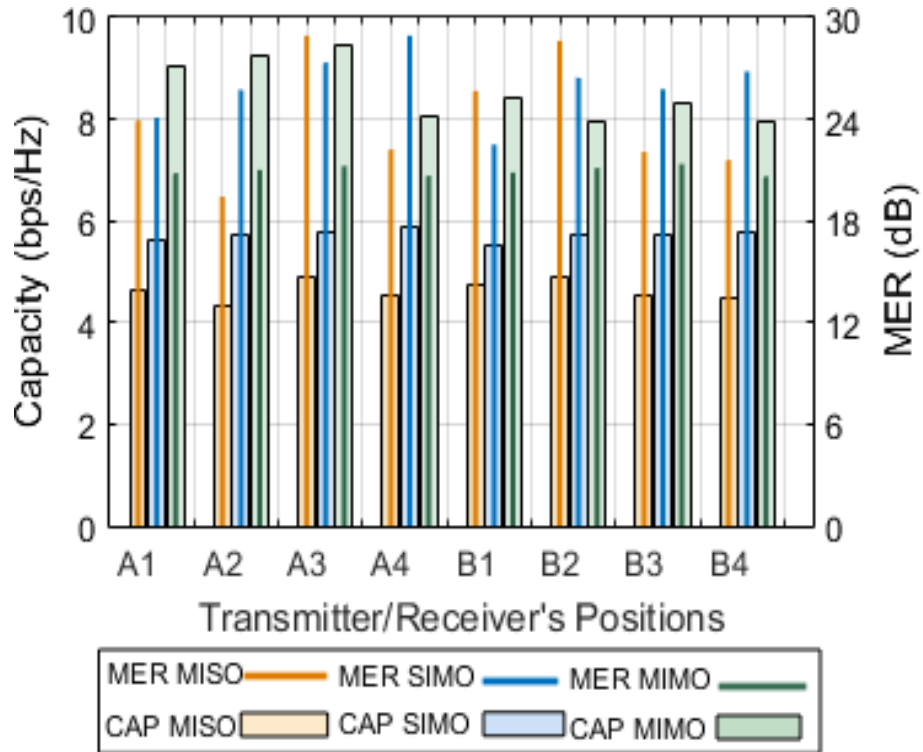
Figure 4.22 Capacity and MER of **Alamouti STBC-MISO**, **MRC-SIMO** and **ZF-MIMO** measured at inter-RAU distance of 4m at different positions.

4.6. Wide antenna separation results

The typical spacing between individual antennas of an AP is ¼ wavelength [24] but it has been reported in Chapter 2 that wider antenna separation thus improves the throughput performance of the MIMO systems, and RoF-DAS opens up new possibilities for this wider separation.

Fig. 4.23 shows the EVM result of a 2x1 downlink MISO scheme using Alamouti STBC algorithm at 0.3m, 4m, 6m and 10m inter-RAU separation distance. It can be observed that most of receiver's positions for 0.3m antenna separation has high EVM, especially positions A4 and B4 that were both above the 11.2% limit for 16-QAM. The EVM performance was generally reduced at 4m and 6m antenna separation, below the 11.2% limit for 16-QAM in all receivers' positions. However, the EVM performance increases at 10m antenna separation.
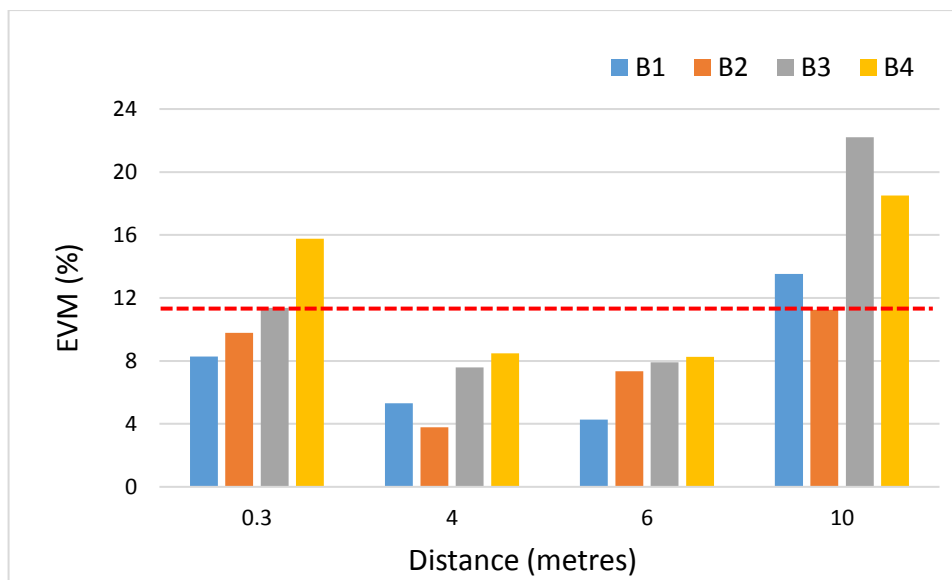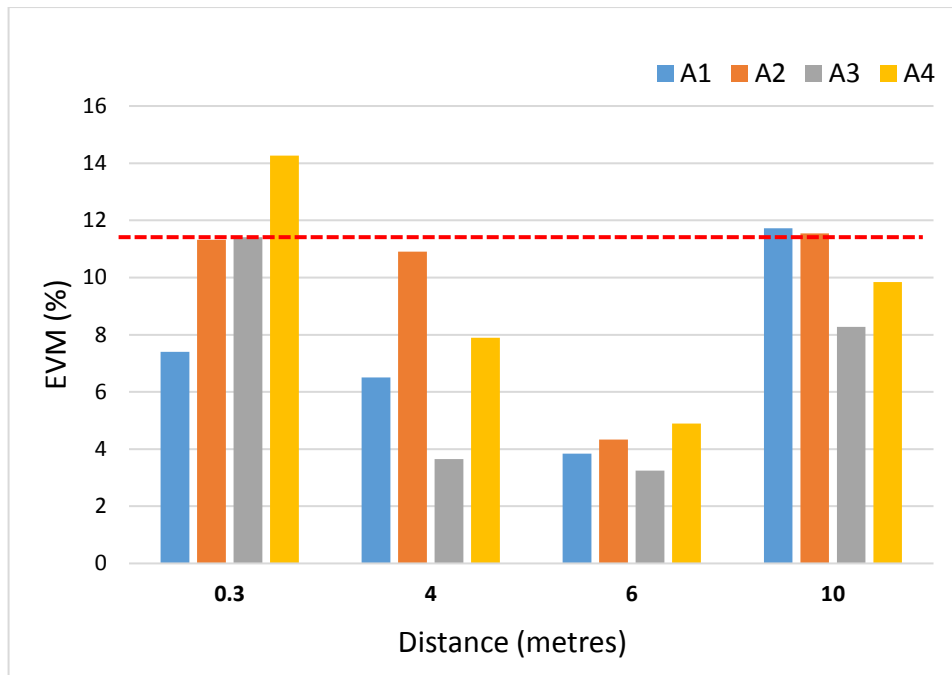
Figure 4.23 EVM of downlink **2x1 STBC Alamouti-MISO** measured at inter-RAU distance of 0.3m, 4m, 6m and 10m at different positions A1-A4 (top) and B1-B4 (bottom).

Fig. 4.24 shows the EVM result of a 1x2 SIMO scheme using MRC algorithm at 0.3m, 4m, 6m and 10m inter-RAU separation distance. The EVM performance of 0.3m was generally reduced in all transmitters' position and below the 11.2% limit for 16-QAM except for positions A1 and B2. However, the EVM reduced at 4m and 6m antenna separation in all transmitters' positions. This is because as the antenna

separation was increased, the less likely it becomes for the two receiving signals to fade simultaneously. Although at 10m antenna separation the EVM gradually increases.

The increase EVM at 10m antenna separation in Figs. 4.23 and 4.24 is because of the large power imbalance between the received signals for a 9.7 by 8.6 m room (shown in Fig. 4.3). To achieve greater diversity gain, the signal strength of the two received signals should be relatively equal.
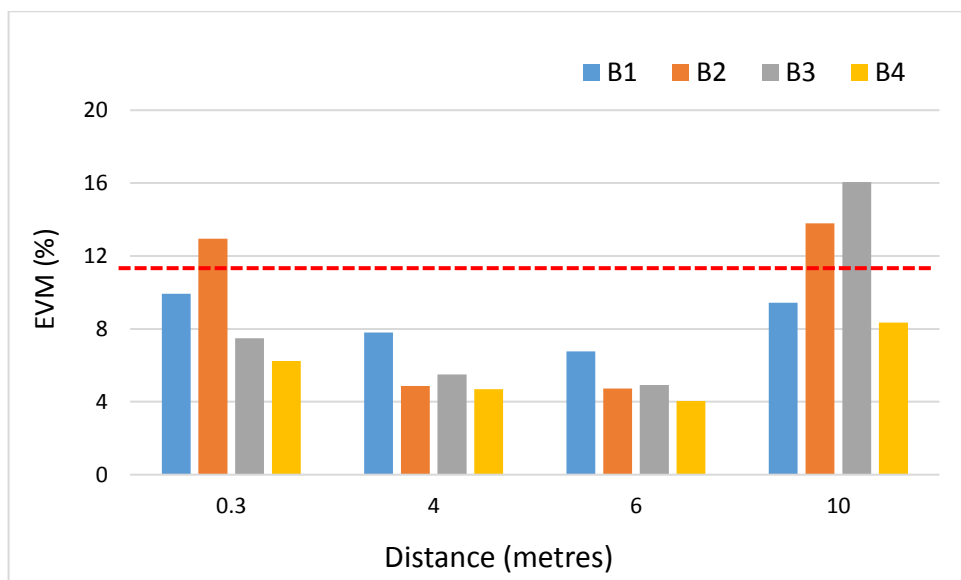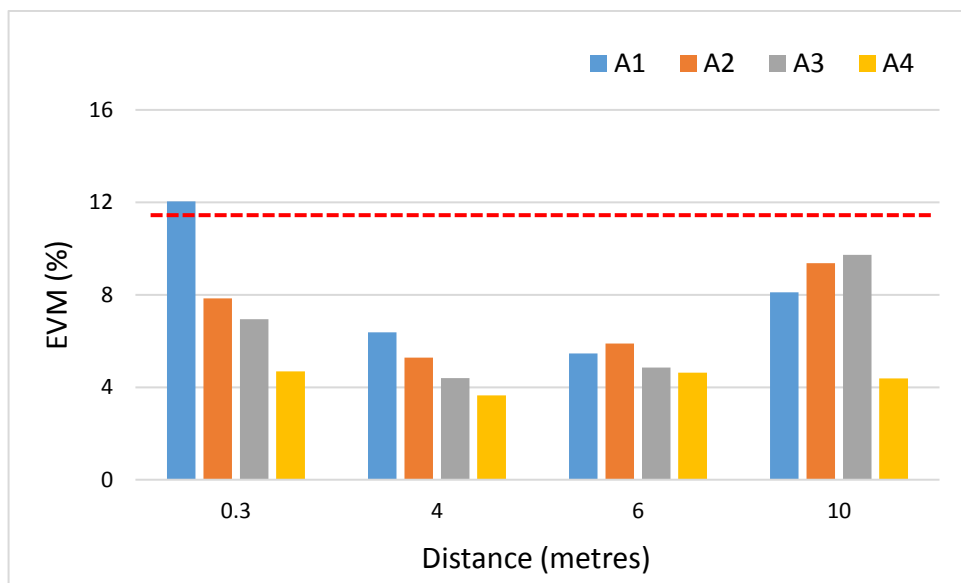
Figure 4.24 EVM of downlink **1x2 MRC-SIMO** measured at inter-RAU distance of 0.3m, 4m, 6m and 10m at different positions A1-A4 (top) and B1-B4 (bottom).
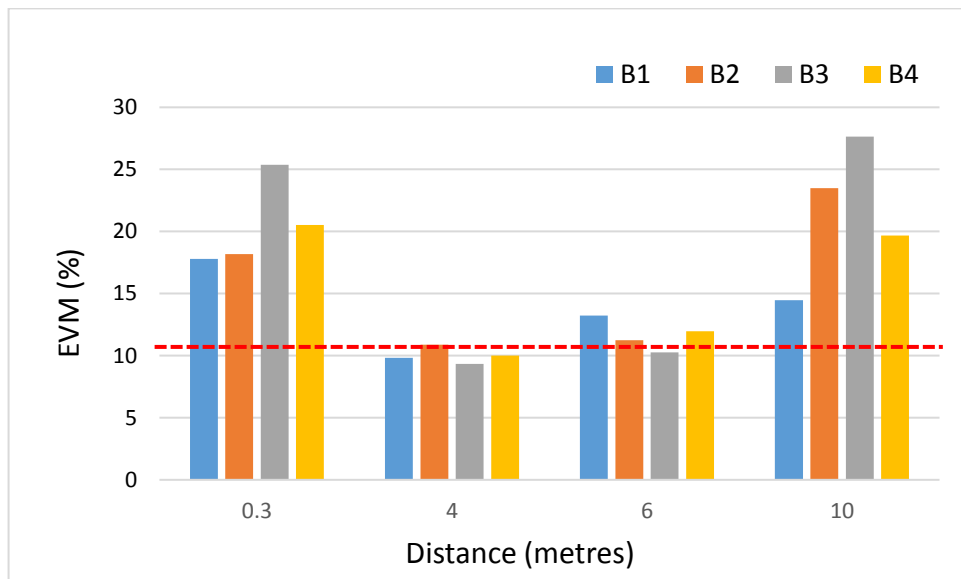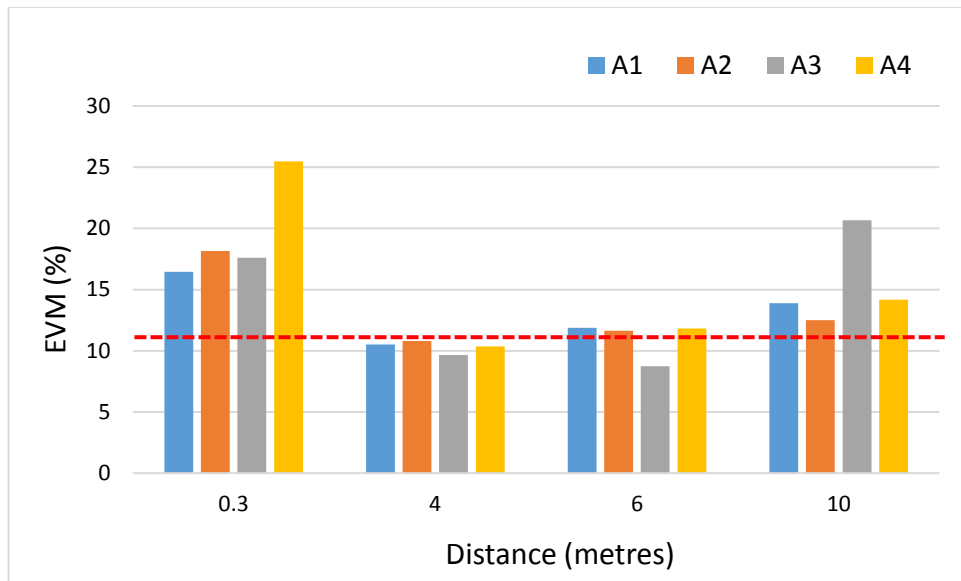
Figure 4.25 EVM of downlink **2x2 ZF-MIMO** measured at inter-RAU distance of 0.3m, 4-m, 6-m and 10-m at different positions A1-A4 (top) and B1-B4 (bottom).

Fig. 4.25 shows the EVM result of a 2x2 MIMO scheme using the ZF algorithm at 0.3m, 4m, 6m and 10m inter-RAU separation distance. It can be observed that the EVM performance for 0.3m is generally high and above the 11.2% limit for 16-QAM but for 4m and 6m antenna spacing, the EVM reduces and falls below the limit in all of the receiver's positions. Again, the EVM performance for 10m antenna separation increases, this is because in spatial multiplexing, both received signals are

multiplexed to achieve the increased data rate and if one of the antennas receives a weak signal and the other receives a strong signal, the EVM of the overall receiver is still high. At 10m antenna separation the chance of both receive antennas receiving a strong signal in the coverage area is unlikely.

4.7. Summary

In this chapter, the benefits of increased antenna spacing in a RoF-DAS when comparing specific multi-antenna transmit/receive schemes to a SISO system has been demonstrated. It has been shown that a wireless 1x2 SIMO uplink when the signals from two RAUs are RoF-transported and then centrally processed using SC, EGC or MRC algorithms can significantly reduce EVM/SER. Also, MRC algorithm provides the optimum performance when compared to other 1x2 SIMO algorithms and it shows small capacity improvement due to reduced EVM/MER. A wireless 2x1 MISO downlink with the signals RoF-transported was also investigated when transmitting from two RAUs using the Alamouti STBC, DD or TAS algorithms. Again the 2x1 MISO scheme algorithms show significantly reduced EVM/SER compared to SISO; the STBC Alaamouti algorithm provides the optimum performance and it also shows modestly increased capacity due to lower EVM/MER.

In addition, a downlink 2x2 wireless spatial multiplexing-MIMO where signals are RoF-transported and transmitted from two RAUs to one mobile unit with two receiving antennas has been investigated. EVM and SER was reduced due to reduced EVM/MER (through a reduction in ISI), and spatial multiplexing gain was achieved with increased RAU spacing, leading to much increased capacity. Also, for 2x2 wireless spatial diversity-MIMO using the STBC Alamouti algorithm, the EVM/SER was reduced even more than in the case of the 2x1 STBC Alamouti-MISO scheme, due to the additional receive diversity 2x2 spatial diversity–MIMO offers. Similarly, combinations of transmit and receive diversity (DD-MRC) in a 2x2 wireless spatial diversity-MIMO scheme where signals are RoF-transported and transmitted from two RAU show that the EVM performance can be reduced significantly when compared to SISO.

Finally, the effect of wide antenna separation in RoF-DAS using 2x1 MISO, 1x2 SIMO and 2x2 spatial multiplexing-MIMO schemes using STBC Alamouti, MRC and ZF algorithms, respectively have been examined. The EVM performance show that for a 9.7 by 8.6 m room fitted with common office furniture and computers, the EVM was generally reduced up to 6m antenna separation due to the uncorrelated channel paths, but as the antenna separation was increased to 10m, the EVM

increases due to large power imbalance between the received signals. It should be noted that the measured EVM performance with these antenna separations are relevant to this specific environment. In the next chapter, these principles will be demonstrated using wider bandwidths and examining the performance when millimetre-wave wireless channels are considered.

REFERENCE

[1]   F. Diehm, J. Holfeld, G. Fettweis, N. J. Gomes, D. Wake, A. Nkansah, et al., "The FUTON prototype: Broadband communication through coordinated multi-point using a novel integrated optical/wireless architecture," IEEE Globecom Workshops, Miami, FL, pp. 757 - 762, 2010.

[2]   L. Cheng, M. M. U. Gul, F. Lu, M. Zhu, J. Wang, M. Xu, et al., "Coordinated Multipoint Transmissions in Millimeter-Wave Radio-Over-Fiber Systems," J. Lightwave Technol, vol. 34, pp. 653 - 660, 2016.

[3]   TE Connectivity Ltd (2011): Distributed Antenna Systems and MIMO Technology

[4] B. R. Tomiuk, N. C. Beaulieu and A. A. Abu-Dayya, "General forms for maximal ratio diversity with weighting errors," IEEE Trans. on Comm., vol. 47(4), pp. 488 - 492, 1999

[5] N. Kaur, "SNR and BER Performance Analysis of MRC and EGC Receivers over Rayleigh Fading Channel," Intl. Journ. of Computer Applns., vol. 132(9), pp 12-17, 2015

[6] A. Annamalai, C. Tellambura and V. K. Bhargava, "Equal-gain diversity receiver performance in wireless channels," IEEE Trans. on Comm., vol. 48(10), pp. 1732 - 1745, 2000

[7] N. Kong, "Performance Comparison Among Conventional Selection Combining, Optimum Selection Combining and Maximal Ratio Combining," IEEE Intl Conf. on Comm., Dresden, 2009. pp. 1 - 6

[8] Y. Chen and C. Tellambura, "Distribution functions of selection combiner output in equally correlated Rayleigh, Rician, and Nakagami-m fading channels," IEEE Trans on Comm., vol. 52(11), pp. 19948 - 1956, 2004

[9]   G. E. Corazza, V. Degli-Esposti, M. Frullone, C. Passerini, and G. Riva, "Performance evaluation of space diversity in indoor communications using a ray-tracing propagation model " Int. Symposium on Personal, Indoor and Mobile Radio Comms, pp. 408 - 413, 1995

[10]   S. Alamouti, "A simple transmit diversity technique for wireless communications," IEEE J. on Sel. Areas in Commun., pp. 1451 - 1458.

[11]   W.C.Y. Lee Vertical vs. Horizontal Separations for Diversity Antennas.Available:http://www.commscope.com/docs/antenna_separation_article_t a.pdf

[12] Rohde & Schwarz (2015). LTE Transmission Modes and Beamforming Application Note.

[13] S Sanayei, A Nosratinia, "Antenna selection in MIMO systems," IEEE Comm. Magazine, pp. 68 - 73, 2004

[14] V.Tarokh, N. Seshadri and A. R. Calderbank, "Space–time codes for high data rate wireless communication: Performance analysis and code construction," IEEE Trans. on Infor. Theory. vol. 44 (2), pp. 744–765, 1988

[15]   J. A. Garcia-Naya, T. M. Fernandez-Carames, H. J. Perez-Iglesias, M. Gonzalez-Lopez, L. Castedo, D. Ramirez, et al., "Performance of STBC transmissions with real data " presented at the Mobile and Wireless Commun. Summit, Budapest, 2007.

[16]   F. J. Vazquez-Araujo, J. A. Garcia-Naya, M. Gonzalez-Lopez, L. Castedo, and J. Garcia-Frias, "Experimental evaluation of MIMO coded modulation systems: Concatenation with OSTBC or spatial multiplexing " in Int. Conf. on Sys., Signals and Image Processing, Vienna, 2012, pp. 93-96.

[17]   Y. Cho, J. Kim, W. Yang, and C. G. Kang, MIMO-OFDM Wireless Communications with MATLAB: John Wiley and Sons Ltd, 2010.

[18]   O. C. Oghre and S. Salous, "BER performance evaluation of HF MIMO spatial multiplexing systems," presented at the URSI General Assembly and Scientific Symposium, Beijing, 2014.

[19] "Emcore Model 1935F Datasheet," Available: http://www.emcore.com

[20] "Appointech 2.5 Gbps InGaAs PIN Photodiode Module Datasheet,". Available: http://www.appointech.com.

[21]   J. A. Altabas, J. A. L. D. Izquierdo, A.Lerin, F. Sotelo, and I. Garces, "1Gbps full-duplex links for ultra-dense-WDM 6.25GHz frequency slots in optical metro-access networks," Opt. Express, vol. 24, pp. 555-565, 2016.

[22]   Z. Al-Qazwini and H. Kim, "Symmetric 10-Gb/s WDM-PON Using Directly Modulated Lasers for Downlink and RSOAs for Uplink," J. Lightwave Technol, vol. 30, pp. 1891 - 1899, 2012.

[23]   MATLAB version R2015a. Communication Toolbox: The MathWorks Inc., 2015

[24] W. Qing, D. D. C. Z. Zheng, N. Ignas, and G. S. H. de, "Performance Analysis of Large Centralized and Distributed MU-MIMO Systems in Indoor WLAN," European Wireless Conf., Budapest, Hungary, 2015.

CHAPTER 5

PERFORMANCE INVESTIGATION OF MULTIPLE-INPUT, MULTIPLE-OUTPUT TECHNIQUES IN MILLIMETRE-WAVE-OVER-FIBRE SYSTEM

5.1. Introduction

The experimental MIMO works presented in Chapters 3 and 4 were carried out in the microwave frequency band, and the radio frequency (RF) spectrum available within this band is limited, especially in the lower region up to 6GHz where many wireless communication applications and services operates [1]. This RF spectrum scarcity has led to interest in millimetre-wave (mm-wave) communication systems where larger bands of frequency are available enabling the possibility of wider bandwidth and higher data rates. For example, 2GHz bandwidth was used in a system operating in the 60 GHz unlicensed mm-wave band, to provide data rates up to 6Gbps in [2].

In this chapter, the error performance of 25GHz and 60GHz radio-over-fibre MIMO systems are investigated using spatial diversity and spatial multiplexing MIMO processing techniques. The theory of millimetre-wave-over-fibre MIMO systems is discussed followed by the experimental setups for 25GHz and 60GHz mm-wave-over-fibre MIMO systems. The measurement results of the systems are then presented, followed by a summary of this Chapter.

5.2. Millimetre-wave-over-Fibre MIMO system

MIMO systems using spatial multiplexing and spatial diversity techniques have been widely deployed in lower-frequency systems, such as the IEEE 802.11n/ac and LTE 4G standards, to improve the reliability and/or increase the data rate of the system [3]. Fundamentally, the performance improvement in MIMO is achieved by exploiting the multipath phenomena of the wireless propagation channel. However, due to the highly directional antennas used in mm-wave frequencies to overcome the wireless channel path loss, it is unclear how well MIMO techniques will work in such a line-of-sight (LOS) propagation environment given the shortage of multipath [4].

Recent studies [5], [6] have proved that the performance of MIMO in LOS can surpass typical multipath Rayleigh faded channels, but the transmitting antennas must be spaced in such a way that the signal from each transmit antenna is received by both receiving antennas as shown in Fig. 5.1. In this Chapter, the optimum transmit antenna separation distance that gives the best possible performance for each MIMO technique is investigated in a realistic indoor mm-wave channel.
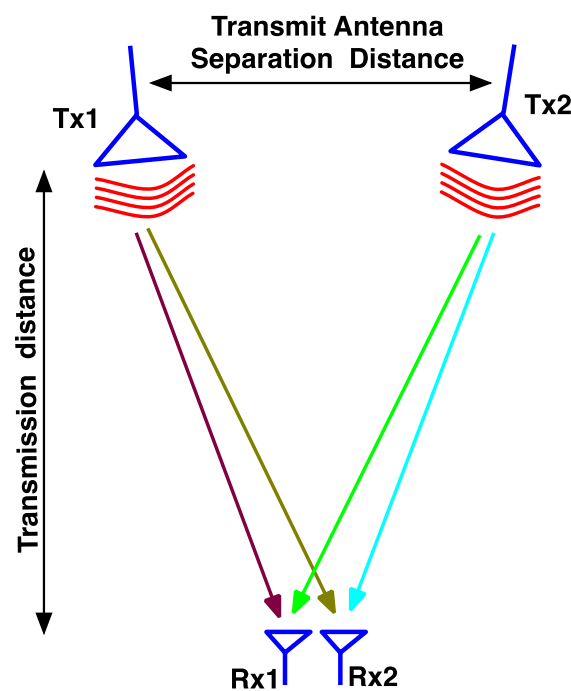

Figure 5.1 MIMO in Line-of-sight (LOS) propagation.

Furthermore, there are several works on RoF transport of mm-wave MIMO signals, for example in [7] and [8], a modulated data was transported to the first RAU, while an optical delay was introduced when transporting the same data to the second RAU. Also in [9], generation of separate sets of the same data has been demonstrated and the same wavelengths were used to transport the data to two RAUs, and performance analysis has only been presented for a single user location at a particular wireless distance.

In this Chapter, the performance of a 25GHz wireless 2x2 MIMO system using specific spatial diversity and spatial multiplexing algorithms are examined in a mm-wave RoF system with over 2km fibre and up to 6m wireless distance. For spatial diversity MIMO, the data symbol was applied to an Alamouti STBC encoder to produce two encoded data streams that were modulated on different wavelengths, and RoF-transported to two RAUs for wireless transmission. The received signals are captured at the mobile unit and saved for offline processing using the Alamouti STBC decoding algorithm. For spatial multiplexing MIMO, two different data streams were modulated on different wavelengths and RoF-transported to two RAUs for wireless transmission, and the captured signals were processed offline using zero-forcing algorithm to separate the data streams before re-combining. The 25GHz DWDM-RoF method of transporting mm-wave MIMO signals presented in this Chapter, has flexibility for wavelength selection/allocation to specific RAUs and it is done in the central unit. This method is useful especially when separate data streams are required to be transported through the RoF link.

The performance of a 60 GHz RoF system using integrated transmitter/receiver circuits is also examined in this Chapter, where an IF signal is RoF-transported to an integrated transmitter circuit that up-converts the IF signal to 60GHz. The 60 GHz signal was received at the mobile unit after wireless transmission and down-converted to IF signal using the integrated receiver circuit. To emulate a 2x2 MIMO system, the complex channel transfer matrix H and the transmitted symbols were captured while moving the antennas to different positions, and the values were saved for offline processing; then, spatial diversity Alamouti STBC and spatial multiplexing zero-forcing algorithms were used.

In addition, the error vector magnitude (EVM) performance metric was used to measure the performance of these MIMO techniques; the EVM requirement varies for every wireless standard. For example, the EVM requirement for wireless local area network (WLAN) modulation schemes for 16-QAM is 11.2% and 6.5% for 64-QAM [10] while for the LTE standard, the requirement for 16-QAM modulation schemes is 12.5% and 8% for 64-QAM. In this Chapter, the LTE standard limit has been used as an EVM requirement, and most modern systems tend to use it to tolerate worse SNR [11].

5.3. Experimental Setup

This section describes the experimental setup for the 25GHz and 60 GHz RoF-systems. These systems were demonstrated using different setups, the 25 GHz experiment was demonstrated using a DWDM-RoF setup where the two 25GHz MIMO signals were modulated on different optical wavelengths and RoF transported to two RAUs for wireless transmission. The 60 GHz experiment on the other hand was demonstrated using an integrated transmitter circuit to up-convert the RoF-transported IF signal to 60 GHz for wireless transmission.

5.3.1. 25GHz Experimental setup

Fig. 5.2 shows the experimental setup for the 25GHz RoF-transported 2x2 MIMO system. The baseband signal was processed offline using MATLAB/Simulink software and pseudo-random data symbols of 177.228MSps were generated and converted to parallel sets of symbols for the 16-QAM-OFDM processing. The OFDM signal processing includes 512 IFFT size, 8 pilot subcarriers for phase tracking, 112 guard bands (zero padding) including 1 DC subcarrier, and 1/8 CP size; 304 OFDM symbols were transmitted including 1 OFDM preamble symbol used for channel estimation. The I/Q samples for the two separate data streams were downloaded onto the Tektronix Arbitrary Waveform generator (AWG) 7122C channels (channel 1 and 2) using RFXpress software running on the AWG. The sample rate was set to 390.625 MHz and the signals were upconverted to an

intermediate frequency (IF) of 1.5GHz and modulated onto a pair of Mach-Zehnder modulators (MZMs), both biased at null point to ensure maximum suppression of the optical carrier.
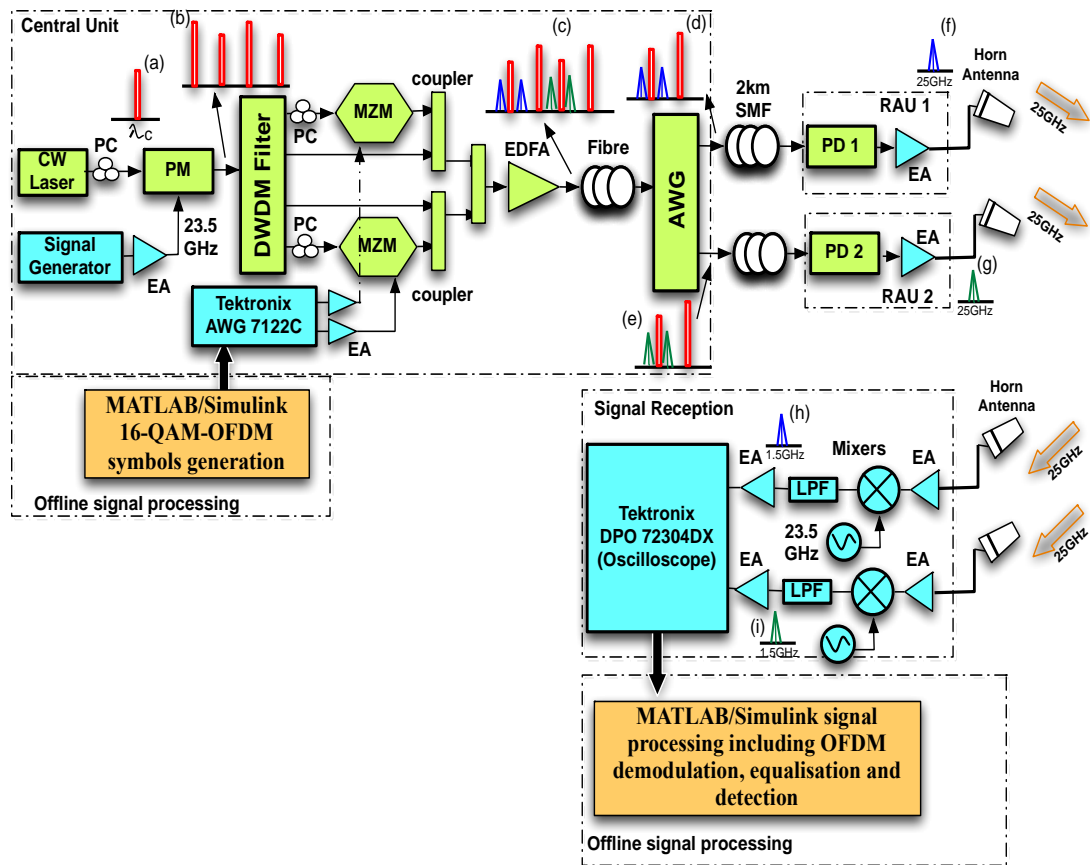
Figure 5.2 Experimental set-up for 25GHz RoF-transported 2x2 MIMO system CW Laser – Continuous-wave Laser, PM- phase modulator, DWDM filter – dense wavelength division multiplexing filter, EA= Electric amplifiers, MZM –Mach-Zehnder modulator, EDFA- Erbium Doped Fiibre Amplifier, AWG - Array Waveform Grating, PD=Photo-detector, RAU=Remote antenna unit, LPF – low pass filter

The optical signal was generated by a continuous lightwave of +5dBm produced by a continuous wave laser (insert (a) in Fig. 2) and transmitted to the optical phase modulator (PM) driven by a 23.5GHz RF signal which produces sidebands (insert (b) in Fig. 5.2). The upper first-order sideband, optical carrier, lower first-order sideband and lower second-order sideband were selected by a 25GHz spacing dense wavelength division multiplexing (DWDM) filter whose polarization was aligned by polarization controllers. One of the data signal was modulated onto the upper first-order sideband and the other was modulated onto the lower first-order sideband using

the MZMs and these modulated optical signals were then coupled together with the optical carrier and the un-modulated second-order sideband using a 3 dB optical coupler (insert (c) in Fig. 5.2). The resultant signal was passed through a 26dB gain Erbium Doped Fiber Amplifier (EDFA) and to the Array Waveguide Grating, which filters one data modulated sideband and the optical carrier to one RAU, and the other data modulated sideband and un-modulated sideband to the second RAU (insert (d) and (e) in Fig. 5.2). After 2 km of optical fibre, the signals are each received at the two RAUs where a high bandwidth photodiode is used for direct photonic upconversion (by the mixing of the data modulated and unmodulated optical sidebands) to generate the mm-wave signals at 25GHz (insert (f) and (g) in Fig. 5.2). The signals are then amplified and transmitted through 20dBi gain horn antennas to the receiver.
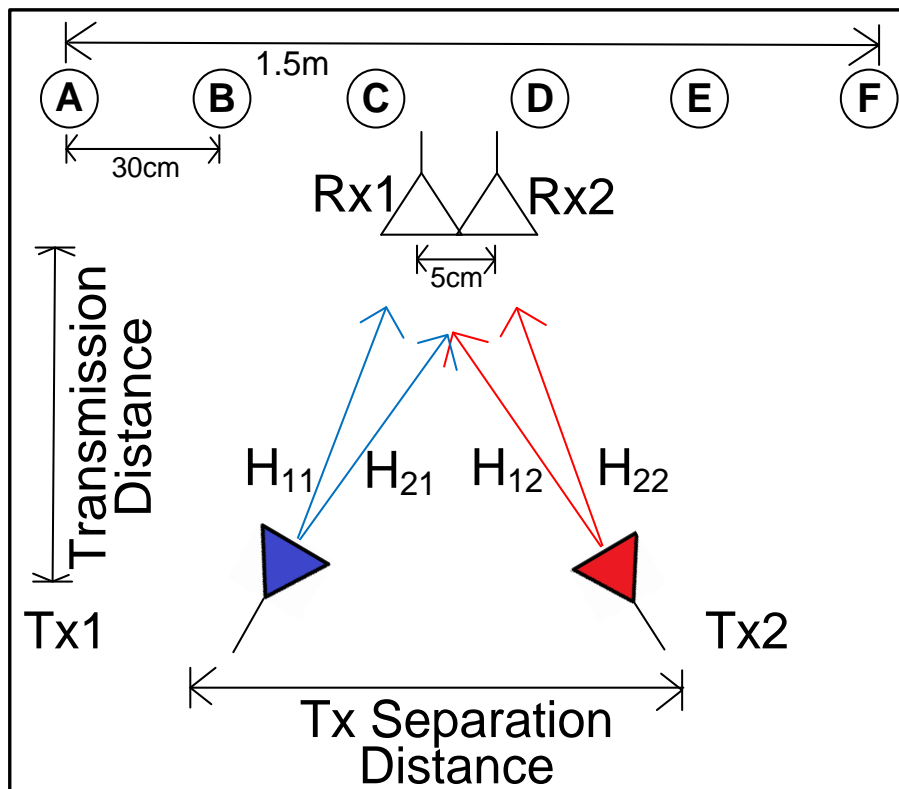

Figure 5.3 Measurement layout of the testing room.

The performance of MIMO systems with different transmit antenna separation distances (40, 60, 80 and 100cm) was examined in a realistic indoor mm-wave

channel to determine the optimum antenna separation. The measurement layout of the testing room is shown in Fig. 5.3, where the transmit antennas (Tx1 and Tx2) were placed on a platform 6m away from two receiving antennas (Rx1 and Rx2), and the receiving antennas were connected to the DPO 72304DX (Oscilloscope) channels 1 and 2 (after down-converting the signal to IF). During each measurement, the transmit antennas were pointing towards the receiving antennas, and manual alignment of both antennas was necessary, to ensure there was good signal strength at the Oscilloscope before capturing the signals for offline processing. Also, the wireless transmission distance was varied to 3, 3.5 and 4m, and at each transmission distance, the EVM results for the transmit antenna separation distances (40, 60, 80 and 100cm) were obtained.

In addition, the receiving antennas were moved between different locations (A to F) in the testing room and at each location, the received OFDM signals were amplified with a pair of 25dB gain 25GHz amplifier to boost the signal strength before mixing them with 23.5GHz local oscillators to downconvert the signals to 1.5GHz IF frequency. Also, a pair of low pass filters (LPFs) were used to filter the signals below 1.8GHz frequency and low-noise figure Mini-Circuits amplifiers (ZX60-242GLN+) were used to boost the signal power level before capturing the signals.

The captured signals at the Oscilloscope were saved in MATLAB format for offline processing, which includes a MATLAB script written to perform OFDM symbol time alignment to detect the starting point of each OFDM symbol, followed by OFDM demodulation involving the removal of the CP, guard bands (zero padding) and DC subcarrier, leaving the pilot and data symbols for channel estimation and detection. The preamble symbol was used for least square (LS) channel estimation and the pilot subcarriers for phase tracking. The signal combining/detection (depending on the MIMO algorithm) was done before the QAM demodulation.

5.3.2. 60GHz Experimental setup

Fig. 5.4 shows the experimental setup for the 60GHz Radio-over-Fibre System. The baseband signal was processed offline using the same parameters as the 25GHz experimental setup in section 5.3.1. The baseband signal was upconverted to an

intermediate frequency (IF) at a carrier frequency of 1.5GHz and modulated onto a distributed feedback laser (DFB) as shown in Fig. 5.5. The optically modulated signal from the central unit was transmitted through single mode fibre (SMF) to the remote antenna unit (RAU) where a photodiode converts the optically modulated signal to 1.5 GHz IF signal. The IF signal was fed into a differential baluns that produces I, Ī, for the gTSC0020 60GHz integrated transmitter circuit.
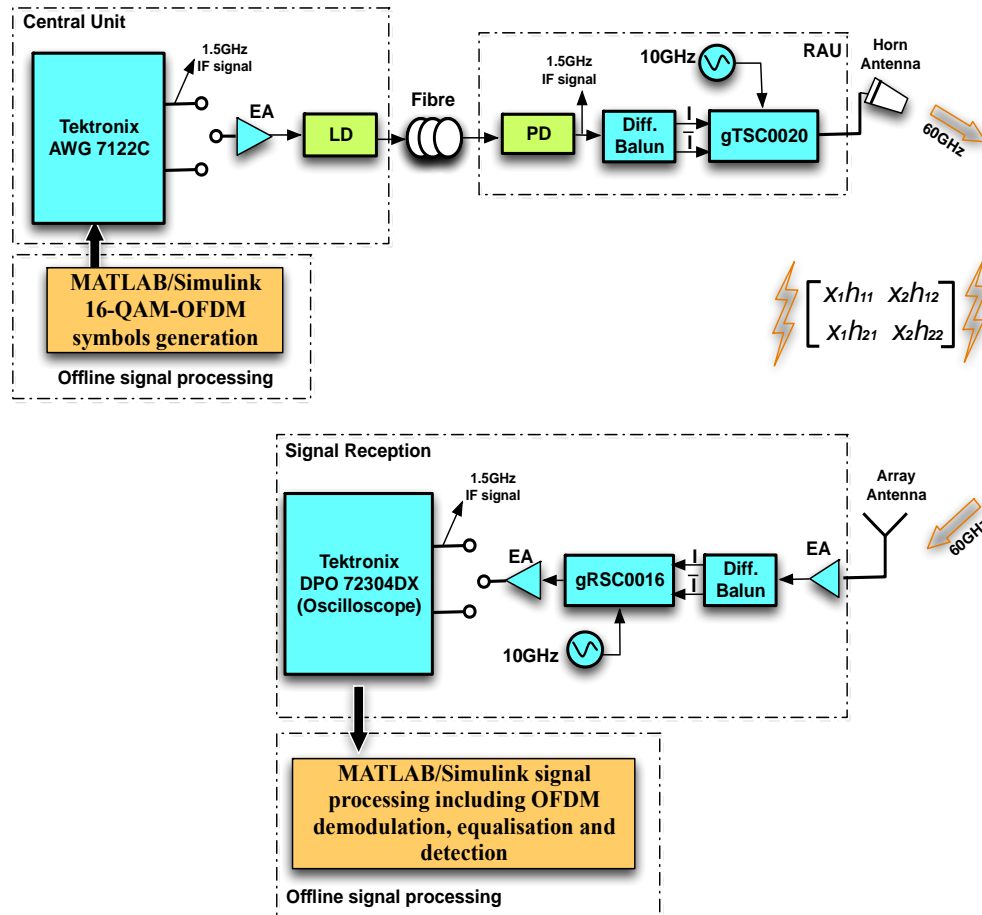
Figure 5.4 Experimental setup for 60GHz Radio-over-Fibre system using integrated transmitter/receiver circuits.
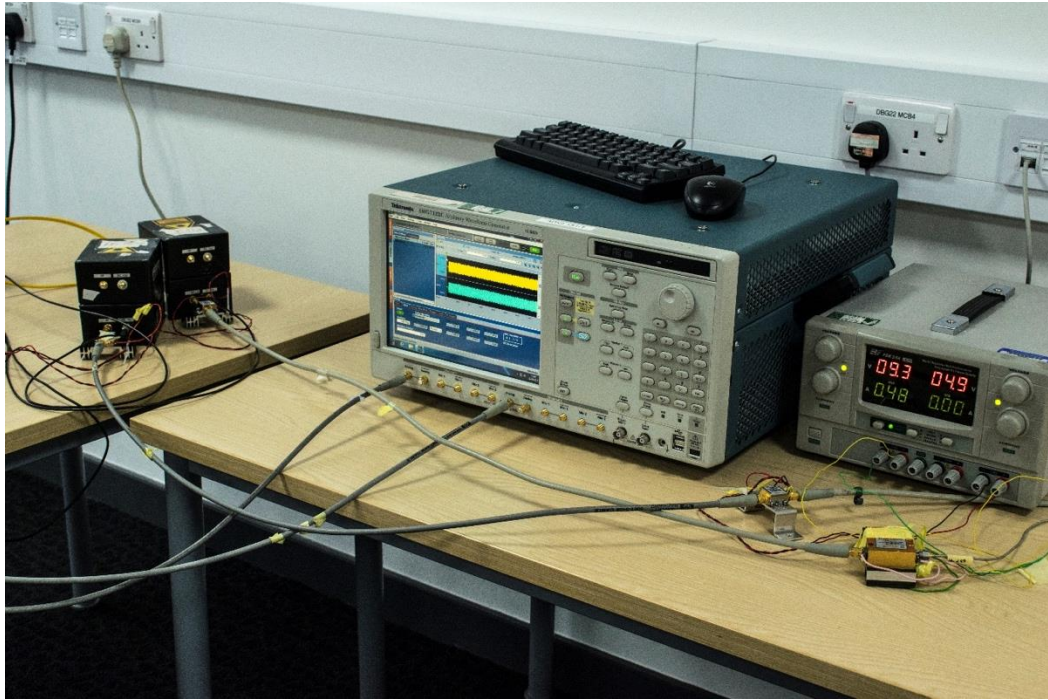
Figure 5.5 Arbitrary Waveform generator (AWG) upconverting baseband signal to an intermediate frequency (IF) and modulating it onto a DFB laser diode.
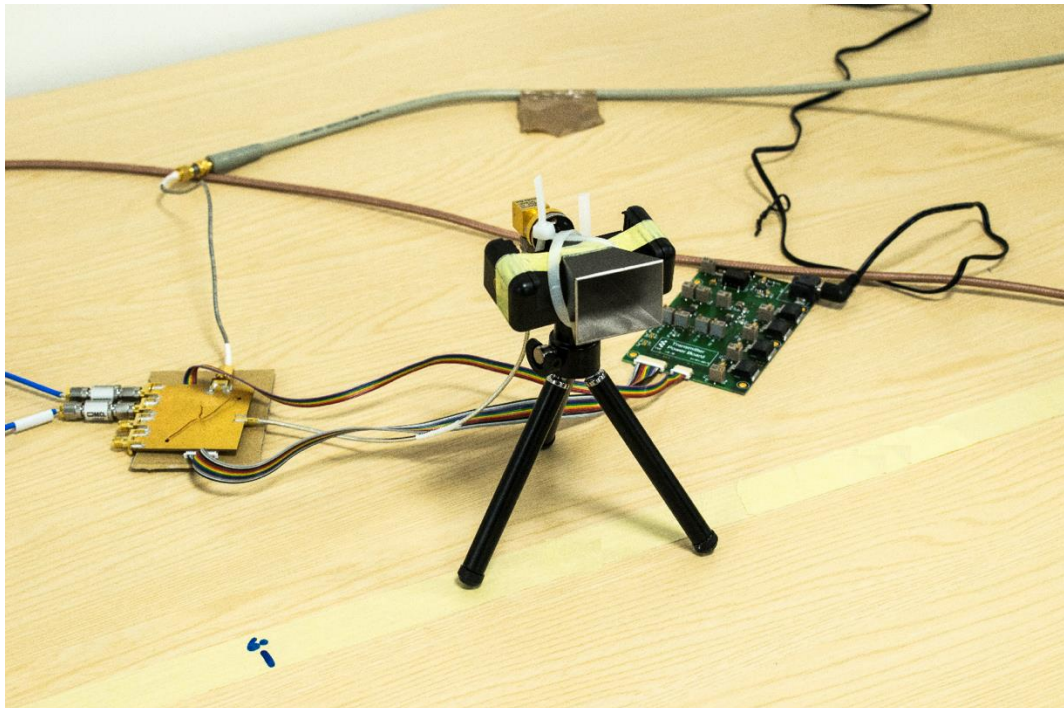
Figure 5.6 IF signal fed into a differential baluns that produces I, $\bar{\text{I}}$, for the gTSC0020 60GHz integrated transmitter circuit and wirelessly transmitted through an horn antenna.
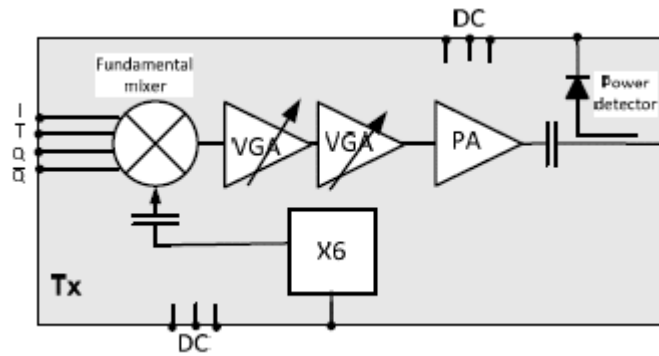
Figure 5.7 gTSC0020 60GHz integrated transmitter circuit [12].

The layout of the gTSC0020 integrated circuit is shown in Fig. 5.7, where the 1.5 GHz I, Ī signals were mixed with a sextupling frequency multiplier that takes a 10GHz local oscillator (LO) input and multiplies it internally to produce a 60 GHz LO, which is then employed to produce the 61.5GHz signal; this signal was wirelessly transmitted using an 18dBi gain horn antenna as shown in Fig. 5.6.
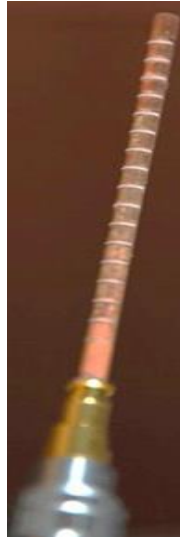
Figure 5.8 A 16.8 dBi quasi-discoidal radiation pattern antenna array [13].
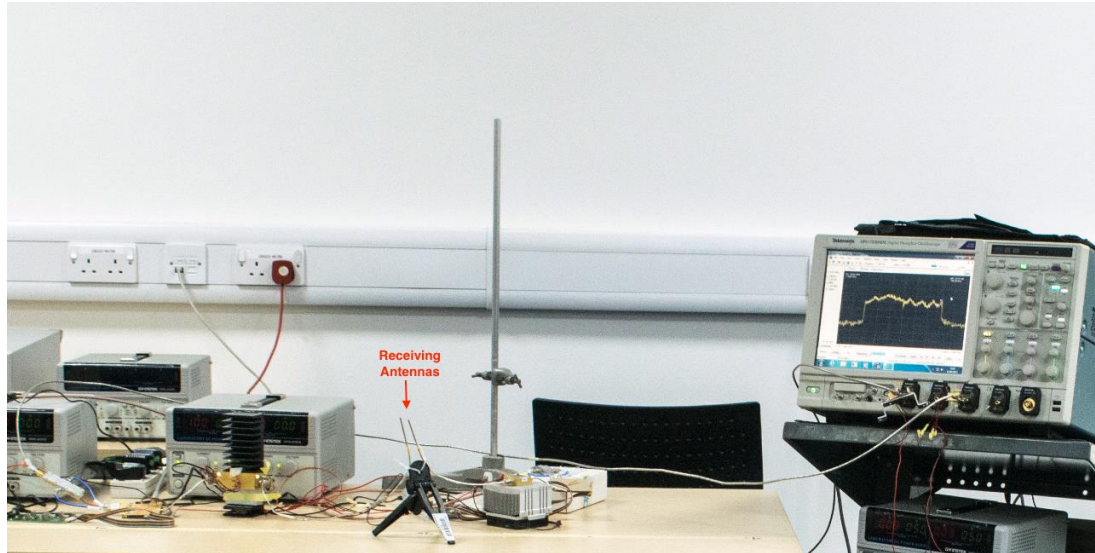
Figure 5.9 Receiving antenna connected to the differential baluns that produces I, Ī, signal for the gRSC0016 60GHz receiver circuit and the signal captured at the Oscilloscope for offline processing.

The transmitted signal was received by a 16.8 dBi gain quasi-discoidal radiation pattern antenna array [13] shown in Fig. 5.8 and it was connected to a 30dB gain V-band Quinstar amplifier QPI-V02030 and to the differential baluns that produce the I, Ī, signal for the gRSC0016 60GHz receiver circuit [14]. The 60GHz integrated receiver circuit takes a 10GHz LO input with +7dBm power to down-convert the 61.5GHz signal to IF of 1.5GHz. The IF signal was amplified using a +17dB gain broadband amplifier and captured at the Oscilloscope for offline processing as shown in Fig 5.9.
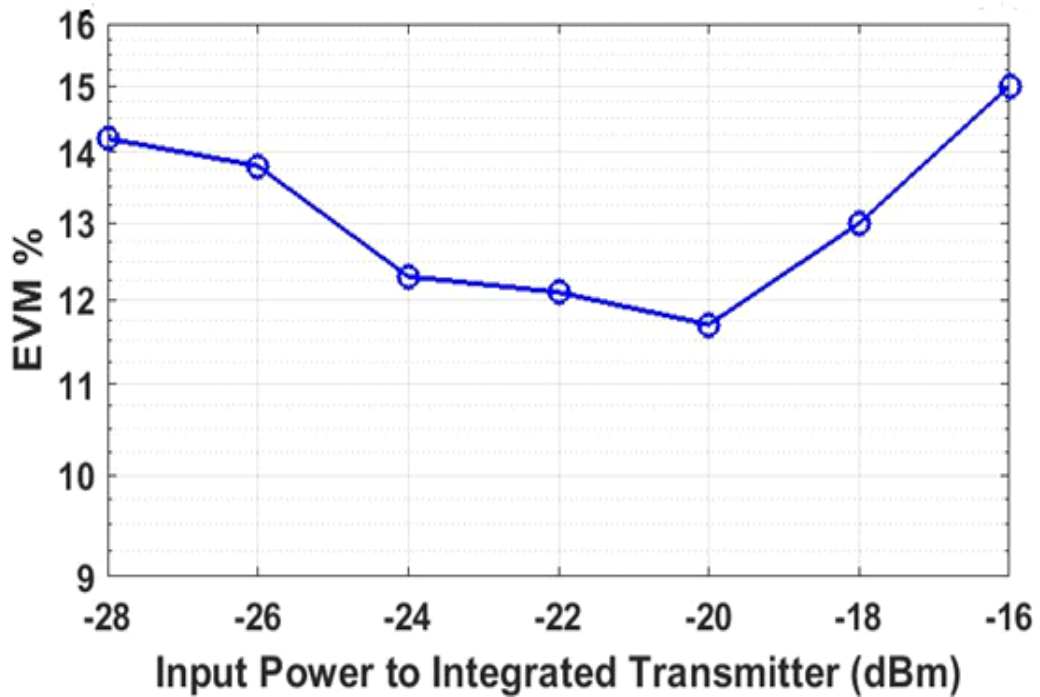
Figure 5.10 EVM result showing the performance of the 60 GHz integrated transmitter at different IF power levels.

Fig. 5.10 shows the EVM result when the IF input power to the 60GHz integrated circuit was varied and connected directly to the Oscilloscope to measure the optimum transmit power to use for the experiment. It can be seen that the lowest EVM of 11.6% was achieved at -20dBm IF input power to the 60GHz integrated circuit.

A 2x2 MIMO system was emulated with the 60GHz experiment, this was achieved by marking the transmit and receive antenna locations with a masking tape on the measurement space according to the layout in Fig 5.11. The SISO transmit antenna location was marked facing where receive antenna location *C* was marked, while the 20, 30, 40 and 60cm transmit antenna separations were marked by putting masking tapes 10, 15, 20 and 30cm to the left of where the SISO transmit antenna location was marked, and 10, 15, 20 and 30cm right of where the SISO transmit antenna location was marked, respectively. These marks represented where the transmit antenna Tx1 or Tx2 would be placed during the measurement.
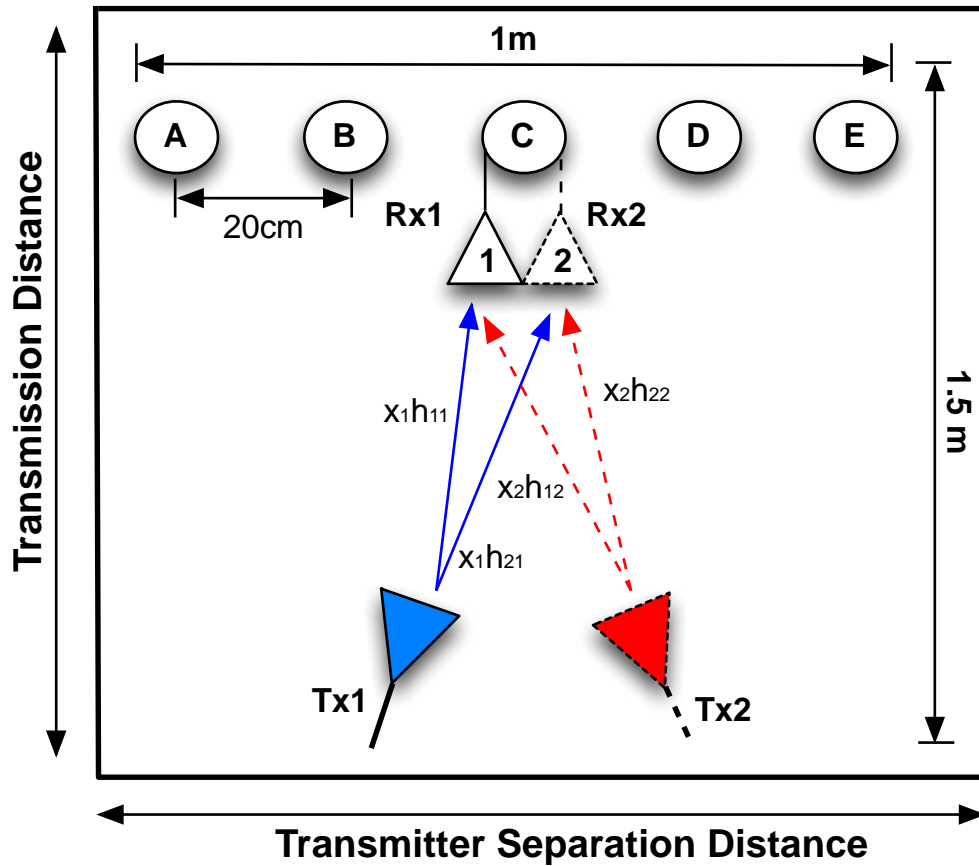
Figure 5.11 Measurement layout of 60GHz experiment

The receive antenna locations were also marked at locations (A-E) according to the layout in Fig 5.11 and at each receiver's location, two masking tapes were placed 5cm away from each other representing where Rx1 or Rx2 would be placed during the measurement. For example, the measurement result for 20cm transmit antenna separation was obtained by placing the transmit antenna 10cm to the left of where the SISO antenna was marked, and the signal was captured when the receiving antenna was placed at the marked receive antenna locations. Thereafter, the transmit antenna was moved 10cm right of where the SISO antenna was marked, and the signal was captured again at the marked receive antenna location.

To determine the EVM performance of the emulated 2x2 MIMO system, the values of the complex channel transfer matrix H together with the transmitted symbols were measured, with the values represented as:

$$\begin{array}{c} y_1 \\ y_2 \end{array} = \begin{bmatrix} x_1 h_{11} & x_2 h_{12} \\ x_1 h_{21} & x_2 h_{22} \end{bmatrix} + \begin{array}{c} n_1 \\ n_2 \end{array} \qquad (5.1)$$

where y_1, y_2 are the received symbol on the first and second antenna respectively, h_{11} is the channel from the first transmit antenna to the first receive antenna, h_{12} is the channel from the second transmit antenna to the first receive antenna, h_{21} is the channel from the first transmit antenna to the second receive antenna, h_{22} is the channel from the second transmit antenna to the second receive antenna, x_1, x_2 are the transmitted symbols and n_1, n_2 is the noise at the receive antennas.

The value of $x_1 h_{11}$ was captured by placing one transmit antenna in position *Tx1* and one receive antenna in position *Rx1* while the value of $x_1 h_{21}$ was captured by moving the receive antenna to *Rx2*, keeping the transmit antenna in *Tx1*. Also, to capture the value of $x_2 h_{12}$, the transmit antenna was moved to *Tx2* and the receive antenna was kept in *Rx1* while the value of $x_2 h_{22}$ was captured by moving the received antenna to *Rx2* and the transmit antenna was kept in *Tx2*. These measurements will give the values of $x_1 h_{11}$, $x_1 h_{21}$, $x_2 h_{12}$ and $x_2 h_{22}$ and they were used to calculate the values of the received signal on the first and second receive antenna given by:

$$y_1 = x_1 h_{11} + x_2 h_{12} + n_1 \qquad (5.2)$$

$$y_2 = x_1 h_{21} + x_2 h_{22} + n_2 \qquad (5.3)$$

The receive antenna was moved to the different receiver's locations (A to E) in the testing room as shown in Fig. 5.11 to capture the OFDM signal and the calculated values of y_1 and y_2 were used in MATLAB/Simulink software for offline processing with spatial diversity Alamouti STBC and spatial multiplexing zero-forcing algorithms. The EVM results of the emulated 2x2 MIMO were obtained for each receiver's location and compared with the EVM results obtained for the SISO system. It should be noted that for each measurement, the receiving array antenna was manually aligned to ensure that good signal strength was achieved before capturing the signal.

5.4. Measurement Results

This section presents the experimental measurement results for the 25 GHz RoF-transported wireless 2x2 MIMO system, and the results of the 60 GHz RoF-transported wireless 2x2 emulated-MIMO system using spatial diversity and spatial multiplexing techniques.

5.4.1. 25GHz Measurement Results

The EVM results of 40cm, 60cm, 80cm and 100cm transmit antenna separation at 3, 3.5, 4m wireless transmission distance for spatial diversity-MIMO and 80, 100, 120 and 140cm transmit antenna separations at 4.5, 5, 5.5 and 6m wireless transmission distance for spatial multiplexing-MIMO systems at 25GHz are examined. The results are compared with the individual SISO transmit antenna performance i.e. Tx1-Rx1 and Tx2-Rx2. To compare the performance of MIMO with SISO, the overall transmit power was kept the same. During the experiment, both transmit antennas were angled such that they always faced towards the centre of the receive antenna and since the half-power beamwidth of the two transmitting antennas was found to be similar, around 20° from anechoic chamber measurements as plotted in Fig. 5.12, the signals from each transmit antenna can be received by both receiving antennas.

The spatial diversity-MIMO technique used the Alamouti STBC algorithm to process a 1Gbps data stream sent from two transmit antennas to two receiving antennas. The spatial multiplexing-MIMO technique used the zero-forcing algorithm to process two different data streams, transmitted from two antennas (each transmitting at 0.5Gbps) to two receiving antennas and the data streams are multiplexed to give an overall data rate of 1Gbps. For both techniques, the receiver was moved between six receiver locations (A-F) at different transmit antenna separation distances to determine the optimum spacing between the transmitting antennas for transmission. The EVM results of the optimum transmit antenna separation distance is then compared with the EVM results of the SISO system.
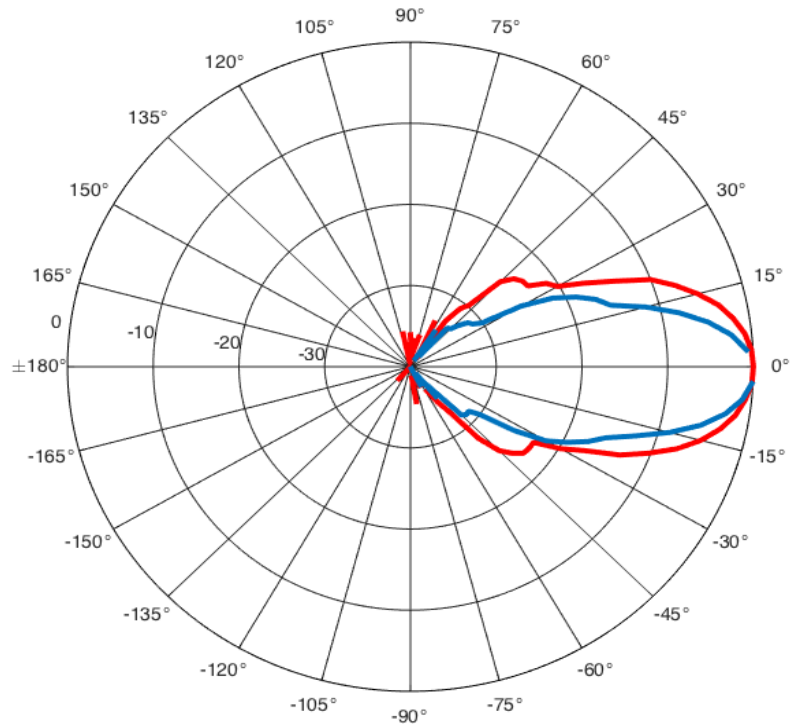
Figure 5.12 Radiation pattern of the two transmitting horn antennas.

Figure 5.13 EVM result of 2x2 spatial diversity-MIMO at receiver location A to F for 40cm, 60cm, 80cm and 100cm transmit antenna separation distances at 3m wireless transmission distance.

Figs. 5.13 shows the EVM result of 2x2 spatial diversity-MIMO using the Alamouti STBC algorithm for 3m wireless transmission distances at 40cm, 60cm, 80cm and 100cm transmit antenna separation distance in different receiver locations. The 12.5% LTE limit for 16-QAM is shown with the red dashed line in the graphs. It can be observed that the EVM result at all receiver's locations are below the 12.5% LTE limit for 16-QAM, for all transmit antenna separation distances. The case is different in Fig. 5.14 showing the EVM result for 3.5m wireless transmission distances, where the EVM results are above the 12.5% LTE limit for 16-QAM in some receiver locations in the 60cm, 80cm and 100cm transmit antenna separation cases.

Figure 5.14 EVM result of 2x2 spatial diversity-MIMO at receiver location A to F for 40cm, 60cm, 80cm and 100cm transmit antenna separation distances at 3.5m wireless transmission distance.

As the wireless transmission distance is increased to 4m for deeper investigation as shown in Fig. 5.15, the EVM result is significantly improved at all receiver locations and all transmit antenna separations, with EVM below the 12.5% LTE EVM limit for 16-QAM in all locations except for receiver location A at 100cm transmit antenna

separation, where the EVM increased above the limit. This is most likely due to the transmitting antennas not properly aligned with the receiving antennas.
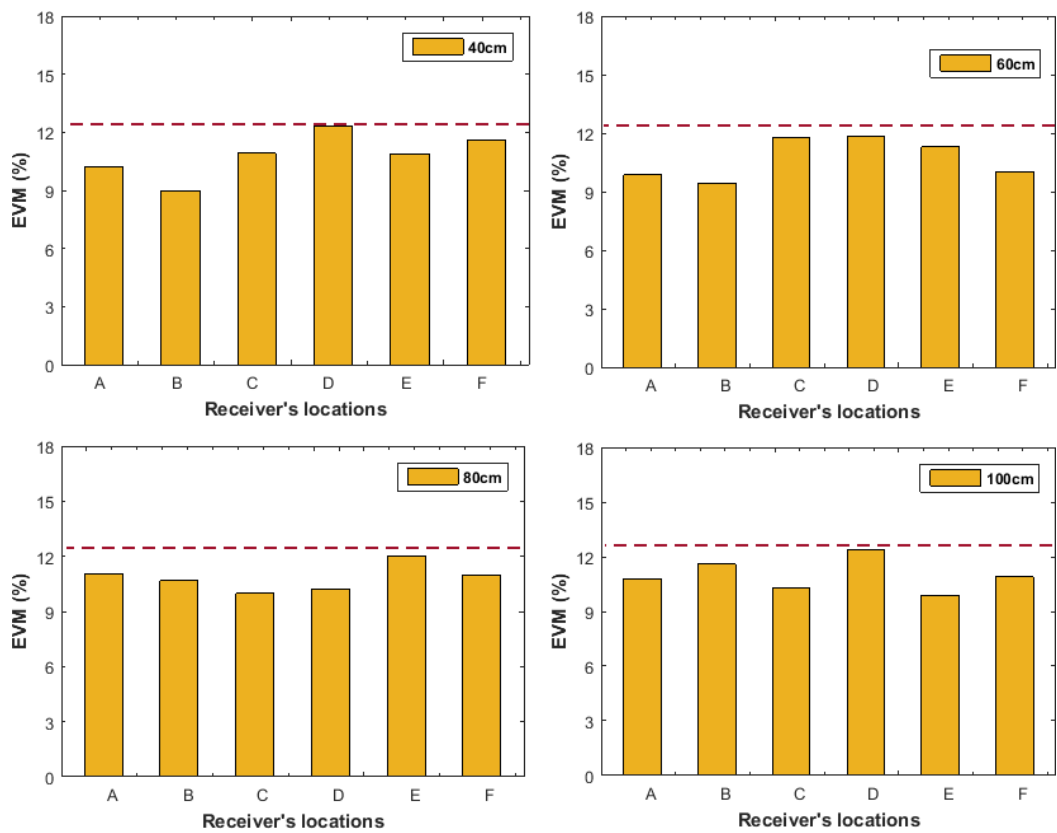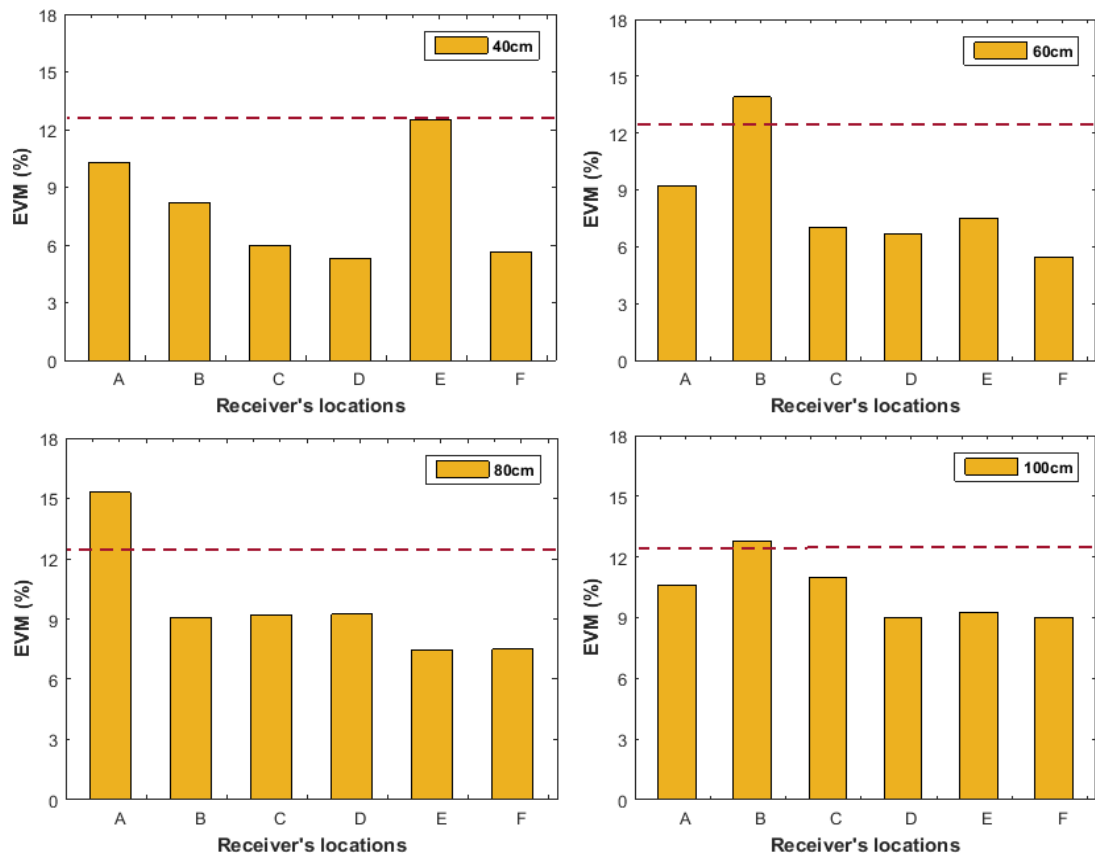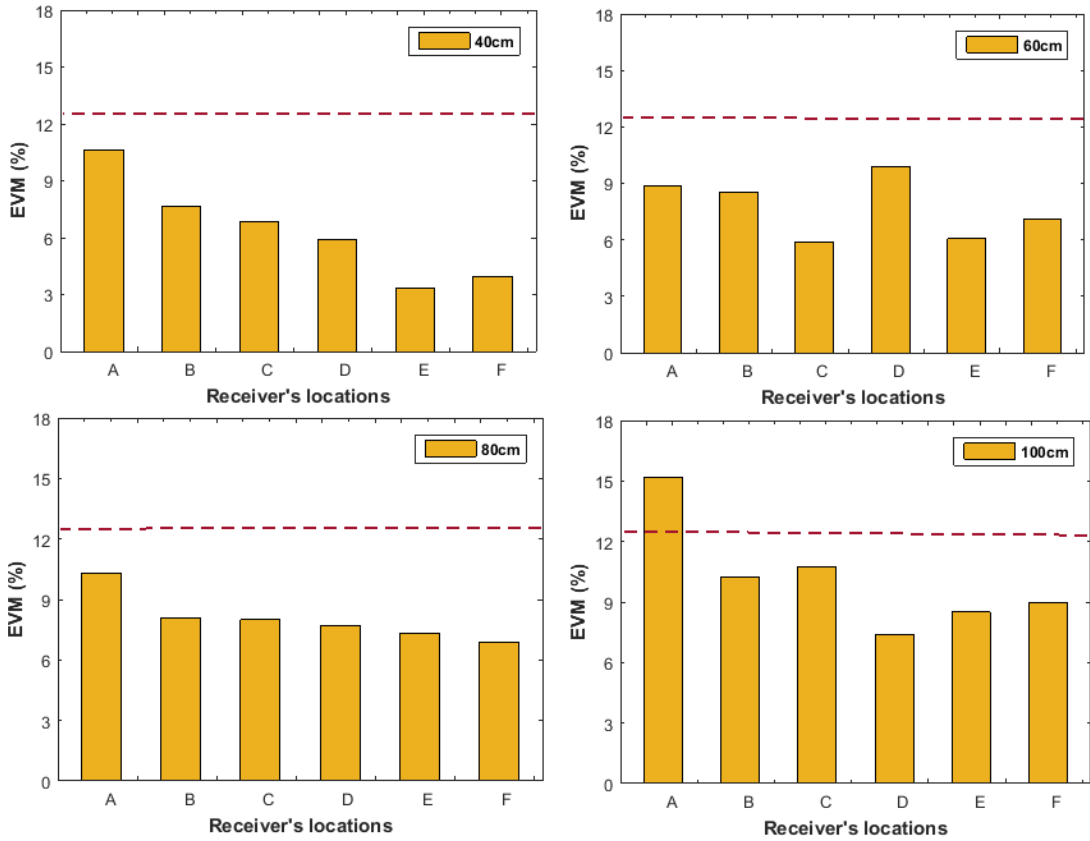

Figure 5.15 EVM result of 2x2 spatial diversity-MIMO at receiver location A to F for 40cm, 60cm, 80cm and 100cm transmit antenna separation distances at 4m wireless transmission distance.

Fig. 5.16 shows the EVM results of the 2x2 spatial diversity-MIMO using the Alamouti STBC algorithm at different receiver's location compared to individual SISO transmit antenna performance. The measurements were taken after 3m wireless transmission distance and at 60cm transmitter separation distance. It can be observed from the results that the EVM performance of spatial diversity-MIMO using Alamouti STBC algorithm generally improves in all the receivers' location below the 12.5% LTE limit for 16-QAM when compared to the individual SISO transmit antenna performance for Tx1 and Tx2. This improvement is due to the Alamouti STBC linear processing at the receiver and using an optimum transmitter separation (as shown in Fig. 5.13). Also, it can be observed that the coverage for SISO transmission is limited to only two receiver locations (for EVM < 12.5%) i.e. receiver

locations C and D, while for 2x2 spatial diversity-MIMO using Alamouti STBC algorithm, the coverage is increased to all six receiver locations.
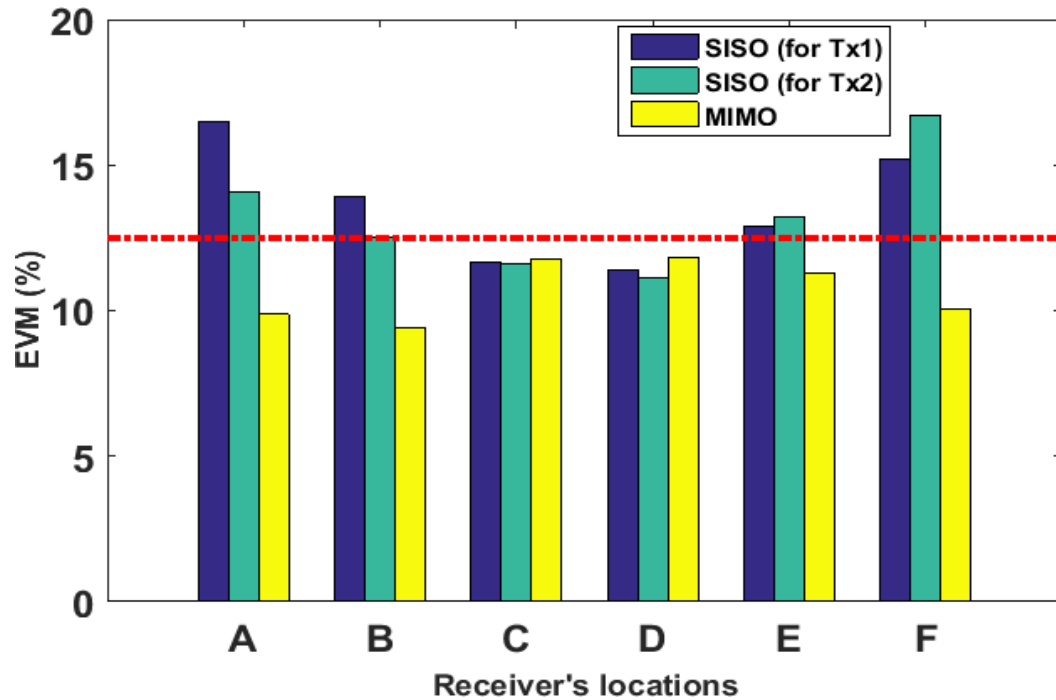
Figure 5.16 EVM results of 2×2 spatial diversity-MIMO using Alamouti STBC at different user locations compared with the performance of SISO system.

To examine the receiver sensitivity for 2x2 spatial diversity-MIMO, Fig. 5.17 shows the EVM result as the received power was varied from -54 to -38 dBm for 2.5m, 3m, 3.5m and 4m wireless transmission distances at a fixed transmitter separation of 80cm. It can be observed that the EVM result drops below the 12.5% LTE limit for 16-QAM at -50dBm received power for most of the wireless transmission distances and further decreases as the received power increases. This shows that the wireless transmission distances are limited by the received power, when there is sufficient power at the receiver (below -50dBm), the EVM result can be reduced.
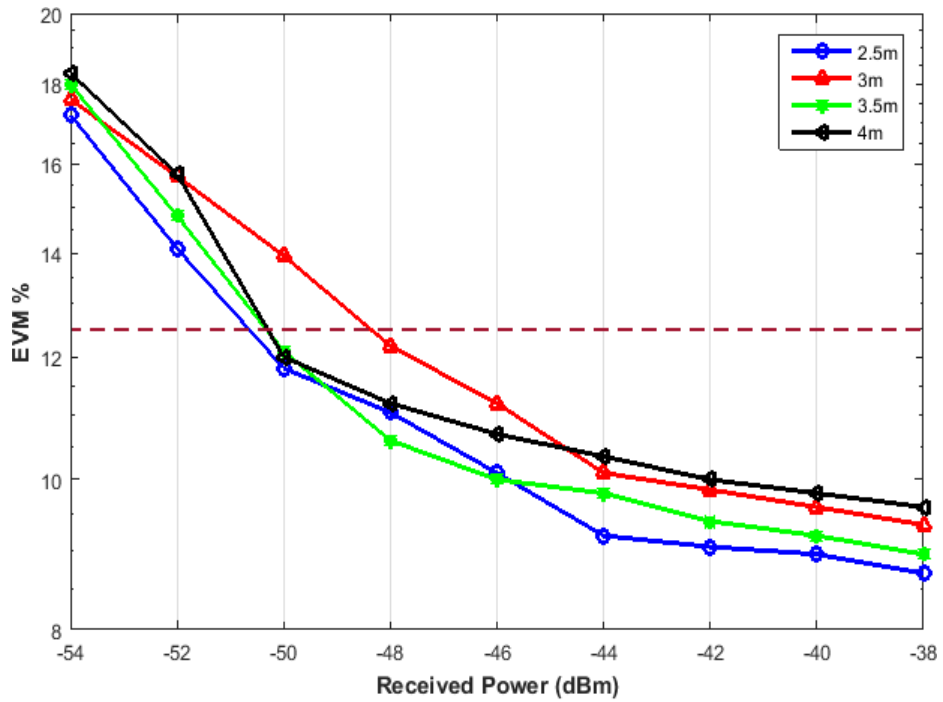
Figure 5.17 EVM results of 2x2 spatial diversity-MIMO using Alamouti STBC algorithm as the received power is increased for 2.5m, 3m, 3.5m and 4m wireless transmission distances at 80cm transmit antenna separation distance.
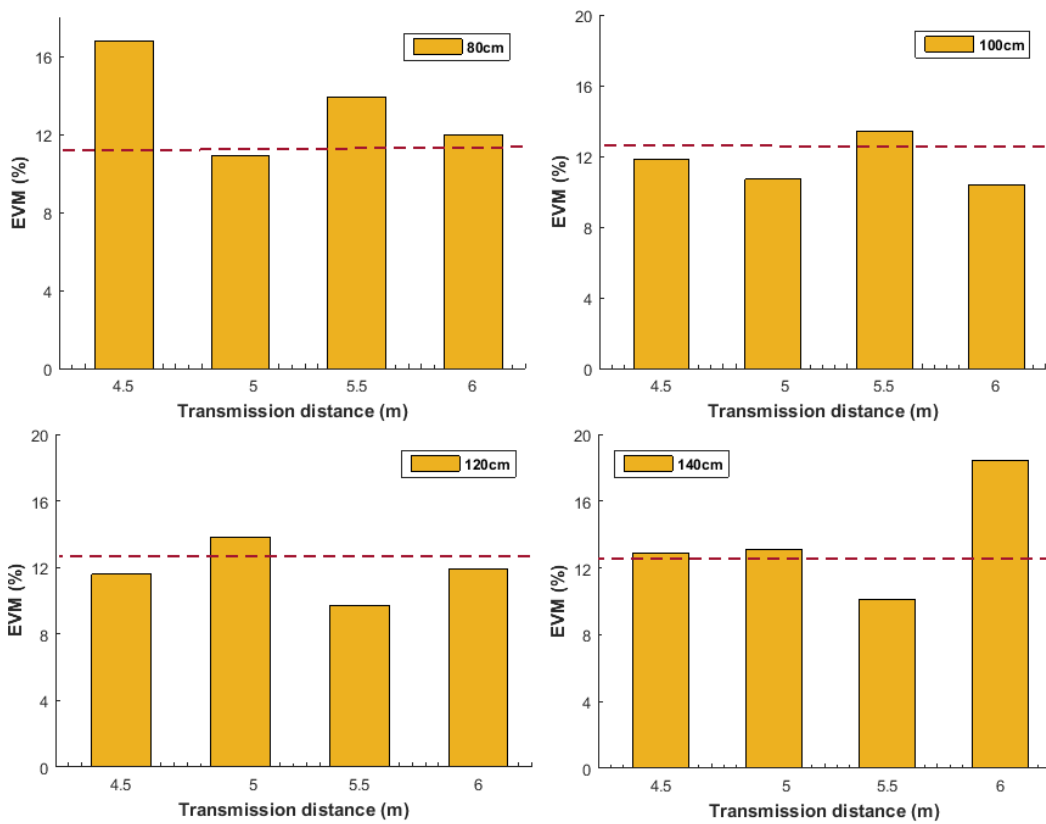
Figure 5.18 EVM result of 2x2 spatial multiplexing-MIMO for 80cm, 100cm, 120cm and 140cm transmit antenna separation distances at 4.5m, 5m, 5.5m and 6m wireless transmission distance.

The EVM result of 2x2 spatial multiplexing-MIMO using the zero forcing algorithm for 80cm, 100cm, 120cm and 140cm transmit antenna separation and at 4.5m, 5m, 5.5m and 6m wireless transmission distance is shown in Fig. 5.18. The results presented are for longer wireless transmission and larger transmit antenna separation distances. This is because after several manual antenna alignments, the EVM results for wireless transmission distance below 4.5m and 80cm transmit antenna separation generally gave high EVM, above 20%. This is most likely be because the received signal could not achieve enough spatial decorrelation at smaller transmit antenna spacing and shorter wireless distance.

In Fig. 5.18, the EVM result for 80cm transmit antenna separation at 4.5m and 5.5m wireless transmission distances were above the 12.5% LTE limit for 16-QAM while at 5m and 6m they were below the limit. For 100cm and 120cm transmit antenna separation, the EVM was below the 12.5% LTE limit for 16-QAM for most of the wireless transmission distances expect 5.5m and 5m for 100cm and 120cm transmit antenna separation, respectively. Also, the EVM for some of the wireless transmission distances for 140cm transmit antenna separation were above the 12.5% LTE limit for 16-QAM. Therefore, the overall best transmit antenna separation in this case was at 100cm and 120cm, since most of the wireless transmission distances were below the EVM limit.

In Fig. 5.19, the EVM result of the 2x2 spatial multiplexing-MIMO was compared with the two individual SISO transmitter (Tx1 and Tx2) at different receivers' locations when the wireless transmission distance was 5m and the transmit antenna separation was 100cm. It should be noted that 2x2 spatial multiplexing-MIMO is meant to double the data rate of SISO while spatial diversity-MIMO is targeted at improving the EVM results of SISO. Therefore, the EVM performance of 2x2 spatial multiplexing-MIMO in Fig. 5.19 does not show improved performance to SISO in terms of EVM, but it is generally below the 12.5% LTE limit for 16-QAM and at lower EVM, higher data rates can be achieved. In particular, the data rate for the SISO cases is 0.5 Gbps while that of spatial multiplexing-MIMO is 1Gbps but the full multiplexing gain can only be achieved when the EVM is below the 12.5% LTE limit for 16-QAM. While the receiver's locations A and F were slightly above the EVM limits, the other positions were significantly below the EVM limit.
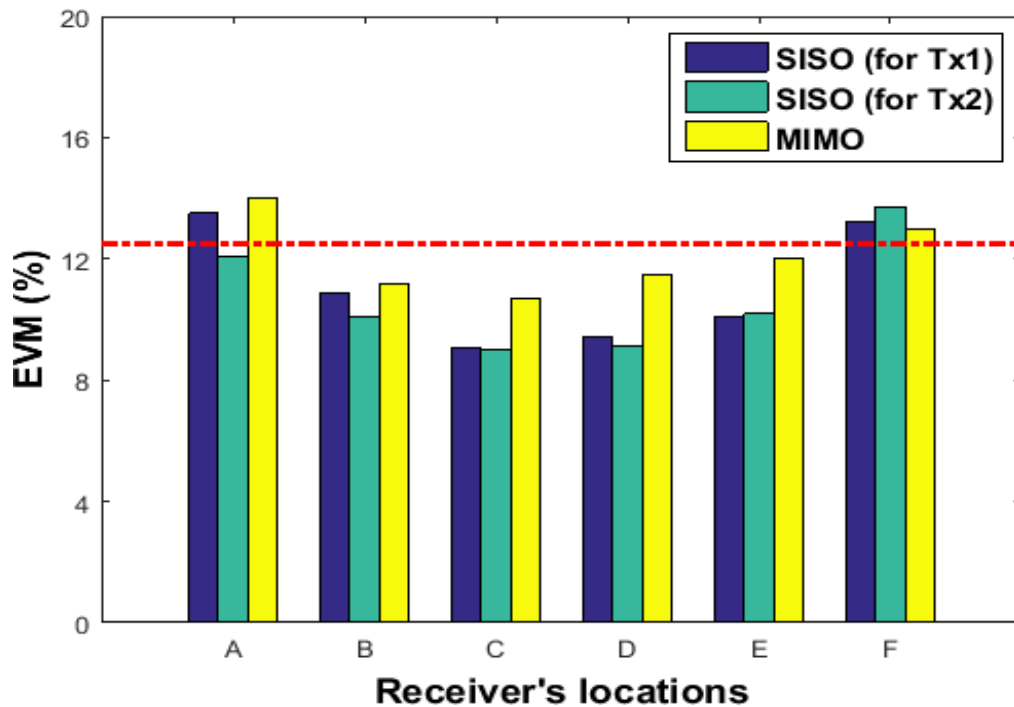
Figure 5.19 EVM of SISO with 0.5Gb/s at different receiver locations compared to spatial multiplexing-MIMO with each antenna transmitting 0.5Gbps.

5.4.2. 60GHz Measurement Results

The EVM results of the RoF-transported 60 GHz 2x2 emulated-MIMO are examined for a wireless transmission distance of 1.5m (the distance limitation was due to the lack of availability of a 60GHz amplifier before the transmit antenna) and 20cm, 30cm, 40cm and 60cm transmit antenna separation distances. The complex channel transfer matrix H and the transmitted symbols were captured when the antennas were moved around to emulate a 2x2 MIMO system. The receiver was moved between five receiver locations (A-E) at different transmit antenna separation distances to determine the optimum spacing between the transmitting antennas for transmission. The EVM results of the optimum transmit antenna separation distance was then compared with the EVM results of the SISO system.

Fig. 5.20 shows the EVM results that were obtained for receiver's locations A to E (shown in Fig. 5.11) after the received signal on the first and second receive antenna (y_1 and y_2) were processed using Alamouti STBC spatial diversity algorithm. The EVM results were obtained for transmitter antenna separation distances of 20cm,

30cm, 40cm and 60cm to determine the optimum separation when 1Gbps data rate was transmitted.

Figure 5.20 EVM result of 60GHz experiment at 20cm, 30cm, 40cm and 60cm transmit antenna separation distances using Alamouti STBC spatial diversity algorithm.

It can be observed from the results in Fig. 5.20 that at 20, 30 and 40cm transmit antenna separation distances, the EVM results were below the 12.5% LTE limit for 16-QAM (shown with the red dash line) in all receiver's location. However, at 60cm transmit antenna separation, the EVM results were generally high for most receiver's locations and above the 12.5% limit. The higher EVM resulting at 60cm transmit antenna separation was because, with the larger antenna spacing, the distance between the transmitting and receiving antenna increased and the received power reduced. Also, the received power imbalance issue might cause a deterioration in the EVM performance since the path loss for the received antennas can be different as a result of the large transmit antenna separation.

Figure 5.21 EVM result of SISO compared with the emulated 2x2 MIMO for 20cm transmit antenna separation at different receiver's locations using Alamouti STBC spatial diversity algorithm.

Fig. 5.21 compares the EVM result of SISO with the emulated 2x2 MIMO at different receiver's locations using Alamouti STBC spatial diversity algorithm, both transmitting 1Gbps data rate. To compare the performance of the emulated 2x2 MIMO with SISO, the overall transmit power is kept the same. It can be observed that the EVM performance of SISO was generally high and above the 12.5% LTE limit for 16-QAM in some receiver's location (D and E) while the EVM performance of the 20cm transmit antenna separation was below the 12.5% LTE limit in all receiver locations. The improved EVM performance for the emulated 2x2 MIMO is due to the Alamouti STBC spatial diversity algorithm and the 20cm antenna spacing that enabled the receiving antennas to see several versions of the transmitted signal.

Fig. 5.22 shows the EVM results that were obtained for receiver locations A to E (as shown in Fig. 5.11) after the received signal on the first and second receive antenna (y_1 and y_2) were processed using zero-forcing spatial multiplexing algorithm. The transmitter sends two independent sets of data, i.e. two 0.5Gbps data streams and they were re-combined at the receiver using the zero-forcing algorithm to give an overall data rate of 1Gbps. The EVM results were obtained for transmit antenna separations of 20cm, 30cm, 40cm and 60cm to determine the optimum separation.
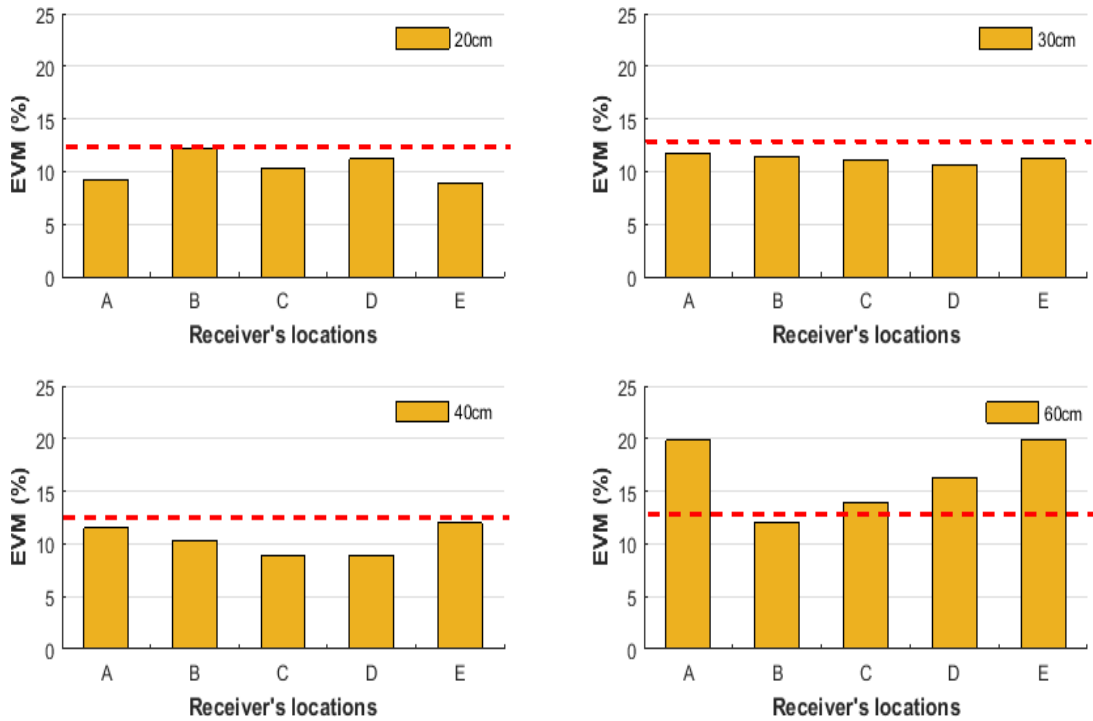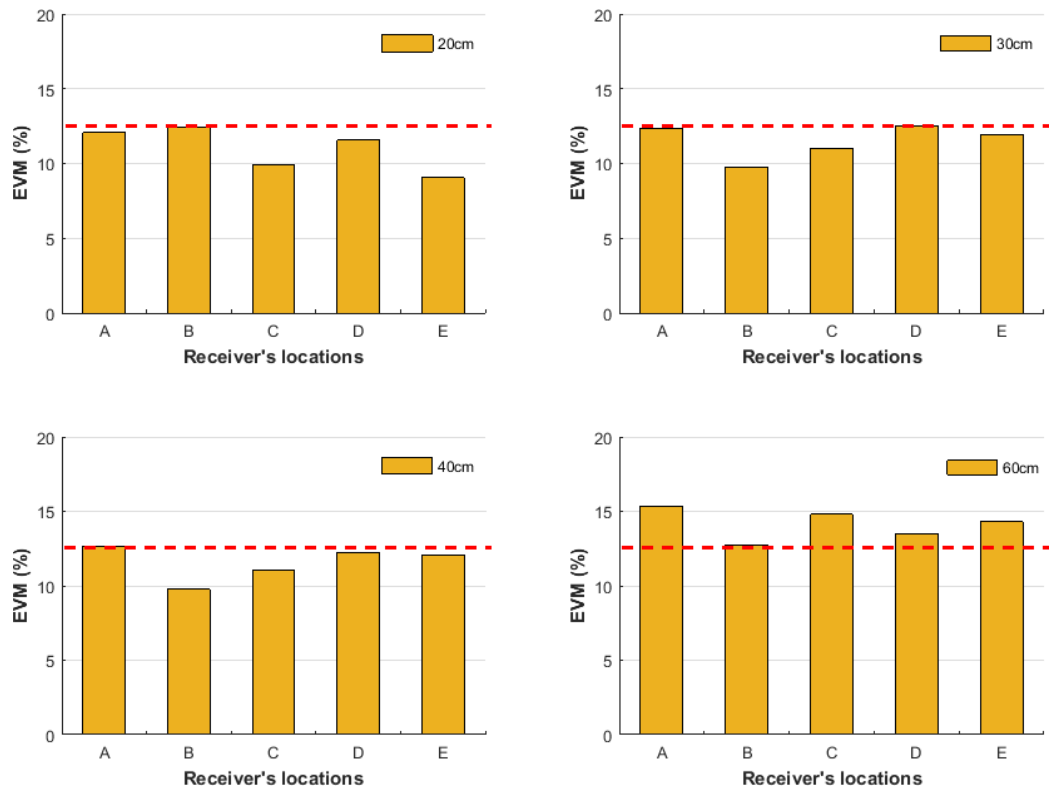
Figure 5.22 EVM result of 60GHz experiment at 20cm, 30cm, 40cm and 60cm transmit antenna separation distances using zero-forcing spatial multiplexing algorithm.

It can be observed that at 20, 30 and 40cm transmitter separation distance, the EVM results in Fig. 5.22 were below the 12.5% LTE limit for 16-QAM in all receiver locations, while at 60cm transmit antenna separation, the EVM results were generally high for all receiver locations and above the 12.5% limit. The reason for this is similar to the EVM result of 60cm transmit antenna separation for Alamouti STBC spatial diversity: the high EVM result at 60cm transmit antenna separation using zero-forcing spatial multiplexing is also due to the low received power caused by an increase in path loss in contributing to the received power imbalance issue.

Fig. 5.23 compares the EVM result of SISO transmitting 0.5Gbps with the emulated 2x2 MIMO transmitting two 0.5Gbps data streams (overall multiplexed data rate of 1Gbps) at different receiver locations using the zero-forcing spatial multiplexing algorithm. To compare the performance of the emulated 2x2 MIMO with SISO, the overall transmit power is kept the same.
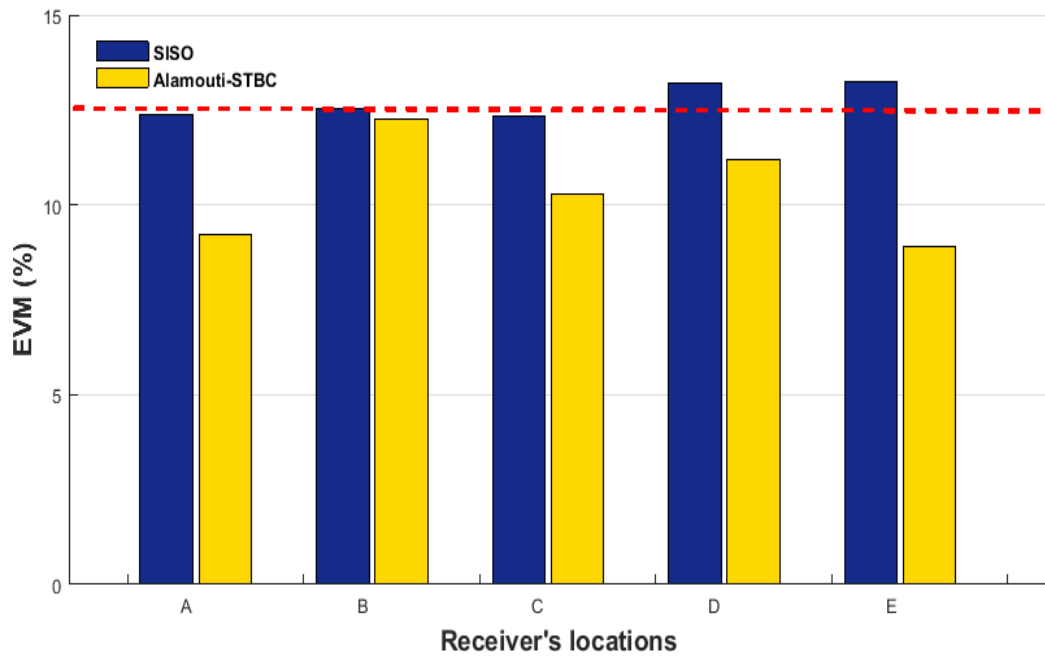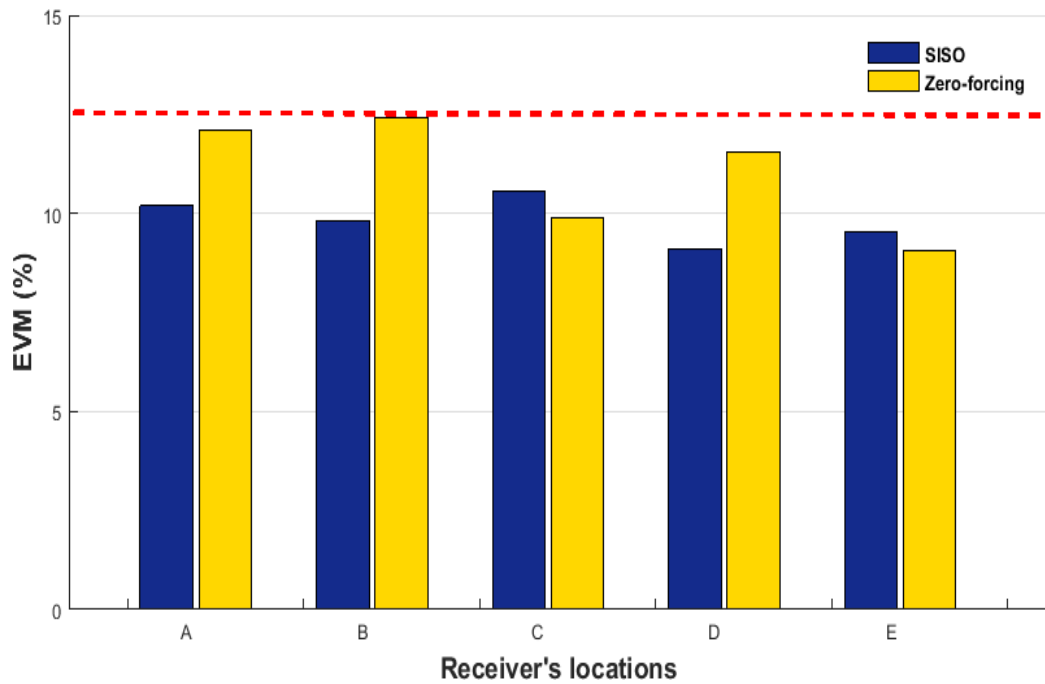
Figure 5.23 EVM result of SISO compared with the emulated 2x2 MIMO for 20cm transmit antenna separation at different receiver's locations using zero-forcing spatial multiplexing algorithm.

It can be seen that both the EVM result of 20cm transmit antenna separation and SISO in Fig. 5.23 are below the 12.5% LTE limit for 16-QAM. However, the EVM result of 20cm transmit antenna separation shows that using the zero-forcing spatial multiplexing algorithm delivered a data rate of 1Gbps across all receiver's locations since the EVM is below the 12.5% LTE limit for 16-QAM, while the EVM result for SISO is for a system only delivering 0.5Gbps data rate across all receiver's locations.

5.5 Summary

A wireless 2x2 MIMO system has been experimentally investigated in a 25GHz DWDM-RoF setup. The experiment was carried out with the encoded OFDM data processed in MATLAB/Simulink and downloaded onto the AWG for upconversion to IF frequency. The resultant signals are modulated on different optical wavelengths and transported over 2km fibre to two RAUs. The signals were captured after up to 6m wireless transmission distance at six user locations and the results were saved in MATLAB format for offline processing using spatial diversity Alamouti STBC and spatial multiplexing zero-forcing algorithms.

The results for 3, 3.5 and 4m wireless transmission distances were obtained when the transmit antennas were separated at 40, 60, 80 and 100cm, and the EVM result revealed that 60cm was the optimum transmit antenna separation for spatial diversity-MIMO at 3, 3.5 and 4m wireless transmission distances for 25 GHz frequency signals and when 20° half power bandwidth horn antennas are used. Also, the EVM performance of 2x2 spatial diversity-MIMO at 60cm transmit antenna separation was compared with the performance of SISO, the result shows that improved performance can be achieved for spatial diversity-MIMO in all the receiver locations with the EVM results below the required limit, while SISO failed to meet the EVM requirement in some receiver's location.

The EVM results for spatial multiplexing-MIMO were also examined when different data streams were transmitted from two antennas and the zero-forcing algorithm was used to remove the ISI and re-combine the data at the receiver. The results for 80, 100, 120 and 140cm transmit antenna separations were obtained at 4.5, 5, 5.5 and 6m wireless transmission distances. The EVM results for smaller transmit antenna separations (<80cm) and shorter wireless transmission distances (<4.5m) were generally high (EVM above 20%), this was most likely be because the received signal could not achieve enough spatial decorrelation at smaller transmit antenna spacing and shorter wireless distance. Overall, 100cm and 120cm transmit antenna separations were the optimum at 4.5, 5, 5.5 and 6m wireless transmission distances, for 25 GHz frequency signals and when 20° half power bandwidth horn antennas are used, since the EVM was generally low and below the required EVM limit. In

addition, the EVM performance of 2x2 spatial multiplexing-MIMO at 100cm transmit antenna separation was compared with the performance of SISO. The results revealed that the EVM for spatial multiplexing-MIMO and SISO were below the required limit in most of the user locations even though the data rate for spatial multiplexing-MIMO was double that of SISO.

In another experiment, the EVM performance of a 60 GHz wireless transmission was obtained in a RoF setup using integrated transmitter and receiver circuits. The experimental setup involved an IF signal modulated onto an optical carrier and transported over a RoF link for up-conversion to 60 GHz using an integrated transmitter circuit. The signal was received after 1.5m wireless transmission distance and down-converted to an IF signal using a 60GHz integrated receiver circuit. A wireless 2x2 MIMO experiment was emulated by moving the transmit and receive antennas between specific locations to capture the complex channel transfer matrix H and the transmitted symbols. The results were captured at five receiver locations and at 20, 30, 40 and 60cm transmit antenna separation using spatial diversity Alamouti STBC and spatial multiplexing zero-forcing processing algorithms.

The EVM results of the 60 GHz RoF experiment reveals that when Alamouti STBC processing algorithms was used, the EVM results were below the required limit for 20, 30 and 40cm transmit antenna separation while for 60cm transmit antenna separation, the EVM was above the limit in most receiver's location. The EVM performance of 20cm transmit antenna separation using Alamouti STBC was compared with the performance of SISO and the results showed improved performance can be achieved for spatial diversity-MIMO in all user locations and that it was always below the required limit. Similarly, the results obtained at 20, 30, 40 and 60cm transmit antenna separation and processed using zero-forcing algorithms show that the EVM at 20, 30 and 40cm was below the required limit, while that of 60cm transmit antenna separation was above the limit.

Finally, the EVM result at 20cm transmit antenna separation for the 60 GHz RoF system using zero-forcing algorithm was compared with the performance of SISO, and the results showed that similar EVM performance can be obtained for 20cm transmit antenna separation and SISO across all user locations while the data rate for the spatial multiplexing-MIMO was, obviously, double that of SISO. These

experiments verify that spatial diversity and spatial multiplexing MIMO techniques can be implemented in a mm-wave RoF system, but it requires setting an optimum transmit antenna spacing for MIMO to achieve improved performance over SISO system.

REFERENCES

[1] N. J. Gomes, P. P. Monteiro, A. Gameiro, Next Generation Wireless Comunications Using Radio Over Fiber., 2012, Wiley.

[2] R. Heath, N. Gonzalez-Prelcic, S. Rangan, W. Roh, and A. Sayeed, "An Overview of Signal Processing Techniques for Millimeter Wave MIMO Systems", IEEE Journal on Selected Topics in Signal Processing, 2016. pp. 436 - 453

[3] IEEE Wireless LAN Medium Access Control (MAC) and Physical Layer (PHY) Specifications – Higher Speed Physical Layer Extension in the 2.4 GHz Band, IEEE Amendment 802.11b-1999, 1999

[4] Y. Niu, Y. Li, D.Jin, L. Su, and A. V. Vasilakos, "A survey of millimeter wave communications (mmWave) for 5G: opportunities and challenges", . Wirel. Netw., vol. 21(8), 2015, pp. 2657-2676.

[5] L. Liu, W. Hong, H. Wang, G. Yang, N. Zhang, H. Zhao, et al., "Characterization of line-of-sight MIMO channel for fixed wireless communications," IEEE Antennas and Wireless Propagation Letters, vol. 6, pp. 36-39, 2007.

[6] I. Sarris, A.R. Nix, "Design and performance assessment of high-capacity MIMO architectures in the presence of a line-of-sight component," IEEE Transactions on Vehicular Technology, vol. 56(4), pp. 2194-2202, 2007.

[7] C.H. Ho, W.R. Jiang, R. Sambaraju, W.Y. Lee, T.H. Lu, C.Y. Wang, et al., "Performance Evaluation of a 60 GHz RoF System Employing MIMO and OFDM Modulation," IEEE Journal on Selected Areas in Communications, vol. 31(12), pp. 780-787, 2013.

[8] A. Kanno, T. Kuri, I. Hosako, T. Kawanishi, Y. Yoshida, Y. Yasumura, K.I. Kitayama, "Optical and millimeter-wave radio seamless MIMO transmission based on a radio over fiber technology," Optics Express, vol. 20(28), pp. 29395-29403, 2012.

[9] L. Cheng, M.M.U. Gul, F. Lu, M. Zhu, J. Wang, M. Xu, et al.,"Coordinated Multipoint Transmissions in Millimeter-Wave Radio- Over-Fiber Systems," Journal of Lightwave Technology, vol. 34, pp. 653-660, 2016.

[10] C. D. Ziomek and M. T. Hunter "Extending the Useable Range of Error Vector Magnitude (EVM) Testing" 2012, [online] Available: http://www.ztecinstruments.com/zconnect/wpcontent/uploads/2012/03/EVM_Opti mization.pdf

[11] Rohde & Schwarz: "LTE System Specifications and their Impact on RF & Base Band Circuits" 2013.

[12] Göteborg Microwave Integrated Circuits (2014): gTSC0020 Complete Transmitter 57-66 GHz

[13] T. Quinlan, S. Walker. "A 16.8 dBi quasi-discoidal radiation pattern antenna array for 60GHz non-line-of-sight applications.", Loughborough Antennas and Propagation Conference (LAPC), pp.210- 213, 2014

[14] Göteborg Microwave Integrated Circuits (2014): gRSC0016 Complete Receiver 60 GHz

CHAPTER 6

CONCLUSION AND FUTURE WORK

6.1. Conclusions

The increasing demand for higher data rate by the growing numbers of mobile users has motivated the development of alternative communication systems that will improve wireless coverage and capacity, especially in an indoor environment. In-building RoF-based DAS provides high quality signal coverage, with low interference and high signal-to-noise ratio (SNR), and its integration with MIMO can bring about further improvement in throughput performance taking advantage of the largely separated multiple RAUs (enabling greater spatial decorrelation).

In this thesis, the performance of two practical issues with commercial MIMO AP in a RoF-DAS infrastructure i.e. the fibre-length difference and power imbalances effects have been analyzed. Previous works have analyzed these issues with non-MIMO APs but here, the analysis has been carried out in a typical office environment with a commercial MIMO-supported AP and spatial diversity-supported AP in a RoF-DAS infrastructure. Further, the previous works on RoF-DAS for improving MIMO systems have been based on commercial products and the specific algorithms used within these products were unknown but here, the performance verification of the benefits of increased antenna spacing in a RoF-DAS has been demonstrated when using specific multi-antenna transmit/receive scheme algorithms. This has been performed by comparing the schemes with a SISO system and with systems using the techniques but with small antenna spacing only. Finally, RoF-transport of mm-wave MIMO has attracted a lot of interest recently due to the availability of larger bands of frequency enabling the possibility of wider bandwidth and higher data rates. The performance of RoF-transport of mm-wave 2×2 MIMO for spatial diversity and multiplexing have been demonstrated at 25GHz and 60GHz, and compared with the performance of a SISO system.

The key conclusions from this thesis are as follows:

- The fibre-length difference analysis in a RoF-DAS infrastructure shows that for MIMO, the throughput drops rapidly due to severe Inter-Symbol Interference (ISI) caused by differential delay when the fibre-length difference exceeds a certain distance, while for spatial diversity the analysis shows that high throughputs can be maintained even at large fibre-length difference.

- The power imbalance effect analysis shows that for a typical office environment, fitted with common office furniture and computers, the throughput performance drops in specific wireless user's positions when the received power imbalance was above 12-15dB for a MIMO-supported AP while for a spatial diversity-supported AP the power imbalance does not affect the throughput performance.

- In a wireless 1x2 spatial diversity-SIMO uplink when the signals from two RAUs are RoF-transported and then centrally processed using MRC algorithm, it was experimentally verified that significantly reduced SER and small capacity improvement due to reduced EVM/MER can be achieved by a large transmitter spacing compared to SISO and smaller transmitter spacing.

- In a wireless 2x1 spatial diversity-MISO downlink with the two Alamouti STBC encoded data signals RoF-transported and then transmitted from two RAUs using the Alamouti STBC scheme significantly reduced SER and modestly increased capacity due to lower EVM/MER can be achieved by a large transmitter spacing compared to SISO and smaller transmitter spacing.

- In a wireless 2x2 spatial multiplexing-MIMO downlink, where two different data signals are RoF-transported and transmitted from two RAUs to one mobile unit with two receiving antennas and processed using the zero-forcing algorithm, it was experimentally verified that SER can be reduced due to reduced EVM/MER (through a reduction in ISI) compared to SISO. Further, the spatial multiplexing gain can be significantly enhanced with increased RAU spacing, leading to much increased capacity.

- For greater antenna spacing of up to 10m, and in a typical office environment, fitted with common office furniture and computers, it was experimentally verified that using a wireless 1x2 SIMO uplink at +3dBm transmit power, and wireless 2x1 MISO and 2x2 MIMO downlink at +11dBm transmit power, the EVM generally reduced at 4m and 6m antenna separation for all user's positions but increases at 10m antenna separation due to power imbalance problem.

- For a 25/60GHz wireless 2x2 spatial diversity-MIMO where two Alamouti STBC encoded data signals are RoF-transported and transmitted from two RAUs to one mobile unit with two receiving antennas, and combined using Alamouti STBC, it was experimentally verified that EVM can be significantly reduced at all user's positions compared to a SISO system when an optimum transmit antenna spacing was used.

- For a 25/60GHz wireless 2x2 spatial multiplexing-MIMO where two different data signals are RoF-transported and transmitted from two RAUs to one mobile unit with two receiving antennas, and processed using zero-forcing processing algorithm, it was experimentally verified that similar EVM performance can be achieved when an optimum transmit antenna spacing was used, compared to SISO even though the data rate for the spatial multiplexing-MIMO is obviously doubled.

6.2. Future Work

Future work can explore other techniques to improve the performance of MIMO in an experimental RoF-DAS.

- The Minimum Mean Square Error (MMSE) algorithm can be explored to process the received signal from a wireless 2x2 MIMO, since it can maximize the post-detection signal-to-interference plus noise ratio (SINR). Unlike the zero-forcing algorithm used in Chapter 4 and 5, which is ideal for noiseless channels because it removes only the inter symbol interference (ISI), MMSE will also benefit interference-limited channels. Also, the large antenna separation enabled by

RoF-DAS will provide sufficient decorrelation for the channel to improve the overall performance. The results of RoF-transported MIMO using MMSE can be compared with RoF-transported MIMO using ZF algorithm to determine the performance improvement.

- A single user pre-coding technique can take advantage of RoF-DAS to provide sufficient decorrelation for the channels in order to achieve lower error rates and higher capacity. A wireless 2x2 downlink MIMO signals can be RoF-transported and transmitted from two RAUs to one mobile units with two receiving antennas, and the channel state information (CSI) can be estimated and applied to the transmitting signal to improve SNR at the receiver. The results of RoF-transported single-user pre-coding MIMO can be compared with a RoF-transported non-precoding MIMO and a SISO system to determine the performance improvement.
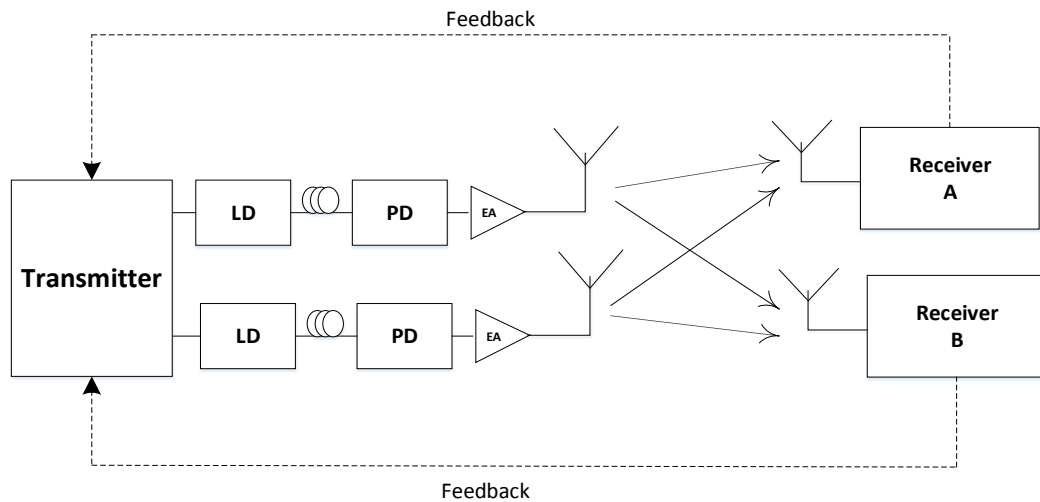

Figure 6.1 An example of the experimental setup of a multi-user pre-coding MIMO in RoF-DAS.

- A multi-user precoding technique can also take advantage of a RoF-DAS to provide sufficient decorrelation for the channels. A wireless 2x2 downlink MIMO signals can be RoF-transported and transmitted from two RAUs to two mobile units, each with one receiving antenna as shown in Fig. 6.1 and the CSI can be estimated and applied to the transmitting signal to improve SNR at the

receiver. The results of multi-user pre-coding MIMO can be compared with a single user pre-coding MIMO and a SISO system.
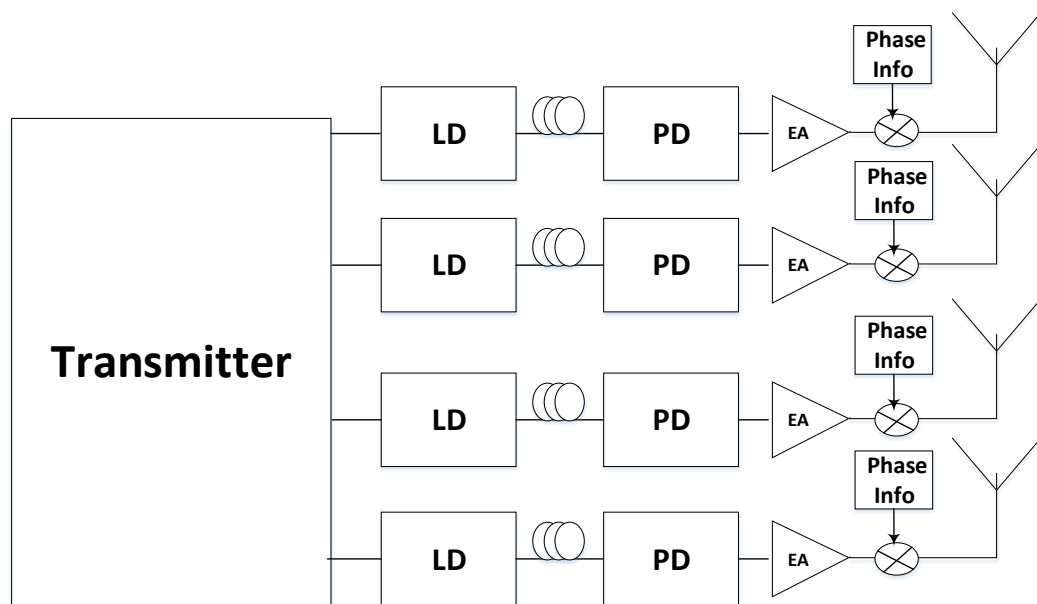

Figure 6.2 An example of the experimental setup of an analogue beamforming in RoF system.

- There has been a dramatic increase in the shipment of WLAN products compliant with IEEE 802.11ac and one distinct characteristic of IEEE 802.11ac/ad standards is the use of beamforming technique to send targeted Wi-Fi signals to individual wireless user. One of the advantages of RoF system is its easy upgrade of existing services to emerging wireless services due to its centralized architecture. Although, large physical antenna separation is not required in beamforming, RoF can still provide an efficient means of transporting the signal over a long distance while centralizing the WLAN product. Beamforming can be implemented either at the analogue or digital domain.

- Analogue beamforming in a RoF system can be demonstrated once the phase of the channel information is known, then, an electronic phase shifter can be introduced before each antenna in the RAU and the signals can be adjusted to form a beam in the direction of the user as shown in Fig. 6.2. Digital

beamforming technique in a RoF system can also be demonstrated once the amplitude and phase information is available to the transmitter. The information can be applied to the transmitting signals, before RoF-transporting them to the RAUs. The advantage of digital beamforming is the cost of phase shifter it saves especially at higher frequencies. The analogue and digital beamforming can be compared to determine the performance, and it can also be compared with other multi-antenna schemes and a SISO system.

APPENDIX A

```
function x = fcn(h₁₁,h₂₁,y1,y2)


%# maximal ratio combining


x = (conj(h₁₁).*y1) + (conj(h₂₁).*y2);
```

APPENDIX B

```
function [x1,x2]  = zeroForcing(y1,h₁₁, h₁₂, y2, h₂₁, h₂₂)


%# Zero-forcing detection


H=complex(zeros(2));
Y=complex(zeros(2,1));
G=complex(zeros(2,1));
x1=complex(zeros(N,1));
x2=complex(zeros(N,1));


for i=1:N
    H(1,1)=h₁₁(i,1,1);
    H(1,2)=h₁₂(i,1,1);
    H(2,1)=h₂₁(i,1,1);
    H(2,2)=h₂₂(i,1,1);
    W= pinv (H);
    Y(1,1)=y1(i,1,1);
    Y(2,1)=y2(i,1,1);
    G=W*Y;
    x1(i,1)=G(1,1);
    x2(i,1)=G(2,1);
end
```